UNIVERSIDAD PONTIFICIA COMILLAS
**ESCUELA TÉCNICA SUPERIOR DE INGENIERÍA (ICAI)**
**INGENIERO INDUSTRIAL**

MASTER THESIS

# EVALUATION OF NOVEL ENERGY MANAGEMENT CONCEPTS FOR EV CHARGERS IN FUTURE SMART CITY INFRASTRUCTURE

**AUTOR: Ignacio Basallote Muñoz**

**DIRECTOR: Milica Bogdanovic**

**MADRID, Junio de 2019**

I, hereby, declare that I am the only author of the project report with title:

**Evaluation of Novel Energy Management Concepts for EV Chargers in Future Smart City Infrastructure**

which has been submitted to ICAI School of Engineering of Comillas Pontifical University in the academic year 2018/19. This project is original, has not been submitted before for any other purpose and has not been copied from any other source either fully or partially. All information sources used have been rightly acknowledged.

Fdo.: Ignacio Basallote Muñoz          Date: 17/06/2019

I authorize the submission of this project

PROJECT SUPERVISOR

Fdo.: Milica Bogdanovic          Date: 17/06/2019

# AUTHORIZATION FOR DIGITALIZATION, STORAGE AND DISSEMINATION IN THE NETWORK OF END-OF-DEGREE PROJECTS, MASTER PROJECTS, DISSERTATIONS OR BACHILLERATO REPORTS

## *1. Declaration of authorship and accreditation thereof.*

The author Mr. /Ms. Ignacio Basallote Muñoz

**HEREBY DECLARES** that he/she owns the intellectual property rights regarding the piece of work:
Evaluation of Novel Energy Management Concepts for EV Chargers in Future Smart City Infrastructure
that this is an original piece of work, and that he/she holds the status of author, in the sense granted by the Intellectual Property Law.

## *2. Subject matter and purpose of this assignment.*

With the aim of disseminating the aforementioned piece of work as widely as possible using the University's Institutional Repository the author hereby **GRANTS** Comillas Pontifical University, on a royalty-free and non-exclusive basis, for the maximum legal term and with universal scope, the digitization, archiving, reproduction, distribution and public communication rights, including the right to make it electronically available, as described in the Intellectual Property Law. Transformation rights are assigned solely for the purposes described in a) of the following section.

## *3. Transfer and access terms*

Without prejudice to the ownership of the work, which remains with its author, the transfer of rights covered by this license enables:

a) Transform it in order to adapt it to any technology suitable for sharing it online, as well as including metadata to register the piece of work and include "watermarks" or any other security or protection system.

b) Reproduce it in any digital medium in order to be included on an electronic database, including the right to reproduce and store the work on servers for the purposes of guaranteeing its security, maintaining it and preserving its format.

c) Communicate it, by default, by means of an institutional open archive, which has open and cost-free online access.

d) Any other way of access (restricted, embargoed, closed) shall be explicitly requested and requires that good cause be demonstrated.

e) Assign these pieces of work a Creative Commons license by default.

f) Assign these pieces of work a HANDLE (*persistent* URL). by default.

## *4. Copyright.*

The author, as the owner of a piece of work, has the right to:

a) Have his/her name clearly identified by the University as the author

b) Communicate and publish the work in the version assigned and in other subsequent versions using any medium.

c) Request that the work be withdrawn from the repository for just cause.

d) Receive reliable communication of any claims third parties may make in relation to the work and, in particular, any claims relating to its intellectual property rights.

## *5. Duties of the author.*

The author agrees to:

a) Guarantee that the commitment undertaken by means of this official document does not infringe any third party rights, regardless of whether they relate to industrial or intellectual property or any other type.

b) Guarantee that the content of the work does not infringe any third party honor, privacy or image rights.

c) Take responsibility for all claims and liability, including compensation for any damages, which may be brought against the University by third parties who believe that their rights and interests have been infringed by the assignment.

d) Take responsibility in the event that the institutions are found guilty of a rights infringement regarding the work subject to assignment.

### 6. Institutional Repository purposes and functioning.

The work shall be made available to the users so that they may use it in a fair and respectful way with regards to the copyright, according to the allowances given in the relevant legislation, and for study or research purposes, or any other legal use. With this aim in mind, the University undertakes the following duties and reserves the following powers:

a) The University shall inform the archive users of the permitted uses; however, it shall not guarantee or take any responsibility for any other subsequent ways the work may be used by users, which are non-compliant with the legislation in force. Any subsequent use, beyond private copying, shall require the source to be cited and authorship to be recognized, as well as the guarantee not to use it to gain commercial profit or carry out any derivative works.

b) The University shall not review the content of the works, which shall at all times fall under the exclusive responsibility of the author and it shall not be obligated to take part in lawsuits on behalf of the author in the event of any infringement of intellectual property rights deriving from storing and archiving the works. The author hereby waives any claim against the University due to any way the users may use the works that is not in keeping with the legislation in force.

c) The University shall adopt the necessary measures to safeguard the work in the future.

d) The University reserves the right to withdraw the work, after notifying the author, in sufficiently justified cases, or in the event of third party claims.

Madrid, on .17........ of .June 2019 ........................, ..........

**HEREBY ACCEPTS**

Signed. Ignacio Basallote Muñoz

Reasons for requesting the restricted, closed or embargoed access to the work in the Institution's Repository

# Documents Index

# UNIVERSIDAD PONTIFICIA COMILLAS

**ESCUELA TÉCNICA SUPERIOR DE INGENIERÍA (ICAI)**

**INGENIERO INDUSTRIAL**

MASTER THESIS

# EVALUATION OF NOVEL ENERGY MANAGEMENT CONCEPTS FOR EV CHARGERS IN FUTURE SMART CITY INFRASTRUCTURE

**AUTOR: Ignacio Basallote Muñoz**

**DIRECTOR: Milica Bogdanovic**

**MADRID, Junio de 2019**

# Acknowledgments

First of all, I would like to thank all my professors and colleges from Comillas and RWTH Aachen for their support during these last six months in the development of this thesis.

Thanks to all my grandparents, especially to Ciriaco for encouraging me studying engineering.

Thanks to my family for the patience and support during these last years and for providing me the opportunity of studying at Comillas (ICAI).

Finally, thanks to you Paola, for your daily support and for all the good moments that we shared in this extraordinary adventure abroad and for the ones that are about to come.

# EVALUACIÓN DE CONCEPTOS NOVELES DE GESTIÓN DE DEMANDA PARA ESTACIONES DE CARGA DE VEs EN FUTURAS CIUDADES INTELIGENTES

**Autor: Basallote Muñoz, Ignacio**
Director: Bogdanovic, Milica.
Entidad Colaboradora: RWTH Aachen.

## RESUMEN DEL PROYECTO

Uno de los retos de las futuras ciudades inteligentes es coordinar la carga de vehículos eléctricos (VE), con el fin de minimizar su impacto en el sistema eléctrico. Si no se controla de forma óptima, esta demanda podría remodelar el perfil de potencia demandada pudiendo ocasionar congestiones en las redes de distribución. Además, variaciones significativas en el perfil de potencia pueden implicar cambios en el dimensionado del sistema eléctrico, lo que conllevaría gastos innecesarios. Este trabajo incluye un estado de la cuestión sobre los sistemas de gestión de energía para estaciones de carga. Además, de acuerdo a lo estudiado, se propone una arquitectura de control basada en un control predictivo (MPC) de dos niveles para coordinar la demanda de VEs en redes de distribución. El nivel de control inferior agrega la demanda de energía de todas las estaciones de carga de la misma subestación de Media-Baja tensión (MT-BT). El segundo nivel distribuye la demanda agregada de VEs en el tiempo, minimizando las pérdidas totales del sistema y considerando el estado futuro del sistema eléctrico. Se utilizan un conjunto de relajaciones para convexificar las ecuaciones de flujo de potencia (FP). De esta manera, el óptimo global puede ser fácilmente alcanzado para topologías radiales. Finalmente, se analiza el rendimiento del algoritmo desarrollado con diferentes topologías de red de la IEEE y para distintos niveles de penetración de VEs.

**Palabras clave:** Sistemas de Gestión de Energía (EMS), Redes Inteligentes, Ciudades Inteligentes, Estaciones de Carga.

### Introducción

El número de estaciones de carga ha aumentado significativamente en la última década. La Figura 1 representa el notable aumento de las estaciones de carga en Europa durante los últimos ocho años. La integración de esta nueva infraestructura en los sistemas de distribución tiene desafíos económicos, políticos, regulatorios y técnicos que deben ser abordados [1]. Por otro lado, surgen nuevos agentes, y la comunicación entre ellos y los existentes es crucial para alcanzar la operación óptima del sistema [2].

Algunos estudios han explorado como afectará en el futuro la demanda de VEs a las redes eléctricas. Estos informes estiman que la demanda de VEs presentará una pequeña porción de la demanda total del sistema. El trabajo en [4] estima que sólo el 5 % del consumo total de electricidad estará relacionado con la demanda energética de VEs en el año 2040. Del mismo modo, un estudio reciente realizado por McKinsey [5] afirma que los VEs no impulsarán un
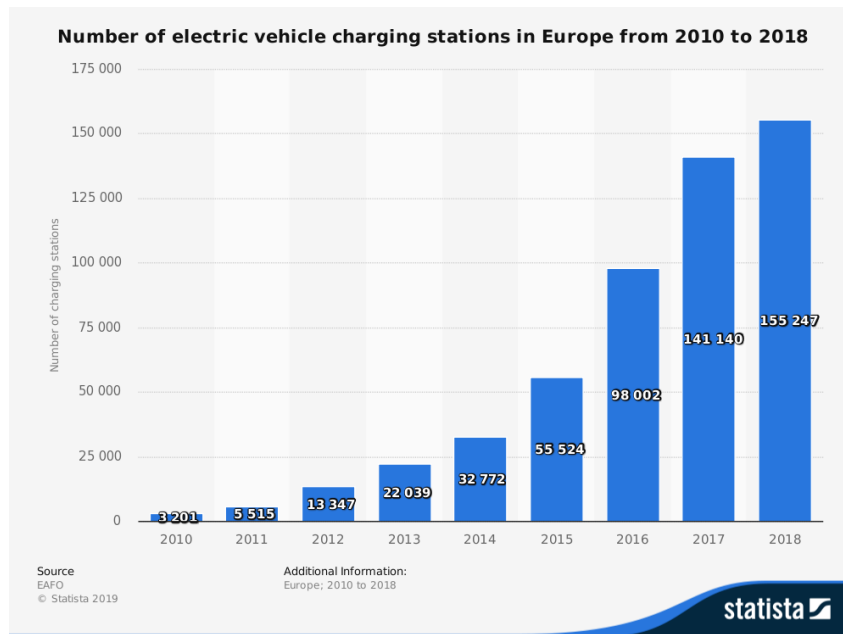
**Figura 1.** Evolución del número de estaciones de carga en Europa en los últimos 8 años [3].

aumento sustancial de la demanda total de electricidad. Utilizando información de Alemania, prevén que la demanda de VEs rondará el 5 % de la demanda total en 2050 en Alemania. Aunque la demanda de VEs no aumentará notablemente la demanda de energía total, alterará los perfiles de potencia demandada, y más especificamente en áreas urbanas y suburbanas, en dónde los ratios de adopción de VEs son más altos. De acuerdo con [6], la demanda total de carga de VEs puede presentar alrededor de un 18 % del pico de verano con un nivel de penetración del 30 %.

Los operadores de la red tienen la responsabilidad de garantizar el funcionamiento y la estabilidad de la misma. Sin embargo, se ha demostrado que la carga masiva descontrolada de VEs aumenta sustancialmente las congestiones en las lineas, las pérdidas totales del sistema y las variaciones de tensiones [7]. Una solución costosa y poco óptima sería aumentar la capacidad del sistema. Alternativamente, el control y planificación de la demanda flexible de VEs ha sido demostrado ser beneficioso para la operación de la red [8].

## Metodología

La planificación y gestión de la demanda de las estaciones de carga puede entenderse como un problema de Flujo Óptimo de Potencia (OPF), con algunos objetivos y limitaciones del sistema, en donde el objetivo principal es minimizar el impacto de la carga sobre el funcionamiento de la red. Para ello, se necesitan recursos de optimización que garanticen el funcionamiento óptimo del sistema. Sin embargo, las ecuaciones de flujo de carga (PF) no son lineales ni convexas, y la resolución del problema de optimización, incluyendo las restricciones de la red, es bastante complicada. En el caso de las redes de transmisión, el modelo DC-PF linealizado es una buena aproximación debido a la pequeña relación R/X. Sin embargo, en las redes de distribución, la relación R/X es mayor, y por lo tanto, esta aproximación conduce a errores significativos.

En primer lugar, este trabajo presenta un estado del arte sobre las estaciones de carga en redes eléctricas, incluyendo: un análisis de algunos controles propuestos en la literatura (e.g. IEEE, Elsevier) para estaciones de carga de VEs, un estudio de la arquitectura de comunicación y los agentes integrantes del proceso de carga y un resumen de diferentes modelos de flujo de potencia

aplicables al control de demanda. Teniendo en cuenta lo anterior, se propone una arquitectura de control basada en un MPC de dos niveles para planificar la demanda de VEs dentro de una red de distribución.

En segundo lugar, se presentan tres problemas de optimización con diferentes modelos de flujo de potencia (DCPF, LACPF y c-BFM). Cada problema incluye un modelo agregador de VEs y las restricciones de la red eléctrica (e.g. tensiones, límites térmicos de la línea y límites técnicos de potencia del transformador). El modelo de optimización con el c-BFM ha demostrado ser el modelo adecuado para el propósito de este trabajo en términos de precisión.

En tercer lugar, los escenarios para demostrar la validez del algoritmo propuesto se forman con dos herramientas desarrolladas en este proyecto: una que produce perfiles de generación y demanda y otra que define el comportamiento de carga de los VEs. La primera genera perfiles de potencia de acuerdo a distintos tipos de carga (e.g. doméstica, comercial, industrial, de oficina, escolar) y a distintas tecnologías de generación (e.g. eólica, fotovoltaica). La segunda herramienta crea una población heterogénea de VEs con dos comportamientos de carga diferentes, es decir, carga diurna y nocturna. Los perfiles de demanda, generación y demanda de VEs se distribuyen de acuerdo a la topología de red, que se obtiene de la biblioteca de MATPOWER [9].

Finalmente, el rendimiento del algoritmo se analiza en dos redes radiales de distribución (18-bus IEEE y 141-bus IEEE) y para dos niveles de penetración de VEs distintos: baja demanda de EV (alrededor del 30 % de penetración y del 4 - 6 % de la demanda total del sistema) y alta demanda de EV (100 % de penetración y del 13 - 15 % de la demanda total del sistema). Nótese que el porcentaje de penetración representa el percentaje de casas que poseen un VE.

El algoritmo de control está implementado en MATLAB y formulado con la libreria YALMIP [10]. Gurobi [11] es utilizado para resolver el problema SOCP de optimización. Los resultados se han obtenido con un PC Intel(R) Core(TM) i7-7500, 2.7 GHz CPU 8 GB RAM.

## Resultados

La Tabla 1 presenta la notable reducción de pérdidas del sistema en el caso de carga coordinada comparado con el supuesto no coordinado, en el que los VEs comienzan a cargar a potencia nominal una vez conectados.

| Pérdidas totales (MWh) | | No Coordinado | Coordinado | Reducción de pérdidas |
|---|---|---|---|---|
| **Baja demanda de VEs** | 18 IEEE | 3,58 | 3,37 | 6 % |
| | 141 IEEE | 7,08 | 6,48 | 9 % |
| **Alta demanda de VEs** | 18 IEEE | 4,96 | 4,16 | 16 % |
| | 141 IEEE | 10,22 | 8,06 | 21 % |

**Tabla 1.** Perdidas totales (MWh) para cada red y cada supuesto de demanda.

El control propuesto en este trabajo considera el estado de la red, mientras que el supuesto no coordinado no lo hace. La Tabla 2 proporciona el número de violaciones de las restricciones térmicas de las lineas para el supuesto no coordinado durante el horizonte de simulación fijado (un día y medio).

---

| Violación de restricción | | Nr. |
|---|---|---|
| **Baja demanda de VEs** | 18 IEEE | 6 |
| | 141 IEEE | 209 |
| **Alta demanda de VEs** | 18 IEEE | 157 |
| | 141 IEEE | 2584 |

**Tabla 2.** Número de veces que se sobrepasa un límite térmico de alguna línea.

Dado que el algoritmo tiene como objetivo minimizar las pérdidas, los VEs se cargarán cuando las líneas estén en los niveles de corriente más bajos, reduciendo así, la variabilidad de la corriente de la línea. De acuerdo con la ley de Ohm, una disminución en la variabilidad del flujo de corriente de línea conduce a una disminución en la variabilidad de la tensiones. Entonces, el algoritmo tiende a cargar los VEs en los períodos cuando las tensiones son más altas y evita la carga en sus valores mínimos. Este efecto se representa en la Figura 2. Además, el algoritmo tiende a asignar la demanda de VEs evitando incrementar los picos de demanda del sistema como se muestra en la Figura 3. Por lo tanto, este algoritmo contribuye positivamente a la calidad del suministro.
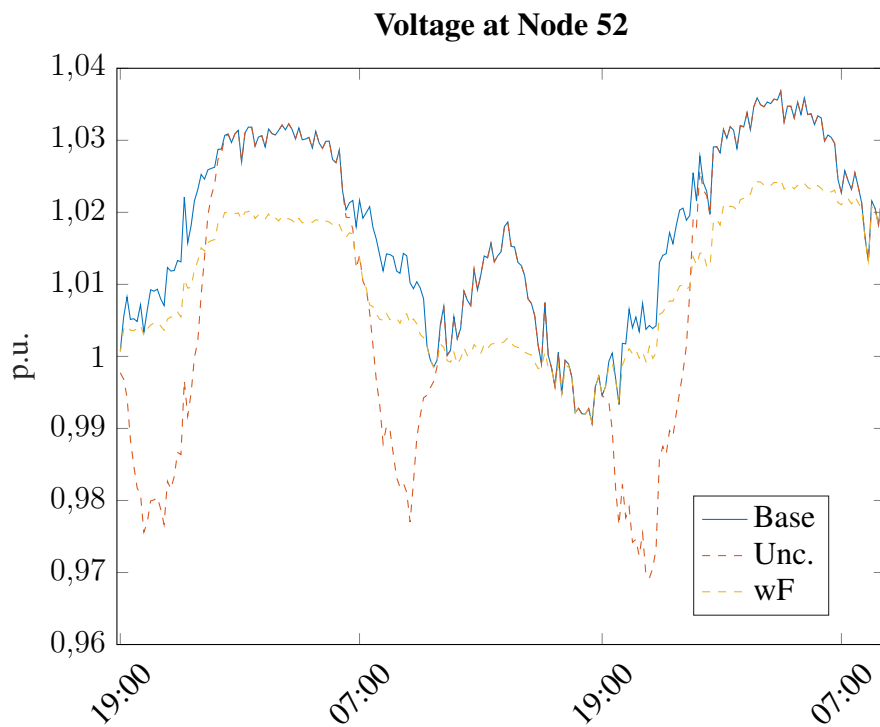


**Figura 2.** 141-bus IEEE High EV demand case - Voltage profile of node 52.

Finalmente, los tiempos medios y máximos para cada escenario y caso se presenta en la Tabla 3. La carga computacional es aceptable para el tiempo de respuesta esperado de 10 minutos.
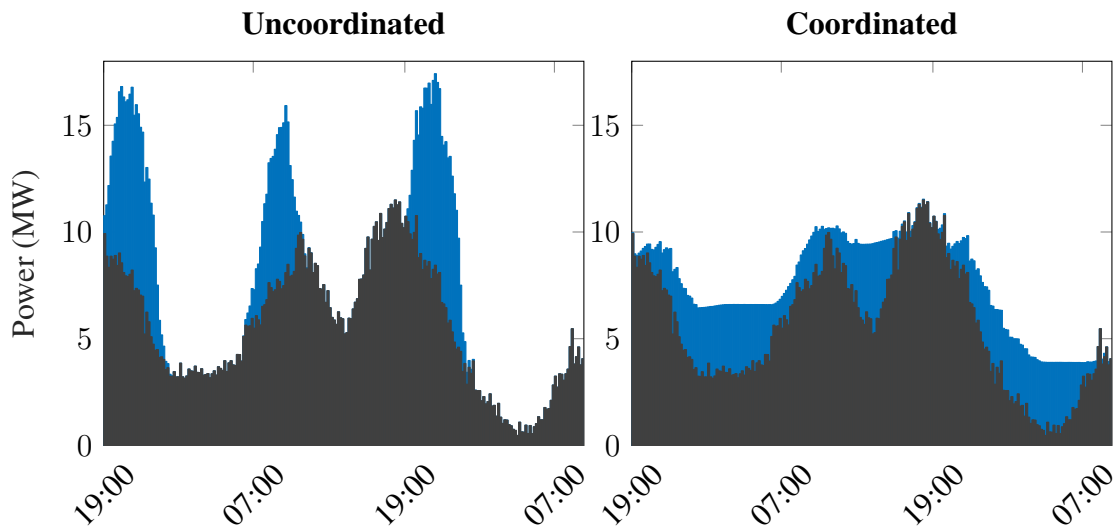
**Uncoordinated** **Coordinated**



**Figura 3.** 141-bus IEEE Alta demanda de VEs - Demanda total del sistema (kW).

| Carga Computacional (s) | | Media | Máxima |
|---|---|---|---|
| **Baja demanda de VEs** | 18 IEEE | 0,25 | 0,43 |
| | 141 IEEE | 14,91 | 23,54 |
| **Alta demanda de VEs** | 18 IEEE | 0,35 | 0,64 |
| | 141 IEEE | 20,37 | 26,70 |

**Tabla 3.** Carga computacional media y máxima (segundos).

## Conclusiones

En definitiva, este proyecto ha contribuido a desarrollar un algoritmo de control para la gestión de estaciones de carga de VEs en redes de distribución, teniendo en cuenta el estado actual y futuro del sistema. Más concretamente, se ha desarrollado un modelo agregador de demanda de VEs, un modelo de optimización SOCP que incluye ecuaciones de flujo de potencia y las herramientas para validar el rendimiento del control. El algoritmo resultante mitiga el impacto de las estaciones de carga sobre la red eléctrica de distribución al evitar congestiones y reducir las pérdidas totales del sistema y, por lo tanto, los gastos de operación totales.

## Referencias

[1] T. G. San Román, I. Momber, M. R. Abbad, and Á. Sánchez Miralles, Regulatory framework and business models for charging plug-in electric vehicles: Infrastructure, agents, and commercial relationships, Energy Policy, vol. 39, no. 10, pp. 6360-6375, 2011.

[2] Carlos Montes Portela,Paul Klapwijk, Lennart Verheijen,Hans de Boer,Han Slootweg,Marko Van Eekelen, Oscp - an open protocol for smart charging of electric vehicles, CIRED 23rd International Conference on Electricity Distribution, no. 15-18, pp. 1-5, June 2015.

[3] Statista, Europe: number of electric vehicle charging stations 2018 statistic.

[4] Fereidoon Sioshansi, The impact of electric vehicles on electricity demand - energy post, November 2018.

[5] Hauke Engel,Russell Hensley,Stefan Knupfer,Shivika Sahdev, The potential impact of electric vehicles on global energy systems, August 2018.

[6] Z. Ma, D. S. Callaway, and I. A. Hiskens, Decentralized charging control of large populations of plug-in electric vehicles, IEEE Transactions on Control Systems Technology, vol. 21, no. 1, pp. 67-78, 2013.

[7] A. Bosovic, M. Music, and S. Sadovic, Analysis of the impacts of plug-in electric vehicle charging on the part of a real medium voltage distribution network, in IEEE PES Innovative Smart Grid Technologies, Europe, pp. 1-7, IEEE, 12/10/2014 - 15/10/2014.

[8] Ahmed R. Abul'Wafa, Aboul'fotouh El'Garably, and Wael A.Fatah Mohamed, Uncoordinated vs coordinated charging of electric vehicles in distribution systems performance, International Journal of Engineering and Information Systems (IJEAIS), vol. 1, no. 6, pp. 54-65, 2017.

[9] R. D. Zimmerman, C. E. Murillo-Sanchez, and R. J. Thomas, Matpower: Steady-state operations, planning, and analysis tools for power systems research and education, IEEE Transactions on Power Systems, vol. 26, no. 1, pp. 12-19, 2011.

[10] J. Lofberg, Yalmip : A toolbox for modeling and optimization in matlab, In Proceedings of the CACSD Conference, Taipei, Taiwan 2004.

[11] L. L. Gurobi Optimization, Gurobi optimizer reference manual, 2018.

# EVALUATION OF NOVEL ENERGY MANAGEMENT CONCEPTS FOR EV CHARGERS IN FUTURE SMART CITY INFRASTRUCTURE

**Author: Basallote Muñoz, Ignacio**
Supervisor: Bogdanovic, Milica.
Collaborator entity: RWTH Aachen.

## ABSTRACT

One of the challenges of future smart cities is to coordinate Electric Vehicle (EV) charging events to reduce their impact on the electrical system. If not optimally controlled, such demand might lead to grid congestions reshaping the net power profile of distribution systems. Significant power profile variations might imply distribution system resizing, driving to unnecessary capital expenditures. This thesis includes a literature review about the state-of-the-art energy management systems for charging stations. Additionally, a two-level MPC-based control architecture is proposed to allocate the EV demand within a distribution system. The lower control level aggregates the energy demand for all charging stations of the same MV-LV substation. The second level allocates the aggregated EV demand in time while minimizing total system losses and considering the future state of the power system. A set of convex relaxations convexifies the power flow (PF) equations. Thus, the global optimum can be easily achieved for radial topologies. Finally, the performance of the proposed algorithm with different IEEE grid topologies and for distinct levels of EV penetration is analyzed.

**Keywords:** Energy Management Systems (EMS), Smart Grid, Smart City, EV-chargers.

## Introduction

The number of charging stations has increased significantly in the last decade. Figure 1 represents the remarkable increase in charging stations in Europe during the previous eight years. The integration of this new infrastructure on distribution systems has economic, policy, regulatory, and technical challenges that must be addressed [1]. New agents emerge in the electricity sector, and the communication between them and the existing ones is crucial to reach optimal distribution network operation [2].

Some studies have explored the potential impacts of Electric Vehicles (EVs) on power grids. These reports estimate that the percentage of EV demand will present a small portion of the overall system demand. The work in [4] states that only 5% of projected global electricity consumption will be related to EVs by 2040. Similarly, a recent study performed by McKinsey [5] claims that EVs will likely not drive a substantial increase in electricity demand. Using information from Germany, they foresee an EV demand portion of 5% by 2050. Although the EV demand will not create a power-demand crisis, it will reshape the load curve. According

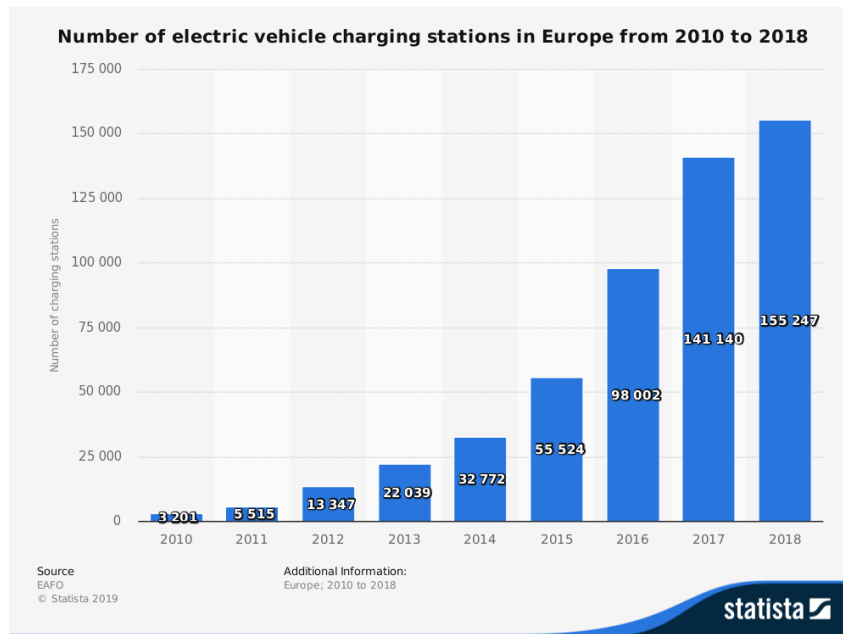**Number of electric vehicle charging stations in Europe from 2010 to 2018**

Figure 1. Increasing number of charging stations in Europe in the last 8 years [3].

to [6], the total charging demand of EVs can contribute nearly 18% of the summer peak at a penetration level of 30%.

Grid operators have the responsibility to guarantee the operation and stability of the grid. However, the massive uncoordinated EV charging schemes have been proved to increase substantially grid congestion, system losses, and voltage variations [7]. One unnecessary expensive and not optimal solution would be to increase the capacity of the system. Alternatively, coordinated charging strategies have been proved to be beneficial for grid operation [8].

## Methodology

The charging station demand allocation problem can be understood as an Optimal Power Flow (OPF) problem with some objectives and system constraints, where the main goal is to minimize the impact of charging. Optimization resources are required in demand management to ensure an optimal grid operation. Nevertheless, the power flow (PF) model is a non-linear and non-convex problem, and the optimization, including grid constraints, is rather complicated. In the case of transmission grids, the linearised DC-PF model is a good approximation due to the small R/X ratio. However, in distribution grids, the R/X ratio is higher, and therefore, this approximation leads to significant errors.

First, this work presents an state-of-the-art regarding EV-chargers in electrical networks including: an analysis of some EV-charger control trends found in the literature (e.g. IEEE, Elsevier), a review of the communication architecture and the agents of the charging process and a summary of different power flow models applicable for demand side response. Thus, an two-level MPC-based control architecture is proposed to allocate the EV demand within a distribution grid.

Second, three optimization problems with different power flow models (DCPF, LACPF and c-BFM) are presented. Each problem includes both an EV aggregate model and the electrical network constraints (e.g. voltages, line thermal limits and transformer power bounds). The

---

optimization model with the c-BFM is proved to be the suitable model for the purpose of this work in terms of accuracy.

Third, the scenarios for proving the validity of the proposed algorithm are formed with two tools: one produces generation and load dynamics and other defines EVs charging behaviour. The first one generates power dynamics according to distinct types of load (e.g. household, commercial, industrial, office, school) and generation resources (e.g. wind and PV). The second creates a heterogeneous population of EVs with two different charging behaviours, i.e., day and night charging. The load, generation and EV demand profiles are distributed according to the grid topology, which is obtained from the MATPOWER library [9].

Finally, the algorithm performance is analyzed in two grid topologies (18-bus IEEE and 141-bus IEEE) and for two distinct EV penetration levels: low EV demand (around 30% penetration and 4 - 6% of overall system demand) and high EV demand (100% penetration and 13 - 15% of overall system demand). Note that the percentage of penetration represents the portion of households that own an EV.

The control algorithm is implemented in MATLAB and formulated with the YALMIP toolbox [10]. Gurobi [11] is used to solve the SOCP problem. The optimization was performed on a PC with an Intel(R) Core(TM) i7-7500, 2.7 GHz CPU 8 GB RAM.

## Results

Table 1 presents the noteworthy system loss reduction in the optimal scheduling case compared to the uncoordinated scheme, in which EVs charge at nominal charging rate once they are connected.

| Total System Losses (MWh) | | Uncoordinated | Coordinated | Loss Reduction |
|---|---|---|---|---|
| **Low EV Demand** | 18 IEEE | 3,58 | 3,37 | 6% |
| | 141 IEEE | 7,08 | 6,48 | 9% |
| **High EV Demand** | 18 IEEE | 4,96 | 4,16 | 16% |
| | 141 IEEE | 10,22 | 8,06 | 21% |

**Table 1.** Total system losses (MWh) for each grid topology and EV demand case (the percentage presents the portion of EV demand compared to the overall system energy demand).

Moreover, the coordinated scheme proposed in this work considers the network state, whereas the uncoordinated scheme does not. Table 2 provides the number of thermal line constraint violations for the uncoordinated scheme during the simulation horizon.

Since the algorithm aims at minimizing losses, EVs will charge when the lines are at the lowest current levels reducing the line current variability. According to Ohm's law, a decrease in the line current flow variability leads to a decrease in the voltage variability. Then, the algorithm tends to charge at the periods where the voltage is higher and avoids charging at its minimum values. This effect is depicted in Figure 2. Furthermore, the algorithm tends to allocate the EV demand avoiding to increase the overall system power peaks as depicted in Figure 3. Therefore, this algorithm contributes positively to the system operation.

ABSTRACT

| Constraint violation | | Nr. |
|---|---|---|
| **Low EV Demand** | 18 IEEE | 6 |
| | 141 IEEE | 209 |
| **High EV Demand** | 18 IEEE | 157 |
| | 141 IEEE | 2584 |

**Table 2.** Number of line thermal bound violation for the simulation horizon for each scenario studied.
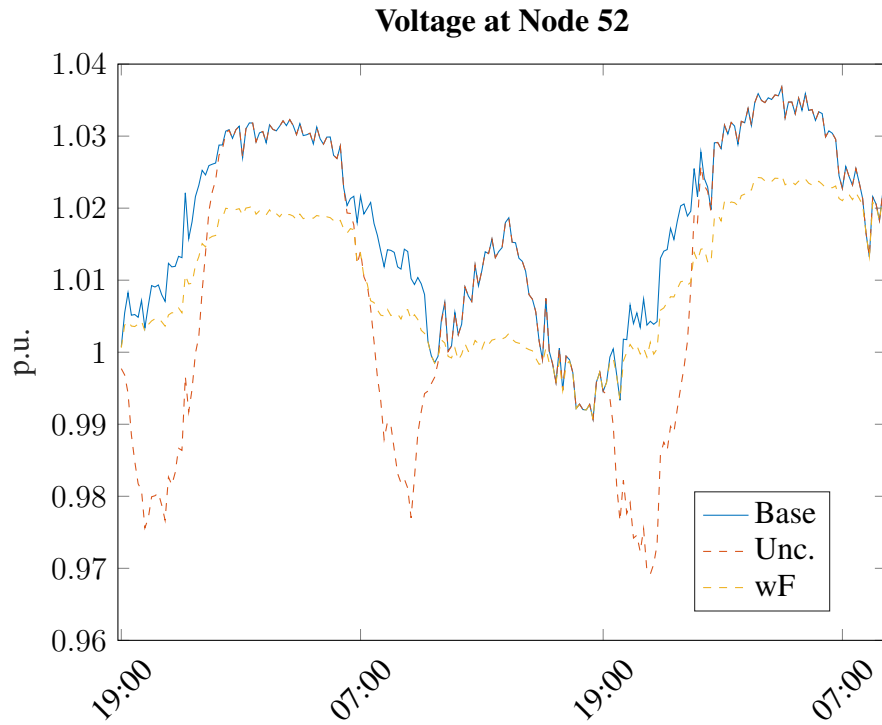


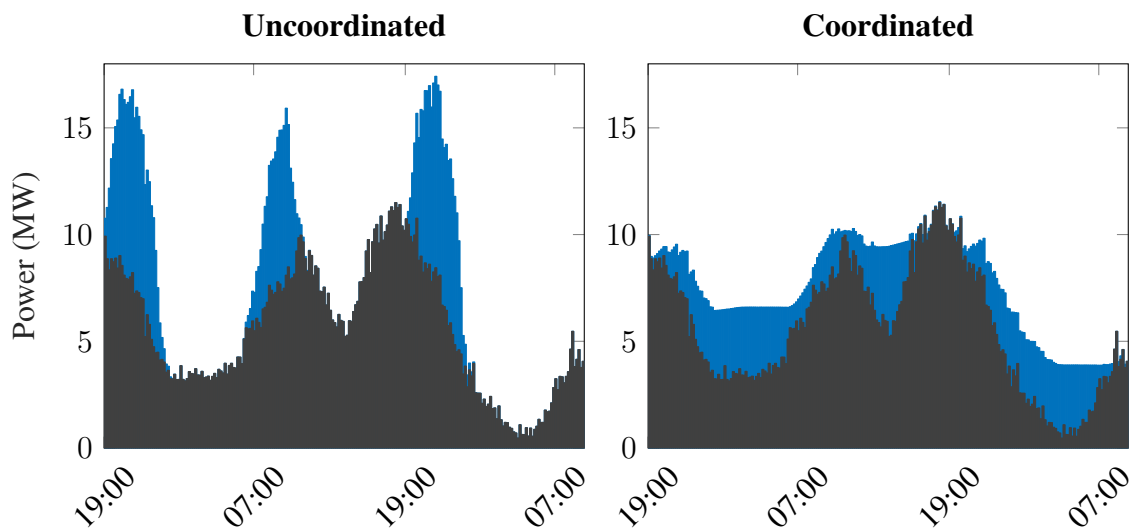**Figure 2.** 141-bus IEEE High EV demand case - Voltage profile of node 52.



**Figure 3.** 141-bus IEEE High EV demand case - Total system demand (kW).

Finally, the time performance for each scenario and case is presented in Table 3. The computational burden is acceptable for the expected time response of 10 minutes.

| Time performance (sec) | | Average | Maximum |
|---|---|---|---|
| **Low EV Demand** | 18 IEEE | 0,25 | 0,43 |
| | 141 IEEE | 14,91 | 23,54 |
| **High EV Demand** | 18 IEEE | 0,35 | 0,64 |
| | 141 IEEE | 20,37 | 26,70 |

**Table 3.** Average and maximum algorithm time burden (seconds).

## Conclusions

To sum up, this thesis has contributed to design a control algorithm for optimal scheduling of EV-chargers in distribution level while considering the present and future electric network state. More precisely, there has been developed an EV aggregate model, an SOCP optimization model including power flow equations and the tools for validating the control performance. The resulting algorithm mitigates EV chargers impact on an electrical network by avoiding system congestions and reducing the overall system losses and hence, the total operational expenses.

## References

[1] T. G. San Román, I. Momber, M. R. Abbad, and Á. Sánchez Miralles, Regulatory framework and business models for charging plug-in electric vehicles: Infrastructure, agents, and commercial relationships, Energy Policy, vol. 39, no. 10, pp. 6360-6375, 2011.

[2] Carlos Montes Portela, Paul Klapwijk, Lennart Verheijen, Hans de Boer, Han Slootweg, Marko Van Eekelen, Oscp - an open protocol for smart charging of electric vehicles, CIRED 23rd International Conference on Electricity Distribution, no. 15-18, pp. 1-5, June 2015.

[3] Statista, Europe: number of electric vehicle charging stations 2018 statistic.

[4] Fereidoon Sioshansi, The impact of electric vehicles on electricity demand - energy post, November 2018.

[5] Hauke Engel, Russell Hensley, Stefan Knupfer, Shivika Sahdev, The potential impact of electric vehicles on global energy systems, August 2018.

[6] Z. Ma, D. S. Callaway, and I. A. Hiskens, Decentralized charging control of large populations of plug-in electric vehicles, IEEE Transactions on Control Systems Technology, vol. 21, no. 1, pp. 67-78, 2013.

[7] A. Bosovic, M. Music, and S. Sadovic, Analysis of the impacts of plug-in electric vehicle charging on the part of a real medium voltage distribution network, in IEEE PES Innovative Smart Grid Technologies, Europe, pp. 1-7, IEEE, 12/10/2014 - 15/10/2014.

[8] Ahmed R. Abul'Wafa, Aboul'fotouh El'Garably, and Wael A.Fatah Mohamed, Uncoordinated vs coordinated charging of electric vehicles in distribution systems performance, International Journal of Engineering and Information Systems (IJEAIS), vol. 1, no. 6, pp. 54-65, 2017.

[9] R. D. Zimmerman, C. E. Murillo-Sanchez, and R. J. Thomas, Matpower: Steady-state operations, planning, and analysis tools for power systems research and education, IEEE Transactions on Power Systems, vol. 26, no. 1, pp. 12-19, 2011.

[10] J. Lofberg, Yalmip : A toolbox for modeling and optimization in matlab, In Proceedings of the CACSD Conference, Taipei, Taiwan 2004.

[11] L. L. Gurobi Optimization, Gurobi optimizer reference manual, 2018.

# DOCUMENT I

—

# REPORT

# Index

# List of Abbreviations

| | |
|---|---|
| *BSS* | Batery Storage System |
| *BFM* | Branch Flow Model |
| *BIM* | Bus Injection Model |
| *c-BFM* | Convexified Branch Flow Model |
| *CSO* | Charging Station Operator |
| *DCPF* | DC Power Flow |
| *DER* | Distributed Energy Resources |
| *DSO* | Distribution System Operator |
| *EMS* | Energy Management System |
| *ESS* | Energy Storage System |
| *EV* | Electric Vehicle |
| *EVSE* | Electric Vehicle Supply Equipment |
| *QP* | Quadratic Programming |
| *QCQP* | Quadratically Constrained Quadratic Programming |
| *LACPF* | Linearized AC Power Flow |
| *MISOCP* | Mixed-Interger Second Order Cone Programming |
| *MPC* | Model Predictive Control |
| *MV-LV* | Medium Voltage - Low voltage |
| *OPF* | Optimal Power Flow |
| *PHEV* | Plug-in Hybrid Electric Vehicle |
| *PV* | Photovoltaic System |
| *SOC* | State of Charge |
| *SOCP* | Second Order Cone Programming |
| *V2G* | Vehicle-to-Grid |

# Chapter 1

# Introduction

## 1.1 Motivation

The number of charging stations has increased significantly in the last decade. Figure 1 represents the remarkable increase in charging stations in Europe during the previous eight years. The integration of this new infrastructure on distribution systems has economic, policy, regulatory, and technical challenges that must be addressed [1]. New agents emerge in the electricity sector, and the communication between them and the existing ones is crucial to reach optimal distribution network operation [2].
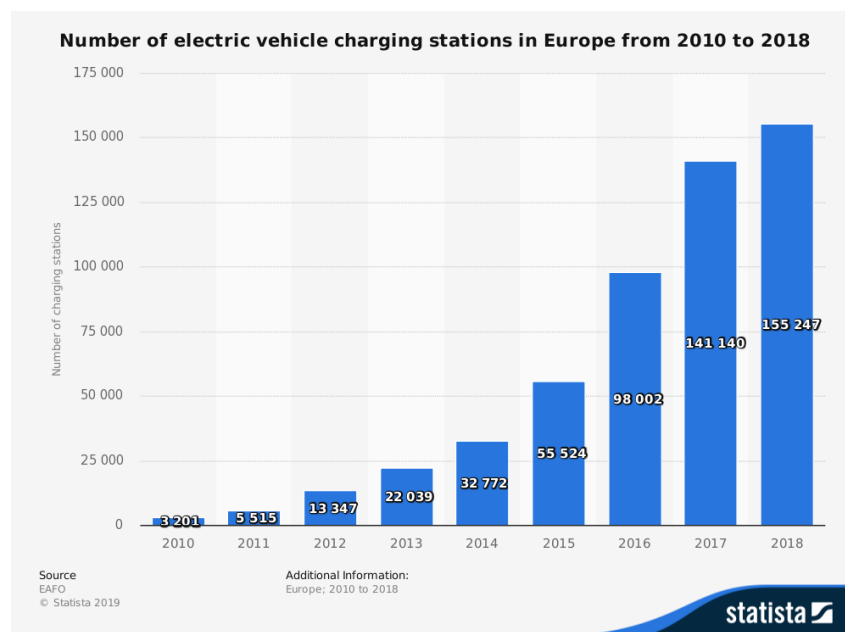


**Figure 1.** Increasing number of charging stations in Europe in the last 8 years [3].

In Europe, the average daily driving distance in 6 member states ranges from an average of 40 km (UK) to an average of 80 km (Poland) [12]. According to the same survey, parking times can be split into two parts. One part can be named "active parking" (e.g., a car parked after a trip

for making an activity: working, shopping). The other one is titled "inactive parking" (e.g., car parked after the last journey of the day). The average active parking time from Monday to Friday in all European countries is around 6 hours per day. On the other hand, the average inactive parking amounts to more than 16 hours per day. These parking durations present attractive charging flexibility that can avoid detrimental power system impacts and minimize operational system costs.

Some studies have explored the potential impacts of Electric Vehicles (EVs) on power grids. These reports estimate that the percentage of EV demand will present a small portion of the overall system demand. The work in [4] states that only 5% of projected global electricity consumption will be related to EVs by 2040. Similarly, a recent study performed by McKinsey [5] claims that EVs will likely not drive a substantial increase in electricity demand. Using information from Germany, they foresee an EV demand portion of 5% by 2050. Although the EV demand will not create a power-demand crisis, it will reshape the load curve. According to [6], the total charging demand of EVs can contribute nearly 18% of the summer peak at a penetration level of 30%.

Grid operators have the responsibility to guarantee the operation and stability of the grid. However, the massive uncoordinated EV charging schemes have been proved to increase substantially grid congestion, system losses, and voltage variations [7]. One unnecessary expensive and not optimal solution would be to increase the capacity of the system. Alternatively, coordinated charging strategies have been proved to be beneficial for grid operation [8].

Most of the literature proposals explore the optimal charging methods for a single station or an aggregation of several charging points, but without considering the interaction of multiple charging stations [13]. Note that for one charging station might be more than one charging point. In these schemes, the charging station is controlled to reach different goals, such as cost minimization or reduction of distributed generation fluctuations. However, they neglect the electrical grid model and hence, a possible system infeasibility might occur.

The charging station demand allocation problem can be understood as an Optimal Power Flow (OPF) with some objectives and system constraints, where the main goal is to minimize the impact of charging. Optimization resources are required in demand management to ensure an optimal grid operation. Nevertheless, the power flow (PF) model is a non-linear and non-convex problem, and the optimization, including grid constraints, is rather complicated. In the case of transmission grids, the linearised DC-PF model is a good approximation due to the small R/X ratio. However, in distribution grids, the R/X ratio is higher, and therefore, this approximation leads to significant errors.

This work studies the different control approaches that have been proposed in the literature recently, the communication interfaces necessary to perform optimal charging station control, a review of the optimal power flow models applied to demand side response and then, according to the previous analysis, proposes an Energy Management System (EMS) for charging stations on a

distribution level. The EMS aims at managing charging stations to avoid system congestions while reducing total system losses.

## 1.2  Thesis Objectives

The main goal of this thesis is to develop a centralized EMS to optimally control EV chargers in a distribution grid at real time. The algorithm can be applied to any radial network. The inputs are the generation and demand forecasts as well as the EV energy demand. The control optimizes for a given time horizon with a constant time step that can be adjusted accordingly to user requirements. The outcome of this thesis is the analysis and comparison of the algorithm performance with an uncoordinated scheme. Some future work is proposed at the end of this work too.

## 1.3  Structure of the Thesis

This thesis is structured as follows: Chapter 2 consists of a literature review about EMS for EV chargers, required interfaces between the grid and charging infrastructure and the control architecture proposal. A theoretical background regarding three different power flow approaches is included in Chapter 3. Chapter 4 presents the development and implementation of the optimal control algorithm. The scenario analysis and evaluation of results are introduced in Chapter 5. Last but not least, Chapter 6 concludes this thesis, and Chapter 7 exhibits future work.

# Chapter 2

# Literature Review

## 2.1 State of the Art

This section presents a literature review of the most crucial issues regarding EV chargers. First, some different concepts of EMSs for EVs are summarized. Second, a brief introduction of the state-of-the-art EV charging communication protocols is addressed. Last but not least, a review of some distinct PF models applied to demand side response is introduced. Most of the documents of this literature review belong to the ScienceDirect and IEEE Xplore Digital Libraries. Some of the keywords used in the search were: smart city, smart grid, charging infrastructures, optimal charging strategies, energy management for EVs, energy management with grid constraints, optimal grid operation, EV line congestion, Model Predictive Control (MPC) and V2G.

### 2.1.1 Energy Management Systems for Charging Stations

Lately in the literature, one can find three distinct smart grid control trends: *centralised*, *decentralised* and *distributed* control approaches. In the first scheme, the application of optimization algorithms seems to be easier since all the information is assumed available at the same point. Additionally, one can achieve the global optimum easily, but the data size can be enormous for large systems and even more if the model requires realistic forecasts about the behavior of all the entities that take part in the system. In practice, this information is difficult to know exactly in advance and can lead to a considerable error, shifting the solution to one less optimal [14]. On the other hand, the decentralized and distributed approaches are far less computationally intensive compared to the centralized. Furthermore, the privacy problem is mitigated since the information is processed locally, and in case of a system size change, this scheme does not require changes in the control program. The main difference between decentralized and distribution is the lack of communication in the first control strategy. Then, the decentralized approach is not an optimal control scheme where interaction between assets

is crucial for optimal operation of a system. However, in the distributed control, the assets can communicate between them to search for the optimal operation of the system. Moreover, there is the possibility of setting different local goals, which in the centralized scheme is not possible. Nevertheless, the solution obtained might not be the global optimum, and depends strongly on the communication order between entities [15].

The literature trends regarding optimal charging station management focus on different levels. One consists of a low stage or microgrid, in which grid constraints are not considered. The other one considers the system state (e.g., voltages, line flows) and can be classified depending on the grid layer (e.g., transmission, distribution, low voltage). Furthermore, researchers have shown particular interest about the optimal control of different system technologies, such as Distributed Energy Resources (DER), charging stations or thermal storage, rather than a specific algorithm for EV chargers. Tailored control strategies for charging stations are frequent at lower levels and, in some cases, without the need for optimization resources. However, the global optimal may not be reached, and for that reason, new trends arise to investigate control schemes that enable optimum system operation.

For instance, the proposal in [16] is an example of a control system without forecasting and optimization resources. Authors investigate optimal operation strategy of a commercial building, which is modeled as a microgrid with photovoltaic systems (PV) and EV charging stations (EVSE). The main objective of the model is to reduce power deviations between PV generation and EV load while serving the maximal EV energy demand possible. It introduces the concept of Feasible Charging Region (FCR), which guarantees that from arrival until departure every EV charges at minimum charging rate to reach the desired SOC. The EVs which leave sooner charge with higher rates than the other that remain longer times at the system. Once a vehicle arrives, it charges if the system constraints are not active. Although it is not a purely coordinated charging scheme, the power demand is always the minimum necessary to fulfill EV driver expectations. One advantage of the model is the reduced computational burden. The control manages EV charging events without demand and generation forecasts to save computational time. However, this approach cannot ensure the best operation of the system, and the control strategy is limited to a local level, since it does not include grid constraints. Nevertheless, this control scheme can be well complemented with an upper control level which optimizes grid operation for a determined time horizon.

Another different approach for a higher level is the one presented in [17]. The proposal consists of two level-control for a hybrid system: one centralized control and two local controls (one per microgrid). The DC system is coupled to the upper grid through an AC/DC converter. The main goal of the algorithm is to reduce local load fluctuations combining EVSE, Energy Storages Systems (ESS), and PV. The centralized controller manages the power taken from the grid and sets the power references for all local controllers. Each local control manages the components of the local system (converters of PV and ESS) to keep the power demand constant and equal to

the reference value. Something interesting of this approach is the two level-control architecture, which saves computation efforts on the centralized level and leaves room for flexibility at the local level. However, this approach is limited to DC feeders, and the line thermal boundaries are not considered. Additionally, the control scheme operates at real-time without considering the future state of the system. Therefore, the charging control strategy is uncoordinated, and it focuses on local load fluctuation minimization instead of optimal charging station operation. In Figure 2, the structure of the control scheme is presented.
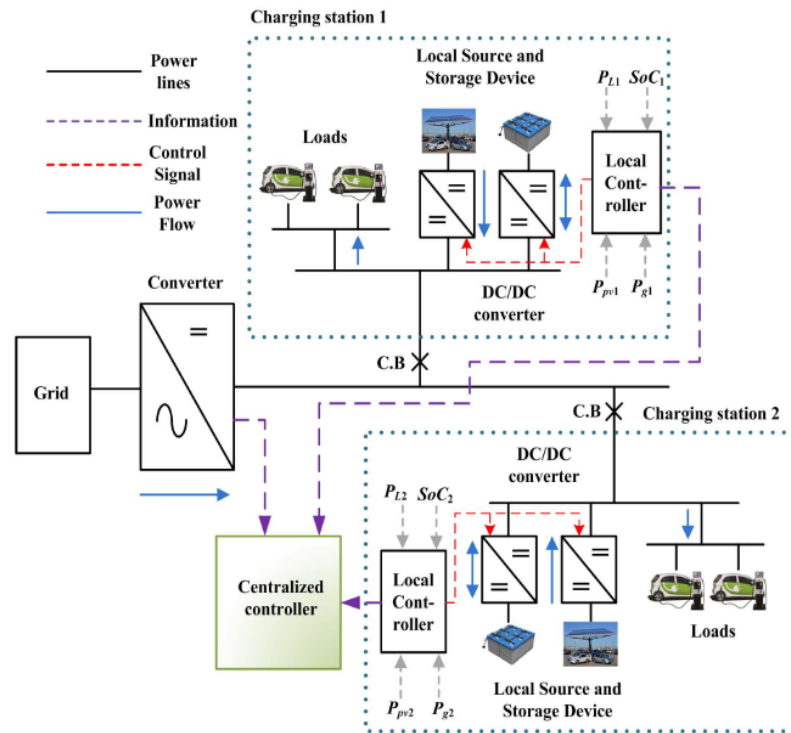


**Figure 2.** Control scheme proposed in [17].

The control strategy in [18] proposes a real-time coordinated scheme for EVSE complemented with DER and ESS at microgrid level. According to Figure 3, the system topology is a DC bus connected to a local grid with an AC/DC converter. All the technologies in the DC bus are interfaced to the Control Center (EMS) with a communication line. This approach consists of a multi-objective optimization with three components: the first one to minimize the total purchase costs from the local grid, the second one to minimize the power deviations between EVSE and RES and the third one to minimize the ESS utilization to prolong the lifetime of the batteries. Moreover, the optimization attempts to minimize the objective function in a predefined time horizon. All the EVs are grouped as a single charging station since the aggregation of EV is an effective way to reduce large computations. Thus, the algorithm considers only one entity (EVSE) during the optimization, which reduces the dimension of the problem, since it is not related to the number of EV connected to the system. Therefore, the resulting charging power is divided into all the EVs that are willing to charge. The EVSE, accordingly to the energy demanded by all EVs, generates two minimum and maximum accumulative energy demand

curves. The minimal limit ensures that user expectations are fulfilled at the end of the time horizon. The maximal bound guarantees that the supplied energy has been provided within the technical limits (regarding the size of the battery and maximal charging power rate). The real accumulative supplied energy curve stays between these two bounds. In other words, the charging power is high enough to meet energy demand expectations, but it never exceeds the maximal EVs' charging power or inject more energy in the EVs' batteries once they are full. Authors test the algorithm with generation forecasts and a real vehicle arrival profile from a university campus with an energy consumption normally distributed. They compare the results to the ones of an uncoordinated charging scheme, and they show an increase in the RES utilization factor as well as a decrease in the peak power from the local grid. Again like in other papers, the control is limited to a local level only for one charging station neglecting distribution grid constraints.
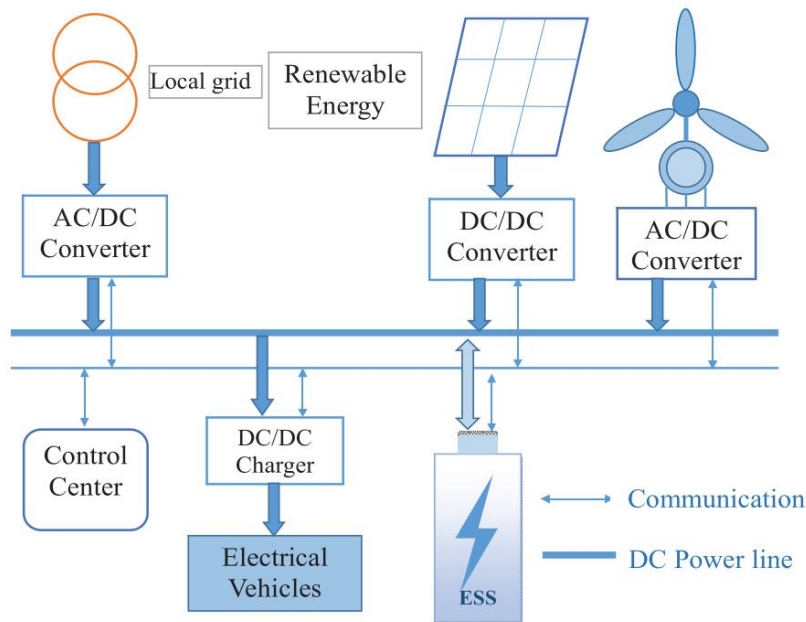


**Figure 3.** System topology in [18].

In [19], a coordinated approach considering V2G is proposed. The main objective of the EMS is the total operation cost minimization while EVs providing frequency regulation. In this case, the EVs are used to compensate power fluctuations due to wind generation, but it focuses again on a microgrid level without grid constraints (only power balance constraint). This approach includes an EV demand model to estimate charging behaviors. The model defines 5 main states: EV user needs to charge at maximal rate, EV user flexible charging, EV user providing V2G, EV user at idle mode, and EV user at driving mode. The state of the EV user is updated at every time step. However, the approach considers only the home charging scenario (charging during the night) neglecting work charging schemes (charging during the day). Alternatively, authors in [20] analyze the impact of V2G in distributed generation systems and the deployment of an EV as a reactive compensator. It can be concluded from their work, that the V2G operation reduces

grid congestion and increases the load factor (smaller load peaks). However, the control scheme does not consider optimization techniques, and hence, it cannot ensure optimal system operation nor EV coordinated charging. Figure 4 represents the system topology in [20]. Even though V2G seems to be a potential EV use, it is not covered by regulations in many countries yet. Furthermore, load stabilization or battery degradation due to excessive cycling are two important drawbacks that might hinder its large scale implementation in the next years [21]. Therefore, it will not be considered in this work.



**Figure 4.** System topology proposed in [20].

An assessment of EV-parking lots effect on congestion management and system reliability is introduced in [22]. This paper analyses the impact of EV charging stations when participating in the electricity market to provide ancillary services (V2G). The chargers behave as distributed generation resources that can leverage electricity prices when congestion occurs. The electricity market model is based on a two-step market clearance method. In the first step, the Independent System Operator runs a market optimization neglecting technical constraints with all generators' participation schedules. This market optimization aims at maximizing social welfare while considering system reliability in the form of a risk cost, which is calculated with the Loss of Load Probability (LOLP). Once the optimal generation planning is calculated, the Independent System Operator informs the generator units and consumers. Then, the Independent System Operator checks whether the transmission lines' bounds are violated. If there is a constraint violation, the Independent System Operator runs a second level optimization minimizing generator re-dispatch cost (congestion cost) including line constraints (DCPF). In this re-dispatch level, the authors include the ancillary services of EV chargers to obtain the optimal schedule. The results show that the participation of EV-parking lots in the electricity market reduce congestion costs and improve system reliability. This approach is limited to a transmission level with a low resistance-reactant ratio (R/X), which is not the case in distribution systems.

The EMS system in [23] controls Plug-in Hybrid Electric Vehicles (PHEVs) in an unbalanced three-phase system for radial and weakly meshed distribution grids. The author uses the Backward/Forward Sweep algorithm to solve the radial power flow and to check the system state.

If there are some constraint violations, the system operator applies load shedding on PHEVs using the Ant Colony Search (ACS) heuristic optimization approach. This EMS considers grid constraints, such as voltage deviations, thermal limitations, and transformer loading. The algorithm performs shedding by a sensitivity analysis maximizing utility of car owner, which depends on the SOC of the PHEV. The algorithm sheds the PHEVs connected to the node with the lowest utility factor, which is overloading the system. Each node has an EV manager, which aggregates all PHEVs that are connected. A global system PHEV manager controls the nodal EV managers. The architecture is shown in Figure 5. However, this approach consists of a corrective real-time optimization instead of a coordinated preventive scheme. Then, this approach does not ensure the optimal system operation.
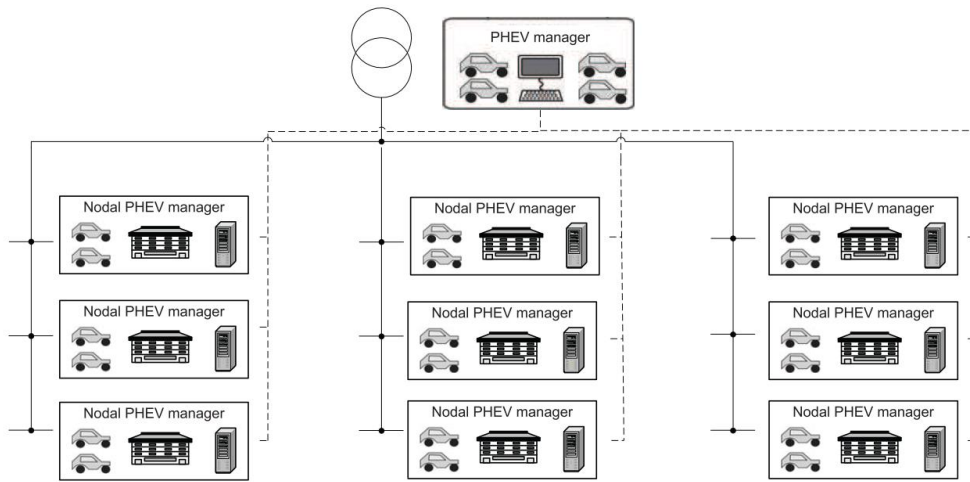


**Figure 5.** System architecture in [23].

The approach in [24] presents a centralized EMS for a three-phase low voltage Smart Polygeneration Microgrid, which has been tested and applied to the study case of the University of Genova Savona Campus. In Figure 6, the electrical grid topology is presented by a set of interconnected nodes at which different generation units and loads are connected. The algorithm processes forecasts and data from SCADA to optimally control all the assets in the microgrid. Some of the elements that compound the system are two different types of battery storage systems (BES), two EV charging stations, and distributed generation sources. The electrical grid is modeled using the DC load flow approach, all voltages are equal and constant to the nominal ones, and a unitary power factor is assumed. The total system losses are approximated as $r \cdot I^2$, where $I \approx P_{line}$. The control scheme is based on a MPC and can generate day-ahead or real-time schedules. The control manages all system components in a way to minimize operation costs and $CO_2$ emissions. However, this algorithm is only applicable for a microgrid level, and the DCPF model has been proved to be insufficient in the analysis of distribution grids [25].
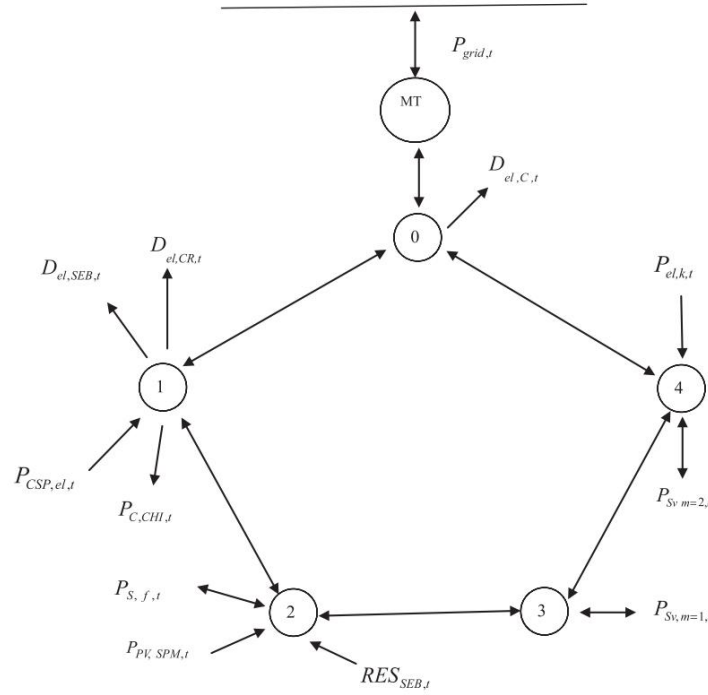
**Figure 6.** Centralized control scheme proposed in [24].

As explained at the beginning of this chapter, another possible trend to approach the problem is the distributed control scheme. The architecture in [13] proposes an on-line distributed MPC-based optimal scheduling for EV charging stations in distribution systems. The MPC is based on the convexified OPF derived in [26]. The main objective is the energy cost minimization while considering the distribution grid and EV charger demand constraints. The distributed problem is formulated as a non-cooperative game in which the converged state is the Nash equilibrium. This state is unique and optimal always on non-heavy loaded radial systems since the convexified PF model exactness conditions are satisfied only if the lines are not heavily loaded. The distributed MPC solves the problem of data privacy and EV uncertainties. However, the algorithm has been only tested on a radial 15-bus IEEE benchmark with a time step of 1 hour, since it is focused on overall monetary cost minimization.

Although it is not directly related to EV, a similar approach like the one implemented in [15] can be mapped to EV chargers. This control scheme proposes a novel decentralized control for electro-thermal heating devices based on a multi-agent system architecture. Each building energy system using an electro-thermal heating device is considered as an agent (see Figure 7). The cluster of agents to be controlled includes all building energy systems in a specific area. The decentralized control consists of a two-layer structure without any centralized resource. The first level generates a pool of possible heating device operation curves according to a local optimization problem. Then, all agents generate schedules for the next 24 hours with a time step of 15 minutes. In the second level, all agents cooperate to serve best, given a system level objective. The agents can communicate with each other. The advantages of the decentralization

compared to the centralized approaches are control robustness, improved data privacy, and reduction of problem complexity. However, the sequence of communication between agents affects the final results, and it may never reach the global optimum of the problem.
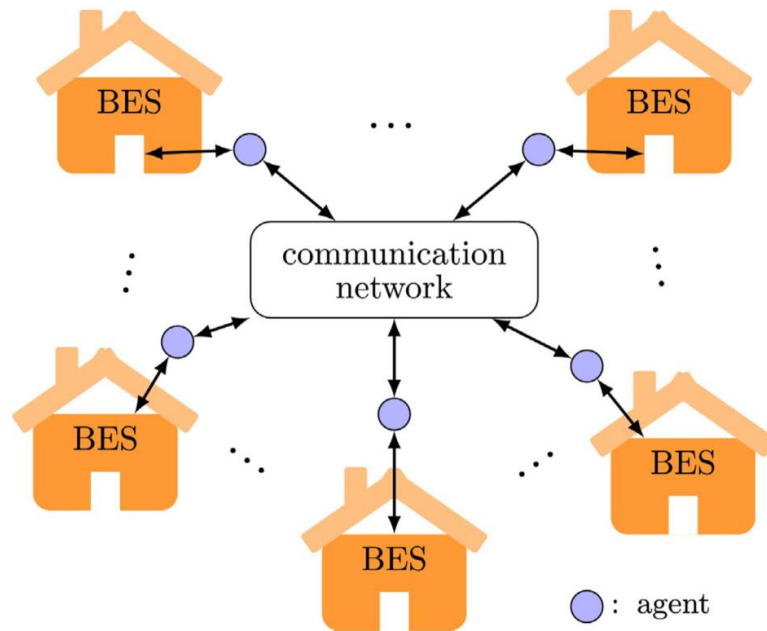


**Figure 7.** System architecture in [15].

Last but not least, the Table 1 shows a summary of all approaches introduced in this Section. The Table provides information regarding the publication year, the main objectives of the control scheme, inclusion of grid constraints, level of applicability, and type of control. Additionally, other schemes that have not been addressed are included, since they are also interesting and related to the control of EV chargers.

| Ref. | Year | Objectives | Grid Constraints | System Level | Control Type |
|------|------|------------|------------------|--------------|--------------|
| [16] | 2015 | Real time EV charging power allocation reducing PV - EV power deviations. | No | Building level | Centralised |
| [17] | 2018 | Two-level control reducing power fluctuations due to EV charges | No | Microgrid | Centralised |
| [18] | 2018 | Coordinated EV charging scheme minimizing energy costs and DER fluctuations. | No | Microgrid | Centralised |
| [19] | 2014 | V2G operation with costs minimization and frequency regulation | No (Only power balance) | Distribution grid | Centralised |
| [20] | 2018 | V2G operation with reactive compensation | No | Charging Station | Centralised |
| [22] | 2012 | V2G impact on congestion costs and system reliability | DCPF | Transmission system | - |
| [23] | 2018 | Optimal EV shedding during a system congestion | ACPF | Distribution system | Centralised |
| [24] | 2015 | Optimal microgrid operation | DCPF | Microgrid | Centralised |

| Ref. | Year | Objectives | Grid Constraints | System Level | Control Type |
|------|------|------------|------------------|--------------|--------------|
| [13] | 2018 | Coordinated EV charging scheduling and system cost minimization | convexified PF | Distribution System | Distributed |
| [15] | 2017 | Global and local system operation optimization | No | City district | Multi-agent based |
| [27] | 2012 | Time-shift control for numerous EV chargers | No | Low voltage | Centralised |
| [28] | 2015 | Reduce building demand peaks because of fast charging | No | Building level | Centralised |

**Table 1.** State-of-the-art EMS approaches.

## 2.1.2 Communication Interfaces

As discussed in previous sections, the coordinated charge of EVs is crucial to avoid unstable scenarios on future smart city infrastructure. For that reason, different control approaches can be found in the literature, as presented in Section 2.1.1. Additionally, the communication between all the involved parts is relevant while designing an energy management system. In this case, different actors are involved in the charging process, such as Distribution System Operator (DSO), EV drivers, Energy suppliers and new market participants (e.g., Charge Station Operator(CSO)), and the communication is divided into different levels. In this Section, all the necessary interfaces and communication standards to manage EV chargers are presented.

The communication architecture is compounded of three levels: user-EVSE, EVSE-CSO, and CSO-DSO. The information flow happens sequentially from one agent to another. From the lower level to the upper level, the EV user set some preferences regarding charging time and energy demand. Then, the EV transfers all these information to the charging station (EVSE) according to a predetermined standard (IEC 15118). Subsequently, the EVSE asks for charging permission to the CSO. At the same time, the CSO must check with the DSO that the grid remains stable once the EV is connected. After receiving an answer, the CSO replies to the charging point with the charging power value. In Figure 8, the overall described system is depicted according to an ongoing project.
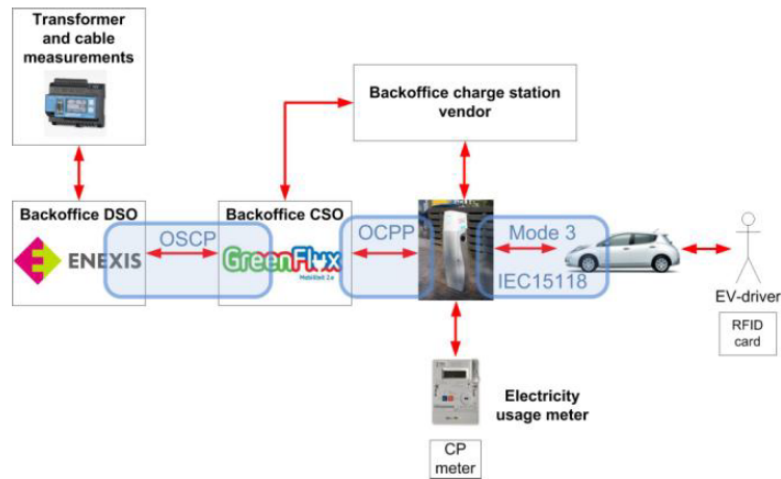
**Figure 8.** OSCP has been implemented in a project between Dutch DSO Enexis and CSO Service provider Greenflux [2].

The first communication level involves the user, EV, and EVSE. Currently, two standards that define this transaction are IEC 61851 and ISO 15118 (V2G). These protocols specify the communication syntax between charging station and electric vehicle. The user specifies its preferences either in the EV or directly in the EVSE through a human-machine interface. On this level, the flexibility of the load is defined by the current SOC of the EV and user departure time.

The second level connects the EVSE with the CSO. In this case, there is a protocol under development called Open Charging Point Protocol (OCPP) which specifies the syntax between charging point and network management system [29]. It is not recognized as a standard yet, but it is the leading candidate in this level. The implementation of this protocol allows the CSO to operate with different chargers regardless of the manufacturer. In Figure 9, several chargers from various vendors are easily connected to the CSO through OCPP.

The third and last level entails the communication interface between CSO and DSO. In this stage, the DSO shall inform the CSO whether it is safe or not to connect the EV. As in the previous level, there is another proposal called Open Smart Charging Protocol (OSCP)[2]. The deployment of OSCP allows a DSO to communicate easily with several CSOs. Therefore, its use would increase both the interoperability and the smart charging points integration avoiding costly ad-hoc implementations between DSO and every CSO.

Note that since there are several agents, each aims at different goals. For instance: EV user demands to charge its vehicle with minimal costs and at a specific time interval, whereas the DSO tries to minimize operation costs and system losses. Then, depending on the level, the objectives are different, and in this thesis, the focus is on the DSO level. Therefore, the approach proposed in this work optimizes distribution system operation.
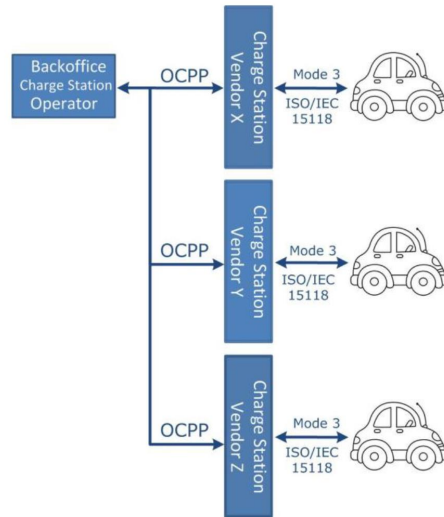
**Figure 9.** Different charging station types connected to the CSO through OCPP[2].

## 2.1.3   Optimal Power Flow Approaches

This thesis aims at managing a distribution system optimally. Therefore, the voltages and line flows shall be monitored to ensure optimal system performance. The power flow equations represent grid behavior. The major challenge of an OPF problem is the non-linearity presented in the system equations. The non-linear relationship between voltages and power demanded lead to a non-convex problem and NP-hard, which hinders the search for the global optimum. For that reason, in the past years, different alternatives to handle this problem have been introduced in the literature. Some of them are tailored to the electric network depending on the voltage level (e.g., distribution system or transmission system) and grid topology (e.g., meshed grid or radial grid). This section presents some of the optimization algorithms and relaxations approaches.

One of the most used is the DCOPF, due to its simple linear formulation. This approach neglects the resistance of the lines assuming that the branches have a small R/X ratio. The performance of this model is accurate in transmission grids. However, this assumption is not suitable for a distribution/low voltage system since the losses cannot be neglected (due to a higher R/X compared to a transmission grid). The optimization model in [22] is based on a DCOPF for transmission level. Alternatively, the control approach in [24] applies this approximation model on a low voltage microgrid, including a loss estimation. This approximation is valid for this case since they consider unity power factor, no voltage deviations, and the microgrid itself can be modeled as one unique bus. Authors in [25] propose a novel linearised power flow model for distribution systems (LACPF). This approach is similar to the DCPF, but including voltages and reactive power besides angles and active power. The voltage angle and magnitudes depend linearly on the power injections (active and reactive). This linearization can be applied for both radial and meshed grids. However, the loss estimation model is uniquely applicable to radial networks. Although the main advantage of linearised optimization models is the simplicity, the

accuracy is often insufficient for the use case, and the solution may include an unacceptable error (e.g., constraint violation).

Alternatively, the utilization of heuristic search techniques is common in practice to solve OPF. Genetic Algorithms (GA) or Particle Swarm Optimization (PSO) are some examples of these approaches. The main advantage of such algorithms is their robustness and their ability to find solutions for complex problems. However, in some cases, these algorithms might get trapped in a local optimum [30], and for that reason, the internal parameters of the model shall be adequately defined according to the problem [31].

Another technique to solve such a non-linear model is the Sequential Quadratic Programming (SQP). The authors in [32] propose an SQP algorithm which is structured with an outer linearisation loop and an inner optimization loop. The QP of the inner loop is solved efficiently using the interior point method. The size of the inner loop is equal to the number of constraint violations. The outer loop is comparable to the Newton power flow approach. Alternatively, the model in [33] combines trust region technique with SQP. The trust region controls the linear step size and ensures the validity of the linear model. Then, the algorithm defines a set of quadratic sub-problems that are solved using the active set method. However, these approaches have been used to solve an OPF for one single time step, and its performance for a set of several time-steps has not been proved in the literature yet. Thus, this technique is discarded since it is insufficient for this work.

Another alternative is the convex relaxation. This technique is commonly applied to derive second-order conic programming for the optimal power flow (OPF-SOCP) problem in a distribution system. The convex relaxation is executed utilizing a set of relaxations. In [34], the authors convexify power flow equations using the branch flow model, and it can be applied to both meshed and radial topologies. To make the problem convex, they apply two relaxations steps: elimination of voltage and current angle, and a conic relaxation on the resulting problem. Alternatively in [13], authors formulate a modified second-order cone programming of the original problem described by the injection model for a radial topology. In this case, some semidefinite relaxations are required as presented in [35]. In both approaches, the problem is quadratically constrained because of the conic constraints and hence, Second Order Cone Programming (SOCP) or Quadratically Constrained Quadratic Programming (QCQP) techniques are necessary. The approaches in [13] and [36] are some examples in which authors integrate convex relaxations for a MPC on a distribution system.

According to [37], solving OPF through convex relaxation offers some advantages: if a relaxed problem is infeasible, it is certificated that the original OPF is infeasible. Moreover, it can be checked whether a solution is globally optimal or not. Additionally, authors in [35] claim that for radial networks, the branch flow model (BFM) is more stable numerically than the bus injection model (BIM). Furthermore, as stated in [38] the branch flow model is always exact for radial systems if either the upper voltage limit or upper power demand limit is unbounded.

Last but not least, distributed OPF approaches are another possibility to face the problem. These methods do not require a central coordination; each node communicates with its adjacent nodes instead. Such approach is not pursued in this work, but is proposed as a future work of this thesis.

In this thesis, the convexified BFM is implemented, and its performance is compared with the linearized ACPF and DCPF.

## 2.2   System Architecture

After reviewing different EMS schemes for EVs, the agents involved in the charging process, and the communication protocols, a centralized 2-level MPC-based control is proposed. This architecture is a good candidate to control the charging stations in a distribution grid optimally. The upper level or *distribution grid level* aims at optimizing grid performance (e.g., system losses minimization). The lower level or *local level* allocates the optimal charging power among the charging stations connected. In the upper level, all the charging points connected in the same MV-LV transformer are aggregated, forming a single charging station or EVSE. Each local manager or CSO sends the cumulative energy demand curves for a determined time horizon to the centralized agent or DSO. The DSO optimizes the grid operation according to the system forecasts and the flexible EV energy demand. The DSO replies to the CSOs with the optimal power profiles for the given time horizon. Then, the lower level allocates the EV charging power rates according to the optimal power reference and user preferences. The system architecture is depicted at Figure 10 and summarized at Table 2.
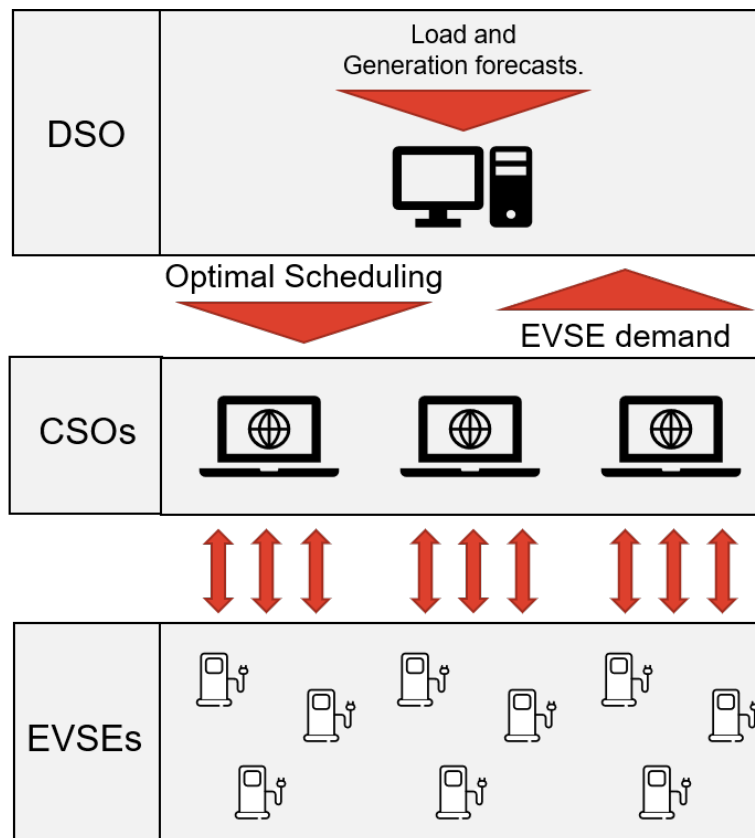


**Figure 10.** Proposed centralised MPC-based two-level control architecture.

| Level | Agent | Inputs | Outputs |
|---|---|---|---|
| Distribution grid | DSO | EV demand, Load and DER forecasts. | Optimal EVSE charging profiles |
| Charging station | CSO | Optimal EVSE charging profile. | EVs' charging rates |

**Table 2.** Proposed control architecture. Manager, inputs and outputs of each control layer.

# Chapter 3

# Theoretical Background

This chapter introduces the theoretical concepts relevant to this thesis. First, the exact non-convex PF problem with three convex alternatives is presented. Accordingly, for each PF model the assumptions are explained in detail. Second, the expressions deployed to estimate wind and PV power generation are presented. Finally, Section 3.3 introduces the key performance indicators (KPI) for analyzing algorithm performance.

## 3.1  Power Flow Models

In this section, the DCPF, linearised ACPF (LACPF) and convexified BFM models are presented. First, the exact ACPF formulation, according to the bus injection model (BIM), is depicted. Second, the DC linearisation assumptions and the DCPF model are stated. Third, the same applies to the LACPF model. Finally, the convexified BFM and the model relaxations are described.

For the sake of clarity, a vectorized variable (e.g. $\vec{V}$) stands for a complex number; on the contrary, the variable stands for its magnitude (e.g. $V$). Moreover, for simplicity reasons, the parallel line admittances are neglected in this work.

### 3.1.1  ACPF Formulation

Let $G = \{N, E\}$ be a connected graph representing a power network, regardless of the system topology, where $N = \{1, 2, ..., n\}$ buses (also called vertices or points) are connected by $E = \{1, 2, ..., l\}$ lines (also called links or edges). The set of lines that connect the node $i \in N$ with any other node $j \in N, j \neq i$ is denoted as $E_i \in E$. Define the line impedance as $\vec{z}_{ij} = r_{ij} + jx_{ij}$ if nodes $(i \to j)$ are connected, otherwise $z_{ij} = 0$. For a node $i \in N$, let $V_i$ be voltage magnitude, $\theta_i$ the voltage angle, $I_i$ the injected nodal current and $s_i$, $p_i$ and $q_i$ the

nodal injected apparent, active and reactive powers respectively. For a line $l = (i, j) \in E$, let $I_{ij}$ be the line current flow and $S_{ij}$, $P_{ij}$ and $Q_{ij}$ the line apparent, active and reactive powers respectively. Then, defining a slack bus with $s_0$ injected (demanded) apparent power and given $V_0$ (included in $V_i$), the system is defined by the set of variables $(V_i, \theta_i, s_0, S_{ij})$. Since this work aims at monitoring voltage magnitudes and power flows, the voltage angles are excluded from the model leaving only the most relevant variables as $(V_i, s_0, S_{ij})$.

According to Kirchhoff's law, the current injected at each node is defined as:

$$\vec{I_i} = \sum_{\forall ij \in E_i} \vec{I_{ij}} = \sum_{\forall ij \in E_i} \left( \frac{\vec{V_i} - \vec{V_j}}{\vec{z_{ij}}} \right) \tag{1}$$

The injected power is equal to the nodal voltage times the conjugated current from (1):

$$\vec{S_i} = \vec{V_i} \cdot \vec{I_i^*} = \vec{V_i} \cdot \sum_{\forall ij \in E_i} (\vec{I_{ij}})^* = \vec{V_i} \cdot \sum_{\forall ij \in E_i} \left( \frac{\vec{V_i} - \vec{V_j}}{\vec{z_{ij}}} \right)^* \tag{2}$$

The apparent power on each line, neglecting parallel admittances, satisfies:

$$\vec{S_{ij}} = \vec{V_i} \cdot \vec{I_{ij}^*} = \vec{V_i} \cdot \left( \frac{\vec{V_i} - \vec{V_j}}{\vec{z_{ij}}} \right)^* \tag{3}$$

being $\vec{V_i}$ and $\vec{V_j}$ the sending and receiving end node voltages respectively and $\vec{z_{ij}}$ the serial line admittance. Dividing equation (3) into its active and reactive terms:

$$\vec{S_{ij}} = P_{ij} + jQ_{ij} \tag{4}$$

$$P_{ij} = \frac{r_{ij}V_i^2 - r_{ij}V_iV_j cos\theta_{ij} + x_{ij}V_iV_j sin\theta_{ij}}{r_{ij}^2 + x_{ij}^2} \tag{5}$$

$$Q_{ij} = \frac{x_{ij}V_i^2 - r_{ij}V_iV_j sin\theta_{ij} - x_{ij}V_iV_j cos\theta_{ij}}{r_{ij}^2 + x_{ij}^2} \tag{6}$$

Both terms can be again divided into two sub-terms:

$$P_{ij_1} = \frac{r_{ij}x_{ij}}{r_{ij}^2 + x_{ij}^2} \cdot \frac{V_i \cdot (V_i - V_j cos\theta_{ij})}{x_{ij}} \tag{7}$$

$$P_{ij_2} = \frac{x_{ij}^2}{r_{ij}^2 + x_{ij}^2} \cdot \frac{V_iV_j sin\theta_{ij}}{x_{ij}} \tag{8}$$

$$Q_{ij_1} = \frac{-r_{ij}x_{ij}}{r_{ij}^2 + x_{ij}^2} \cdot \frac{V_iV_j sin\theta_{ij}}{x_{ij}} \tag{9}$$

$$Q_{ij_2} = \frac{x_{ij}^2}{r_{ij}^2 + x_{ij}^2} \cdot \frac{V_i \cdot (V_i - V_j cos\theta_{ij})}{x_{ij}} \tag{10}$$

Now, combining equations eqs. (2) and (3), the power injected at node $i$ can be written as:

$$\vec{S}_i = \sum_{\forall ij \in E_i} \vec{S}_{ij} \tag{11}$$

Following sections show the different assumptions to obtain the simplified DCPF, and LACPF approaches from the aforementioned exact Bus Injection Model (BIM).

## 3.1.2 Linearised DCPF

The DCPF is broadly used to analyse transmission systems. Although its applicability in distribution grids is not accurate due to the higher $R/X$ ratio, its performance will be compared with the other two approaches. The main assumptions of the DCPF are grouped below:

- All the node voltages are equal to the nominal voltage (1 p.u) and reactive powers are neglected ($\vec{S}_i \approx P_i$).

- Lines are purely inductive (resistance values are neglected in the DCPF formulation, $\vec{z}_{ij} \approx jx_{ij}$).

- Small angle shift between connected nodes ($\theta_i \approx \theta_j \approx 0$, $sin(\theta_i - \theta_j) \approx \theta_i - \theta_j$ and $cos(\theta_i - \theta_j) \approx 1$).

Then, considering the guidelines from above, the eqs. (7) to (10) can be reduced to only one equation:

$$P_{ij} = \frac{\theta_i - \theta_j}{X_{ij}} \tag{12}$$

and hence, the power injected at each node in (11) is simplified as follows:

$$P_i = \sum_{\forall ij \in E_i} \frac{\theta_i - \theta_j}{X_{ij}} \tag{13}$$

Organizing both expression in matrix formulation:

$$[P]_{inj} = [B] \cdot [\theta] \tag{14}$$

$$[P]_{line} = [T] \cdot [\theta] \tag{15}$$

where $[P]_{inj}$ and $[P]_{line}$ are the power injections and power flows respectively, $[B]$ is formed by $B_{ij} = -\frac{1}{X_{ij}}$ and $B_{ii} = \sum \frac{1}{X_{ij}}$, and $[T]$ by $T_{li} = \frac{1}{X_{ij}}$ and $T_{lj} = -\frac{1}{X_{ij}}$ (assuming $i$ to $j$ as positive line flow criteria). The term $l$ represents the line number.

The voltages remain constant and equal to the reference voltage ($V_0 \approx 1$). For that reason, the power flows ($P_{ij}$) are the unique variables which define the system state and they are controlled by changing the nodal injections ($P_i$) in the system. This relation state-control is obtained by

combining eqs. (14) and (15). In order to avoid singularity, all terms (rows and columns) related to the reference bus are excluded from both matrices (resulting $\hat{T}$ and $\hat{B}$). The combination of the resulting matrices leads to the sensitivity matrix of the system, which defines state changes due to nodal power variations:

$$[Q] = [\hat{T}] \cdot [\hat{B}]^{-1} \tag{16}$$

$$[P]_{line} = [Q] \cdot [P]_{inj} \tag{17}$$

According to Ohm's law and DCPF assumptions, the current flow on lines can be approximated by:

$$\vec{I}_{ij} = \frac{\vec{V}_i - \vec{V}_j}{\vec{z}_{ij}} \approx \frac{\theta_i - \theta_j}{x_{ij}} = P_{ij} \tag{18}$$

Note that along this Section, injections have prevailed as positive sign criteria. In the next chapters, the power demanded is adopted as positive sign criteria. Thus, the sign of the sensitivity matrix $Q$ changes too:

$$Q_D = -Q \tag{19}$$

### 3.1.3 Linearised ACPF

The DCPF approach shown in section 3.1.2 is rather limited for a distribution level. Therefore, authors in [25] propose a linearised ACPF to overcome DCPF deficiencies in distribution networks and still preserve linearity. This novel formulation incorporates reactive power components and voltage constraints. Authors claim that the linear approximation for voltage magnitudes remains within an acceptable error range in actual operating conditions. Given a meshed or radial grid, the model assumes that:

- The absolute values of all voltages are approximately equal to the nominal voltage ($|V_i| \approx 1\ p.u.$, $|V_j| \approx 1\ p.u.$), but the difference between voltages is not negligible. This is a strong assumption and can potentially introduce error if the voltages are not close to 1 p.u..

- The distance of two consecutive nodes in a distribution system is generally short and therefore, the voltage drop along the branch is small. Thus, the angle shift should be close to zero ($sin(\theta_i - \theta_j) \approx \theta_i - \theta_j, cos(\theta_i - \theta_j) \approx 1$).

Considering the two points described above, the expressions in eqs. (7) to (10) are simplified as follows:

$$P_{ij_1} \approx \frac{r_{ij}x_{ij}}{r_{ij}^2 + x_{ij}^2} \cdot \frac{(V_i - V_j)}{x_{ij}} \tag{20}$$

$$P_{ij_2} \approx \frac{x_{ij}^2}{r_{ij}^2 + x_{ij}^2} \cdot \frac{(\theta_i - \theta_j)}{x_{ij}} \tag{21}$$

$$Q_{ij_1} \approx \frac{-r_{ij}x_{ij}}{r_{ij}^2 + x_{ij}^2} \cdot \frac{(\theta_i - \theta_j)}{x_{ij}} \tag{22}$$

$$Q_{ij_2} \approx \frac{x_{ij}^2}{r_{ij}^2 + x_{ij}^2} \cdot \frac{(V_i - V_j)}{x_{ij}} \tag{23}$$

Then, according to eqs. (4) and (11) the active and reactive power injected at each node:

$$P_i = \sum_{\forall ij \in E_i} \left( \frac{x_{ij}^2}{r_{ij}^2 + x_{ij}^2} \cdot \frac{(\theta_i - \theta_j)}{x_{ij}} + \frac{r_{ij}x_{ij}}{r_{ij}^2 + x_{ij}^2} \cdot \frac{(V_i - V_j)}{x_{ij}} \right) \tag{24}$$

$$Q_i = \sum_{\forall ij \in E_i} \left( \frac{-r_{ij}x_{ij}}{r_{ij}^2 + x_{ij}^2} \cdot \frac{(\theta_i - \theta_j)}{x_{ij}} + \frac{x_{ij}^2}{r_{ij}^2 + x_{ij}^2} \cdot \frac{(V_i - V_j)}{x_{ij}} \right) \tag{25}$$

Rewrite both expressions in matrix form excluding the terms related to the reference bus:

$$\begin{bmatrix} P' \\ Q' \end{bmatrix} - \begin{bmatrix} B_2^{ref} \\ -B_1^{ref} \end{bmatrix} \cdot \theta_{ref} - \begin{bmatrix} B_1^{ref} \\ B_2^{ref} \end{bmatrix} \cdot V_{ref} = \begin{bmatrix} B_2' & B_1' \\ -B_1' & B_2' \end{bmatrix} \cdot \begin{bmatrix} \theta' \\ V' \end{bmatrix} = B \cdot \begin{bmatrix} \theta' \\ V' \end{bmatrix} \tag{26}$$

where $B_1(i,j) = \frac{-r_{ij}}{r_{ij}^2 + x_{ij}^2}$ , $B_1(i,i) = \sum_{\forall ij \in E_i} \frac{r_{ij}}{r_{ij}^2 + x_{ij}^2}$, $B_2(i,j) = \frac{-x_{ij}}{r_{ij}^2 + x_{ij}^2}$, $B_2(i,i) = \sum_{\forall ij \in E_i} \frac{x_{ij}}{r_{ij}^2 + x_{ij}^2}$, $B^{ref}$ and $B'$ are parts of the $B$ matrix with only the reference bus column and without the reference bus column respectively and $P'$, $Q'$, $V'$ and $\theta'$ are the active and reactive powers and the magnitude and angle voltages excluding the reference bus.

Since the control variables and state variables are the EVSE power demand and the voltages respectively, the suitable matrix form is:

$$\begin{bmatrix} \triangle\theta \\ \triangle V \end{bmatrix} = \begin{bmatrix} B_2' & B_1' \\ -B_1' & B_2' \end{bmatrix}^{-1} \cdot \begin{bmatrix} P \\ Q \end{bmatrix} = \begin{bmatrix} B_{\theta,P} & B_{\theta,Q} \\ B_{V,P} & B_{V,Q} \end{bmatrix} \cdot \begin{bmatrix} P \\ Q \end{bmatrix} \tag{27}$$

$$\theta_i = \theta_{ref} + \triangle\theta_i \tag{28}$$

$$V_i = V_{ref} + \triangle V_i \tag{29}$$

Splitting voltage magnitude and voltage angle, the voltage at each node $b$ can be presented as:

$$V_i = V_{ref} + \sum_{j=1}^{N_B - 1} \left( B_{V_i,P_j} \cdot P_j + B_{V_i,Q_j} \cdot Q_j \right) \tag{30}$$

where $B_{V_i,P_j}$ and $B_{V_i,Q_j}$ are the terms of the matrices $B_{V,P}$ and $B_{V,Q}$ at the row $i$ and column $j$ and $N_B$ is the number of nodes. Thus, the EVSE impact on system voltages can be supervised and included in the optimization model, which is not the case with the DCPF. However, this approach is accurate uniquely if the voltages are near to 1 p.u., because of the first assumption of ($|V_i| \approx 1p.u$). The larger the deviation from 1 p.u., the larger the approximation error as shown in Section 5 later on.

Concerning power on lines, the work in [25] suggests a recursive approach to calculate Load Shift Factors (LSFs) of the system similar to the backward/forward sweep algorithm for solving

radial power flows. The factors are approximated using Taylor's series by omitting the 2nd and higher order terms. Then, the sensitivity matrix is formed by the combination of all LSFs and depends on the initial operating point $x_0 = \{P_{ij}^0, Q_{ij}^0, V_i^0\}$, which includes all uncontrollable loads $P_i^0$ and $Q_i^0$. Then, the active and reactive power flows can be derived as:

$$P_{ij} = P_{ij}^0 + \sum_{k=1}^{N_B-1} (\frac{dP_{ij}}{dP_k})^0 \cdot (P_k - P_k^0) + \sum_{k=1}^{N_B-1} (\frac{dP_{ij}}{dQ_k})^0 \cdot (Q_k - Q_k^0) \tag{31}$$

$$Q_{ij} = Q_{ij}^0 + \sum_{k=1}^{N_B-1} (\frac{dQ_{ij}}{dP_k})^0 \cdot (P_k - P_k^0) + \sum_{k=1}^{N_B-1} (\frac{dQ_{ij}}{dQ_k})^0 \cdot (Q_k - Q_k^0) \tag{32}$$

In this work, we propose a linearisation of the line apparent power as the line flow must be supervised. Thus, following the procedure deployed in [25] the apparent flow is derived as:

$$S_{ij} = \sqrt{P_{ij}^2 + Q_{ij}^2} \tag{33}$$

$$S_{ij} = S_{ij}^0 + \sum_{k=1}^{N_B-1} (\frac{dS_{ij}}{dP_k})^0 \cdot (P_k - P_k^0) + \sum_{k=1}^{N_B-1} (\frac{dS_{ij}}{dQ_k})^0 \cdot (Q_k - Q_k^0) \tag{34}$$

$$(\frac{dS_{ij}}{dP_k})^0 = \frac{1}{2} \cdot ((P_{ij}^0)^2 + (Q_{ij}^0)^2)^{-\frac{1}{2}} (2 \cdot P_{ij}^0 \cdot \frac{dP_{ij}}{dP_k} + 2 \cdot Q_{ij}^0 \cdot \frac{dQ_{ij}}{dP_k}) \tag{35}$$

$$(\frac{dS_{ij}}{dQ_k})^0 = \frac{1}{2} \cdot ((P_{ij}^0)^2 + (Q_{ij}^0)^2)^{-\frac{1}{2}} \cdot (2 \cdot P_{ij}^0 \cdot \frac{dP_{ij}}{dQ_k} + 2 \cdot Q_{ij}^0 \cdot \frac{dQ_{ij}}{dQ_k}) \tag{36}$$

Note that demand is considered as positive sign criteria. Then, eqs. (31) to (36) can be reformulated as matrix form and for each time step:

$$[\hat{Q}(t)] = \begin{bmatrix} \hat{Q}_{pp}(t) & \hat{Q}_{pq}(t) \\ \hat{Q}_{qp}(t) & \hat{Q}_{qq}(t) \end{bmatrix} = \begin{bmatrix} \frac{dP_{ij}}{dP_i}(t) & \frac{dP_{ij}}{dQ_i}(t) \\ \frac{dQ_{ij}}{dP_i}(t) & \frac{dQ_{ij}}{dQ_i}(t) \end{bmatrix} \tag{37}$$

$$\begin{bmatrix} P(t) \\ Q(t) \end{bmatrix}_{line} = \begin{bmatrix} P^0(t) \\ Q^0(t) \end{bmatrix}_{line} + \begin{bmatrix} \hat{Q}_{pp}(t) & \hat{Q}_{pq}(t) \\ \hat{Q}_{qp}(t) & \hat{Q}_{qq}(t) \end{bmatrix} \cdot \begin{bmatrix} P(t) - P^0(t) \\ Q(t) - Q^0(t) \end{bmatrix}_{inj} \tag{38}$$

$$[\hat{Q}_s(t)] = \begin{bmatrix} \hat{Q}_{sp}(t) & \hat{Q}_{sq}(t) \end{bmatrix} = \begin{bmatrix} \frac{dS_{ij}}{dP_i}(t) & \frac{dS_{ij}}{dQ_i}(t) \end{bmatrix} \tag{39}$$

$$\begin{bmatrix} S(t) \end{bmatrix}_{line} = \begin{bmatrix} S^0(t) \end{bmatrix}_{line} + \begin{bmatrix} \hat{Q}_{sp}(t) & \hat{Q}_{sq}(t) \end{bmatrix} \cdot \begin{bmatrix} P(t) - P^0(t) \\ Q(t) - Q^0(t) \end{bmatrix}_{inj} \tag{40}$$

According to the main assumptions of this approach, the line losses can be estimated similarly to the DCPF approach. Let the voltage magnitude be close to 1 p.u. and neglecting the voltage

angles ($\theta_i \approx 0$) the line current magnitude can be approximated to the apparent power magnitude in the line:

$$\vec{S}_{ij} = \frac{\vec{V}_i - \vec{V}_j}{\vec{z}_{ij}} = I_{ij}\angle\phi \tag{41}$$

$$\vec{S}_{ij} = \vec{V}_i \cdot \left(\frac{\vec{V}_i - \vec{V}_j}{\vec{z}_{ij}}\right)^* = S_{ij}\angle - \phi \tag{42}$$

$$S_{ij} \approx I_{ij} \tag{43}$$

This is approximation presents lightly better results compared to the DCPF approximation as shown in chapter 5.

### 3.1.4   Convexified BFM

In this section, the convexified Branch Flow Model (c-BFM) is introduced. First, the BFM formulation is presented. Second, the convex relaxations and the relaxed problem are stated. Finally, the section ends with the assumptions that must be adopted to obtain reliable results.

#### 3.1.4.1   Branch Flow Model (BFM)

The BFM is an alternative power flow formulation to the traditional BIM, which is based on nodal variables (e.g., voltages, current and power injections). The BFM focuses on line variables, such as powers and currents on the lines, and has been mainly used for distribution radial systems [39]. The following power flow formulation is extracted from the works in [39] and [35].

Let $G = \{N, E\}$ be a connected graph representing a power network, where $N$ buses (also called vertices or points) are connected by $E$ lines (also called links or edges). If the graph $G$ is a tree, then the power network is a radial system. In a tree system, the root generally represents the substation bus or reference bus.

In this case, the system is adopted as a directed tree graph assuming that each line points away from the root. A line $(i, j)$ or $i \rightarrow j$ with a complex impedance $z_{ij} = r_{ij} + jx_{ij}$ points from node $i$ to node $j$. The current flowing on the line is denoted as $I_{ij}$ and the *sending-end* complex power as $S_{ij} = P_{ij} + jQ_{ij}$. Let $z_i = r_i + jx_i$ be the nodal shunt admittances, $V_i$ the nodal complex voltage and $s_i = p_i + jq_i$ the nodal complex injection on node $i$. The slack bus is denoted as $0$ with a variable injected power $s_0$ and a constant voltage $v_0$. In Figure 11, the equivalent $\pi$ branch model is presented.

Then, given the line impedances of the grid and the bus power injections, the branch flow model with variables $(S, I, V, s_0)$ satisfies the following equations:

$$V_i - V_j = z_{ij} \cdot I_{ij} \quad \forall(i, j) \in E \tag{44}$$
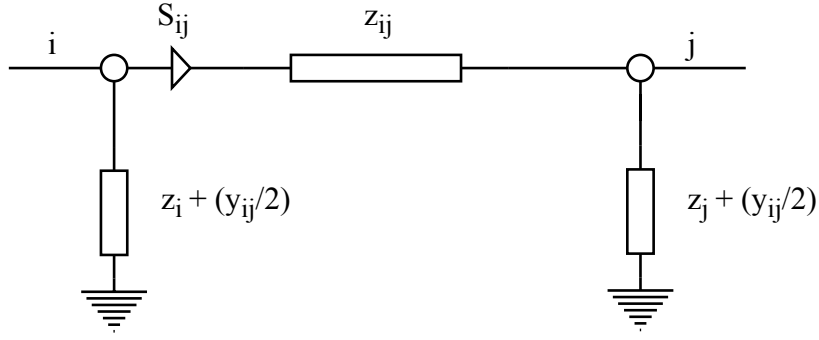
**Figure 11.** $\pi$ branch model. Note that $z_i$ and $z_j$ represent the capacitive devices on buses $i$ and $j$. In this work, the line is modelled without parallel admittances but can be added as $\frac{y_{ij}}{2}$ on each end.

$$S_{ij} = V_{ij} \cdot I_{ij}^* \quad \forall(i,j) \in E \tag{45}$$

$$s_j = \sum_{k:j \to k} S_{jk} - \sum_{i:i \to j}(S_{ij} - z_{ij} \cdot I_{ij}^2) + y_j^* \cdot |V_j|^2 \quad \forall j \in N \tag{46}$$

where equation (44) is the Ohm's law, equation (45) is the branch power flow and equation (46) is the nodal power balance. Note that the previous formulation applies also for meshed networks. If we now assume radial systems, the equation (46) is simplified as:

$$s_j = \sum_{k:j \to k} S_{jk} - (S_{ij} - z_{ij} \cdot I_{ij}^2) + y_j^* \cdot |V_j|^2 \quad \forall j \in N \tag{47}$$

### 3.1.4.2 Relaxations and Convexification

In order to convexify the BFM, two relaxations are necessary according to [39]. These relaxations are described below and summarized in Figure 12 (for further explanation see [39]):
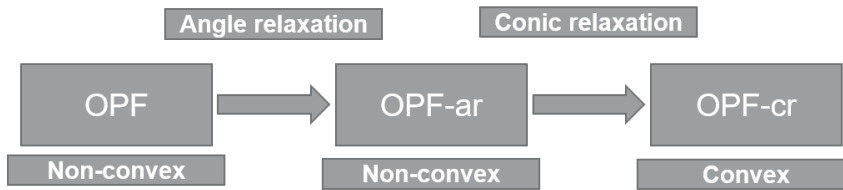


**Figure 12.** Set of convex relaxations according to [39].

- *Angle relaxation*: relax the OPF to OPF-ar by taking the square magnitude of the current ($l_{ij} = I_{ij}^2$) and voltage ($v_i = V_i^2$) to eliminate voltage and current angles from the power flow equations. This problem is still non-convex due to the set of quadratic constraints in (49).

$$v_j = v_i - 2 \cdot (r_{ij} \cdot P_{ij} + x_{ij} \cdot Q_{ij}) + (r_{ij}^2 + x_{ij}^2) \cdot l_{ij} \quad \forall(i,j) \in E \tag{48}$$

$$l_{ij} = \frac{P_{ij}^2 + Q_{ij}^2}{v_i} \quad \forall(i,j) \in E \tag{49}$$

$$p_j = \sum_{k:j \to k} P_{jk} - (P_{ij} - r_{ij} \cdot l_{ij}) + g_j \cdot v_j \quad \forall j \in N \tag{50}$$

$$q_j = \sum_{k:j \to k} Q_{jk} - (Q_{ij} - x_{ij} \cdot l_{ij}) + b_j \cdot v_j \quad \forall j \in N \tag{51}$$

where $g_j$ and $b_j$ represent the shunt admittance ($y_j = g_j - i \cdot b_j^2$) from $i$ to ground, that will be neglected in this work. Note that equation (47) has been divided into two terms: active and reactive powers to control each term individually.

- *Conic relaxation*: relax the OPF-ar to OPF-cr by changing the set of quadratic equality constraints (49) into a set of inequality constraints. This relaxation results in a SOCP when the objective function is linear.

$$l_{ij} \geq \frac{P_{ij}^2 + Q_{ij}^2}{v_i} \quad \forall (i,j) \in E \tag{52}$$

The constraint (52) can be rewritten as:

$$\left\| \begin{matrix} 2 \cdot P_{ij} \\ 2 \cdot Q_{ij} \\ l_{ij} - v_{ij} \end{matrix} \right\|_2 \leq l_{ij} + v_{ij} \tag{53}$$

According to [39], a global solution for radial networks of the original OPF problem can be recovered from the solution of the aforementioned SOCP always when the solution attains equality (53). However, in cases of excessive distributed generation, this is only possible if there are not either upper bounds on the loads or upper voltages limits [38]. Additionally, the following assumptions are essential to obtain reliable results:

- The network graph $G$ is connected.

- The objective function for optimal power flow is convex.

- The objective function is strictly increasing in $l_{ij}$ ($I_{ij}^2$), non-increasing in load $s_i$ and independent of $S_{ij}$.

Note that the line thermal limit is modeled according to the longitudinal current flow neglecting the current flows toward the shunt elements of both ends. This can lead to an infeasible solution of the problem, especially for very long lines [40]. However, for the sake of simplicity, the line shunts are neglected in this work. Generally, distribution lines in city districts do not have extremely long lines, and therefore this assumption should not lead to any problems.

---

## 3.2 Wind and PV Generation Models

Wind and PV generation have been included in the realistic scenarios implemented to demonstrate the effectiveness of the proposed EMS scheme. For that reason, we estimate their behavior with a standard model for PV generation from the literature and a wind speed/power curve. First, wind power can be formulated as a function of wind speed. Considering that the energy is completely transmitted into the system, the wind power can be directly interpolated according to the E40/500 power curve [41]. This turbine is a realistic candidate for distributed generation since the power rates are neither extremely high nor small. The power curve and turbine characteristics are presented below in Figure 13 and Table 3 respectively:
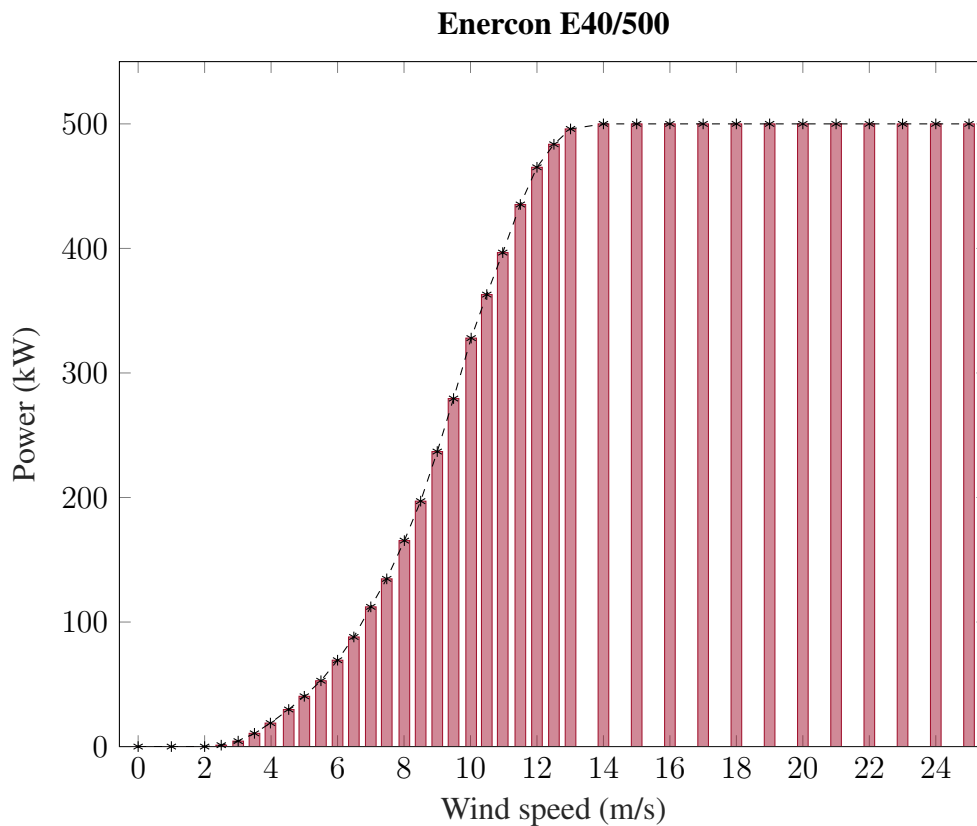


**Figure 13.** Wind power profile of the wind turbine ENERCON E40/500.

| Wind Turbine | |
|---|---|
| Manufacturer | ENERCON |
| Model | E40/500 |
| Rated Power | 500 kW |
| Rotor Diameter | 40 m |
| Number of blades | 3 |
| Cut-in wind speed | 2.5 m/s |
| Rated wind speed | 13.5 m/s |
| Cut-off wind speed | 25 m/s |
| Min./Max. Hub Height | 42-65 m |

**Table 3.** Main characteristics of the ENERCON E40/500 wind turbine.

Then, the expression that determines the wind power depending on the wind speed is:

$$P_{wind} = \frac{P_2 - P_1}{v_2 - v_1} \cdot (v - v_1) + P_1 \tag{54}$$

where 2 and 1 are the upper and lower interval values respectively, $P$ stands for the power and $v$ for the wind speed.

The measured wind speed must be adapted to the wind turbine height since it is measured in a determined height that may not match with the one from the turbine. Thus, the wind speed at the blades is approximated as follows:

$$v \approx v_{measured} \cdot \frac{ln(\frac{h}{z_0})}{ln(\frac{h_{measured}}{z_0})} \tag{55}$$

where $v_{measured}$ and $h_{measured}$ stand for the measured wind velocity and the height at which it was measured, $v$ and $h$ represent the velocity and height of the wind turbine and $Z_0$ is a constant that depends on the surface roughness. In our case we assumed a short grass surface ($Z_0 = 0.01$).

Second, the PV generation behavior can be approximated by a formula that is broadly deployed in the literature [42]. This expression is presented below:

$$P_{PV} = \eta \cdot S \cdot I \cdot (1 - 0.005 \cdot (T_a - 25)) \tag{56}$$

where $\eta$ is the conversion efficiency of PV cells, $S$ is the area of the PV surface, $I$ the solar radiation, and $T_a$ is the ambient temperature. This work neglects the incidence angle, assuming that the total sum of radiation fall on the PV panels. Thus, the resulting radiation is calculated as the sum of the diffused and direct radiation.

## 3.3 Key Performance Indicators (KPI)

In order to evaluate the performance of the algorithm, different parameters are defined.

### 3.3.1 Total System Losses

The overall system losses is calculated as follows:

$$E_{loss} = \sum_{l=1}^{Lines} r_l \cdot I_l^2 \tag{57}$$

### 3.3.2 Loss Reduction

This performance indicator aims at showing the total system losses reduction of the coordinated scheme with regards to the uncoordinated scheme.

$$KPI_{losses}(\%) = 100 \cdot \frac{Losses_{uncoordinated} - Losses_{coordinated}}{Losses_{uncoordinated}} \tag{58}$$

### 3.3.3 Computational Burden

The maximum, minimum and average computational burden for the given simulation horizon are included as a performance indicators.

### 3.3.4 Magnitude Variability

The variability indicator is deployed to analyze the power imported at the slack bus, line current, and voltage magnitudes performance during the whole simulation horizon T ($u = \{P_{imported}, I_{line}, V\}$).

$$\overline{u} = \frac{1}{T} \sum_{t=1}^{T} u \tag{59}$$

$$\sigma = \sqrt{\frac{1}{T} \cdot \sum_{t=1}^{T} (u - \overline{u})^2} \tag{60}$$

$$KPI_{CV}(\%) = 100 \cdot \frac{\sigma}{\overline{u}} \tag{61}$$

### 3.3.5   Absolute Error or Magnitude Deviation

This indicator is used to analyse the performance of each power flow model. The value represent the accuracy on the current and voltage magnitudes. Additionally, this indicator is deployed to prove the magnitude deviation when rounding up the optimal set of charging power profiles.

$$KPI_{error}(\%) = 100 \cdot |\frac{u_{base} - u}{u_{base}}| \tag{62}$$

# Chapter 4

# Implementation

Until now, we have shown the importance of an EMS for EV charging stations, the limitations of different approaches that try to solve the problem and the solution we propose. This chapter describes the methodology for the thesis work and its implementation. The first section describes the methodology followed to accomplish the tasks. In the second section, the system model is explained in detail. The model is formulated in MATLAB and with the help of the YALMIP toolbox [10].

## 4.1  Proposed Methodology

As already mentioned at the beginning of the thesis, the proposed EMS consists of a 2-level MPC-based control. The distribution network is assumed to be radial. Then, we allocate the EV demand minimizing the total system losses and considering EV user flexibility (e.g., arrival and departure times). The EVs are aggregated per node, forming an aggregation of EVs to reduce the size of the problem. Then, all the charging stations connected to the same transformer are aggregated forming a single nodal charging station or EVSE. Thus, the first optimization level handles a smaller number of variables. The optimization outputs are the set of nodal optimal charging power profiles. The second level allocates the optimal charging rate among all the EV users of the same aggregation (second-level control).

Before the algorithm starts running, the program initializes the grid parameters. Then, the control starts with the charging station (EVSE) energy profile aggregation (second-level or local level). Once all the EVSE send the maximum and minimum energy profiles to the upper level, the optimization problem takes place (first level or centralized level). After each time step $\triangle t$, the EVSE sends a new set of energy profiles including the new changes in the system. The flow chart in 14 outlines the methodology proposed graphically.

To accomplish a meaningful algorithm evaluation, we first define a realistic EV user behavior considering day and night charging schemes as in 4.3.1.1. Then, we simulate for a time frame of 2 days, taking into account real system dynamics with load heterogeneity. After each time step, we save the status of each EV, calculate the cumulative energy profiles, and rerun the OPF problem. This process is repeated until the end of the simulation horizon.
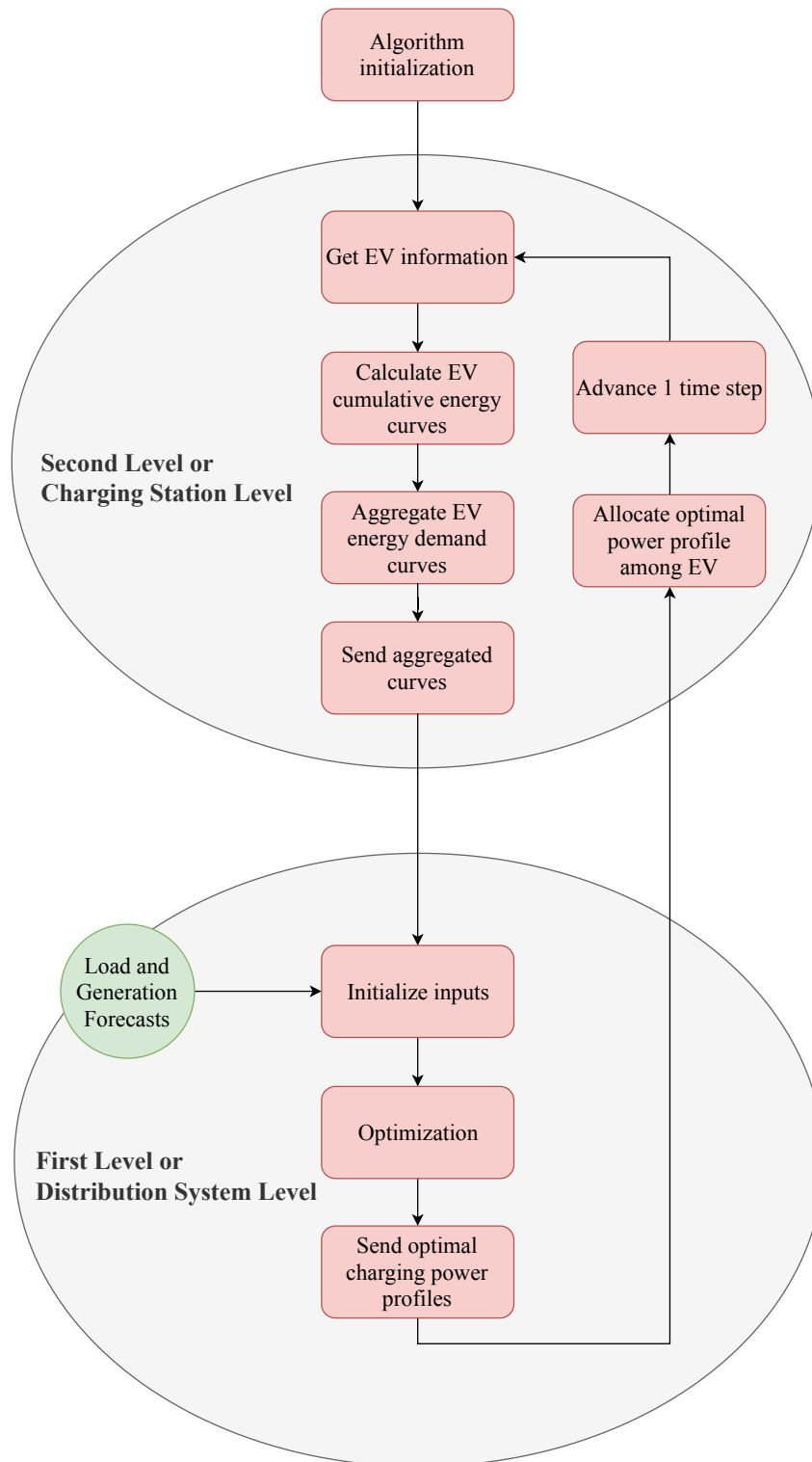


**Figure 14.** Proposed methodology for a set of charging stations and the centralised control. For the sake of simplicity, only one charging station is depicted in the figure.

## 4.2   System Model

This section gives an overview of the system formalization and its implementation. First, the EV aggregate model is introduced. Second, the three different power flow approaches adopted in this work are presented. Finally, the optimization model is formulated for a prediction and control horizon $T$ of $\{1,...,T\}$ time steps of length $\triangle t$. For each $t$ the optimization is recalculated for the control horizon shifted by $\triangle t$ and taking into account the last state of the system.

### 4.2.1   EV Aggregate Model

As we introduced in the previous section, each charging station has to provide the aggregated maximum and minimum cumulative energy demand curves for all the EV it manages. The maximum cumulative energy curve for an EV represents the battery state while providing the maximum charging power constantly until the battery reaches the expected SOC. Thus, the EV will charge up to the expected SOC and once the EV reaches that level, the SOC will remain constant. Equation (63) represents the maximum cumulative energy curve for one EV and for a constant time step $\triangle t$:

$$W_{max}^{EV}(t+1) = W_{max}^{EV}(t) + P_{max}^{EV} \cdot \triangle t \tag{63}$$

where $P_{max}^{EV}$ is the maximum charging power and depends on the current rate and the number of charging phases. There are different charger types and each can have distinct characteristics as can be seen in Table 4. The typical maximum values for a standard charging event (not fast charging) in Europe are either $16A$ or $32A$. Then, the number of phases and the charging current rate are generated randomly among the set of integer numbers $\{1,2,3\}$ and $\{16,32\}$ respectively. The maximum power for each EV is calculated as in equation (64):

$$P_{max}^{EV} = \frac{rand(1,2,3) \cdot rand(16,32) \cdot 230}{1000} \tag{64}$$

| Type | Phases | Voltage (V) | Current per Phase(A) | Power (kW) |
|------|--------|-------------|----------------------|------------|
| Type 1 | 1 | 230 | 16-32 | 3,7-7,4 |
| Type 2 | 1/2/3 | 230 | 16-32 | 3,7-22 |
| Type 2 CCS | dc/1/2/3 | 230 | 16-32 | 3,7-22 (DC - up to 170) |

**Table 4.** EV chargers: Type 1 - AC single-phase, Type 2 - AC single/double/three phase and Type 2 Combined Charging System (CCS) - AC(single/double/three phase)/DC[43, 44].

Alternatively, the minimum cumulative energy curve depicts the minimum battery state while providing the minimum charging power constantly to reach the desired SOC. Then, the optimal

cumulative charging energy profile is located between these two curves. If the optimal energy profile is below the minimum profile there will be some energy that will not be supplied.

$$W_{min}^{EV}(t+1) = W_{min}^{EV}(t) + P_{min}^{EV} \cdot \triangle t \tag{65}$$

where $P_{min}^{EV}$ is the minimum charging power and depends on the energy demand and the parking time. These two values are generated accordingly to realistic data that is presented in the next Section 4.3.1.1. The minimum power for each EV is calculated as in equation (66):

$$P_{min}^{EV} = \frac{W_{demand}^{EV}}{t_{departure} - t_{arrival}} \tag{66}$$

Note that if the energy demand is really high that the minimum power results higher than the maximum power, the EV will not charge all the demanded energy and the minimum and maximum cumulative curves will overlap. In this case, the EV behaves like an uncontrollable load without leaving room for flexibility.

Once the energy curves are defined for each EV, they are aggregated by charging station. All the EV connected to the same node form a charging station or EVSE and the resulting aggregated curves are the inputs of the optimization model, which is defined in Section 4.2.3. In the same way, the maximum charging power is the sum of all the aggregated EV maximum power rates. On the contrary, the minimum EVSE charging power is initially not limited and set to zero. Then the resulting EVSE energy curves and EVSE maximum power are:

$$W_{max}^{EVSE}(t) = \sum_{\forall EV \in EVSE} W_{max}^{EV}(t) \tag{67}$$

$$W_{min}^{EVSE}(t) = \sum_{\forall EV \in EVSE} W_{min}^{EV}(t) \tag{68}$$

$$P_{max}^{EVSE}(t) = \sum_{\forall EV \in EVSE} P_{max}^{EV}(t) \tag{69}$$

Each charging station is modelled similar to a battery storage system, but the operation range change dynamically at each iteration and it can be only charged (V2G not considered). Moreover, the power range depend on the charging characteristics of all the EV aggregated to the same EVSE. Then, the EVSE aggregate model is expressed by the following equations:

$$W_{EVSE}(i_e, t+1) = W_{EVSE}(i_e, t) + P_{EVSE}^{supplied}(i_e, t) \cdot h + P_{EVSE}^{not\ supplied}(i_e, t) \cdot h \tag{70}$$

$$W_{min}^{EVSE}(i_e, t) \leq W_{EVSE}(i_e, t) \leq W_{max}^{EVSE}(i_e, t) \tag{71}$$

$$P_{min}^{EVSE}(i_e, t) \leq P_{EVSE}^{supplied}(i_e, t) \leq P_{max}^{EVSE}(i_e, t) \tag{72}$$

$$P_{EVSE}^{not\ supplied}(i_e, t) \geq 0 \tag{73}$$

$$\forall\, t \in T, \forall\, i_e \in N_{EVSE} \tag{74}$$

where $t$ represents each time step of the time horizon $T$ and $i_e$ each charging station EVSE of the whole set of charging stations $N_{EVSE}$. The energy not supplied represents the part of the energy demand that cannot be supplied because of a system congestion.

### 4.2.2  Power Flow Models

#### 4.2.2.1  DC Power Flow Formulation (DCPF)

In this section, we introduce the simplified power flow model according to the DC model assumptions. The voltages are neglected since they remain invariant and equal to the nominal one (75). The line flows are approximated by a sensitivity matrix proportional to the nodal power demands (76). The overall nodal power demand is calculated as in (77) and the power balance in (77) considers the estimated system losses. As explained in Section 3.1.2, the line current can be approximated to the line power flow in p.u.. Thus, the estimated losses are proportional to the line flows and can be calculated as in (79). Finally, the line and transformers shall not exceed its boundaries (80) and (81).

$$V_i(t) = 1 \; p.u. \tag{75}$$

$$[I(t)]_{lines} = [Q_D] \cdot [P(t)]_{inj} \tag{76}$$

$$P_i(t) = P_i^D(t) + P_{EVSE}^{supplied}(i,t) - P_i^G(t) \tag{77}$$

$$P_{ref}(t) = P_{losses}(t) + \sum_{b=2}^{Buses-1} P_i(t) \tag{78}$$

$$P_{losses}(t) = \sum_{l=1}^{Lines} r_{ij} \cdot I_{ij}(t)^2 \tag{79}$$

$$\underline{I}_{ij} \le I_{ij}(t) \le \overline{I}_{ij} \tag{80}$$

$$\underline{P}_i \le P_i \le \overline{P}_i \tag{81}$$

$$\forall\, t \in T, \forall\, i \in N, \; \forall (i,j) \in E \tag{82}$$

where $P_i$, $P_i^D$ and $P_i^G$ represent the total active power injected, active power demanded and active power generated at node $i$ respectively.

#### 4.2.2.2  Linearised-AC Power Flow Formulation (LACPF):

In this case, the linearised AC power flow does not neglect the voltages that can be calculated as in (83). The line power flows are estimated from the previous system state ($S_{ij}^0$) and with the sensitivity matrix for that operation point (84). Note that the sensitivity matrix includes the loss

factors. Equations (85) and (86) express the nodal active and reactive demand respectively. The power balance defines the imported/exported power at the reference bus (87) and the losses are approximated similarly like in the previous DCPF approach (88). The maximum and minimum voltages, power flows and MV-LV transformer powers are expressed in (89), (90) and (91) respectively. Note that the current flows are approximated to the apparent power in the lines.

$$[V] = V_{ref} + \begin{bmatrix} B_{V,P} & B_{V,Q} \end{bmatrix} \begin{bmatrix} P(t) \\ Q(t) \end{bmatrix}_{inj} \tag{83}$$

$$[S(t)]_{lines} = [S^0]_{lines} + [\hat{Q}^0_{sp}(t)] \cdot [P(t)]_{inj} \tag{84}$$

$$P_i(t) = P_i^D(t) + P_{EVSE}^{supplied}(i,t) - P_i^G(t) \tag{85}$$

$$Q_i(t) = Q_i^D(t) - Q_i^G(t) \tag{86}$$

$$P_{ref}(t) = P_{losses}(t) + \sum_{b=2}^{Buses-1} P_i(t) \tag{87}$$

$$P_{losses}(t) = \sum_{l=1}^{Lines} r_{ij} \cdot I_{ij}(t)^2 \tag{88}$$

$$\underline{V}_i \leq V_i(t) \leq \overline{V}_i \tag{89}$$

$$\underline{S}_{ij} \leq S_{ij}(t) \leq \overline{S}_{ij} \tag{90}$$

$$\underline{P}_i \leq P_i \leq \overline{P}_i \tag{91}$$

$$\forall\, t \in T, \forall\, i \in N,\ \forall (i,j) \in E \tag{92}$$

where $Q_i$, $Q_i^D$ and $Q_i^G$ represent the total reactive power injected, reactive power demanded and reactive power generated at node $i$ respectively.

### 4.2.2.3  Convexified BFM Power Flow Formulation (c-BFM)

The two previously defined power flow models are linearised according to some assumptions that may lead to the wrong solution in our optimization problem (e.g., inaccuracy in the voltage or line flow values). In contrast, the convexified model has been proved to be an effective formulation for radial systems, since it converges in most cases to an optimal solution [37]. Furthermore, in the case of an infeasibility, the original problem is infeasible too, which is completely unknown in the other two linearised approaches. The c-BFM formulation is presented below. The voltage magnitudes are calculated as in (93). Note that complex angles are not considered explicitly since they can be uniquely retrieved in case of radial systems. The line flow constraint is relaxed and modeled as a second order cone constraint (94) to convexify the problem. Expressions eqs. (95) and (96) express the active and reactive power balance respectively. The overall nodal demand is expressed by eqs. (97) and (98). The operational limitations are also considered, like

current in lines (100), voltage deviations (99) and MV-LV transformer power (101). Finally, the c-BFM auxiliary variables (102) and (103) are presented.

$$v_j(t) = v_i(t) - 2 \cdot (r_{ij} \cdot P_{ij}(t) + x_{ij} \cdot Q_{ij}(t) + (r_{ij}^2 + x_{ij}^2) \cdot l_{ij}(t) \qquad \forall(i,j) \in E \qquad (93)$$

$$l_{ij}(t) \geq \frac{P_{ij}^2(t) + Q_{ij}^2(t)}{v_i(t)} \qquad \forall(i,j) \in E \qquad (94)$$

$$p_j(t) = P_{ij}(t) - r_{ij} \cdot l_{ij}(t) - \sum_{k:j \to k} P_{jk}(t) \qquad \forall j \in N \qquad (95)$$

$$q_j(t) = Q_{ij}(t) - x_{ij} \cdot l_{ij}(t) - \sum_{k:j \to k} Q_{jk}(t) \qquad \forall j \in N \qquad (96)$$

$$p_j(t) = p_j^D(t) + P_{EVSE}^{supplied}(i,t) - p_j^G(t) \qquad (97)$$

$$q_j(t) = q_j^D(t) - q_j^G(t) \qquad (98)$$

$$\underline{v}_b \leq v_b(t) \leq \overline{v}_b \qquad (99)$$

$$\underline{l}_{ij} \leq l_{ij}(t) \leq \overline{l}_{ij} \qquad (100)$$

$$\underline{p}_j \leq p_j \leq \overline{p}_j \qquad (101)$$

$$l_{ij}(t) = I_{ij}^2 \qquad (102)$$

$$v_b(t) = V_b^2 \qquad (103)$$

### 4.2.3  Optimization Model

The optimization model contains two main parts: the objective function and the constraints. In the objective function, we set the total system losses minimization as the system performance goal. Namely, in the convexified model, the objective function must strictly increase when the line current flow does. Then, the losses minimization is set as the optimization objective regardless of the power flow model deployed. Additionally, the energy not supplied is penalized to ensure maximum supplied EV demand. Both terms are combined in (104) proportionally to a penalization cost that must be appropriately selected.

$$f = \sum_{t=1}^{Horizon} \left[ C_{loss} \cdot \sum_{l=1}^{Lines} P_{loss}(l,t) \cdot h + C_{ns} \cdot \sum_{b=1}^{Buses} P_{EVSE}^{not\ supplied}(b,t) \cdot h \right] \qquad (104)$$

The performance of different cost values for a 33-bus IEEE scenario are shown in Table 5. Same cost factors of $0.1$ have been empirically proved to be the best in terms of number of iterations to solve an exemplary problem and to provide an optimal valid solution. Note that an infinite penalization cost for the energy not supplied seems to be the most obvious approach. However, the larger this value, the higher the computational load, since the problem becomes numerically

unstable. Furthermore, an infinite value forces the solver to ignore that term from the objective function and hence, the problem leaps into infeasible in cases of extremely high energy demand.

| $C_{loss}$ (€/kWh) | $C_{ns}$ (€/kWh) | Nr. Iterations | Time (sec) |
|---|---|---|---|
| 0,1 | 10 | 22 | 5,15 |
| 0,1 | 1 | 33 | 5,90 |
| 0,1 | 0,1 | 16 | 2,74 |
| 0,1 | 0,01 | 15 | 2,46 |
| 0,1 | 0,001 | 13 | 3,00 |

**Table 5.** Penalization costs and a performance example for the 33-bus IEEE system. The red marked terms relax excessively the energy not supplied penalization and some energy will not be supplied.

The objective function is subject to the distribution system constraints (voltages, line current flows and transformer power bounds) and to the charging station (EVSE) technical limitations and energy demand. The first set of constraints depends on the power flow model deployed from Section 4.2.2. The other set of constraints have been introduced in Section 4.2.1. Then, the controllable outputs are defined as $x = \{I_{line}, V, P_{transformer}, W_{EVSE}\}$ and the control variables as $u = \{P_{EVSE}^{supplied}, P_{EVSE}^{not\ supplied}\}$. The following expressions eqs. (105) to (107) represent the three optimization problem formulations:

### 4.2.3.1 DCPF OPF Problem Formulation:

$$minimize \quad eq.\ (104) \tag{105}$$

subject to

$$eqs.\ (75) to\ (82)$$

$$eqs.\ (70) to\ (74)$$

### 4.2.3.2 LACPF OPF Problem Formulation:

$$minimize \quad eq.\ (104) \tag{106}$$

subject to

$$eqs.\ (83) to\ (92)$$

$$eqs.\ (70) to\ (74)$$

### 4.2.3.3 c-BFM OPF Problem Formulation:

$$minimize \quad eq.\ (104) \tag{107}$$

subject to

$$eqs. \ (93) to \ (103)$$

$$eqs. \ (70) to \ (74)$$

Depending on the power flow model the objective function is linear (c-BFM (107)) or quadratic (DCPF (105) and LACPF (106)), and the problem can be modeled with Second-Order Cone Programming (SOCP) or Quadratic Programming (QP) respectively. Finally, the optimization problem is formulated with the YALMIP toolbox and solved with the academic Gurobi solver [11]. The solver is interfaced directly through YALMIP.

## 4.3  Scenarios Studied

For the validation of the algorithm, different scenarios are introduced in this section. The effectiveness of the algorithm is tested with different grid topologies and load diversity. The grid parameters are loaded directly from the cases of the MATPOWER library. The EV user behaviour and energy demand is estimated according to real data. The load and generation profiles are formed using distinct real measurements and weather data that was extracted from various sources. The section is divided in two subsections. First, the model inputs and their origin sources are presented. Finally, the grid topologies used to show the validity of this algorithm are stated.

### 4.3.1  Model Inputs

#### 4.3.1.1  EV Behaviour

As we explained in Section 4.2.1, the EV behaviour can be classified in 2 types: day or work and night or home charging schemes. There are different papers in the literature which use queueing theory to present realistic EV behaviour [45]. However, they consider arrival rates as the time the EV starts charging. For our case, this is insufficient since we look for the instant the EV is connected to the grid regardless of the charging status (ON or OFF). Moreover, they use charge duration, but the energy demanded is completely unknown since each EV can charge with different power rates.

In this work, EV charging behaviours have been taken into account and have been modelled with truncated normal distributions. First, we set a number of EV entities that will participate in the simulation (e.g. 200 EV users). Second, we assign the charging capabilities to these entities (e.g. charging phases, current rate). Third, we assign each user to a residential node and to a industrial/office/commercial node, in which will charge with home and work charging schemes respectively. Finally, the arrival and departure times for each scheme are generated randomly

with the truncated normal distributions from Table 6. In order to avoid very short driving times, we have fixed the shortest trip to 30 minutes from home to work and vice versa according to the EU mobility survey [12].

| Normal dist. | Mean | Deviation | Min. | Max. |
|---|---|---|---|---|
| Home departure (h) | 7 | 2 | 5 | 9 |
| Work arrival (h) | 8 | 2 | 6 | 10 |
| Work departure (h) | 18 | 2 | 16 | 20 |
| Home arrival (h) | 21 | 2 | 21 | 23 |

**Table 6.** Truncated normal distributions for home/work arrival and departure times.

On the other hand, the energy demand is calculated distinctively depending on the charging scheme. We combine the empirical charging duration from [45] and the EV power rate to estimate home charging demand. The empirical probability distribution function, which is depicted below in Figure 15, is obtained from a training set of 37 EVs. Alternatively, the work charging scenario is estimated according to the daily average work trip in Germany [46] and the estimated energy consumptions from different EV brands [47]. Both are modelled with the truncated normal distributions shown in Table 7.
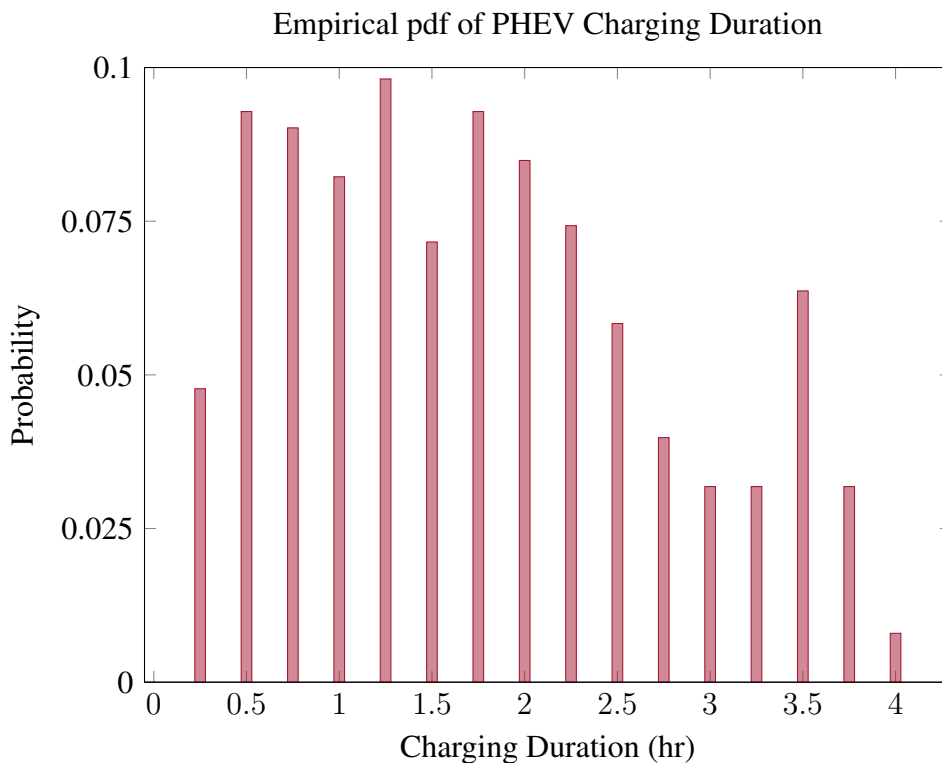


**Figure 15.** Empirical pdf for charging duration [45].

| Normal dist. | Mean | Deviation | Min. | Max. |
|---|---|---|---|---|
| Energy consumption (kWh/100km) | 22 | 5 | 12 | 32 |
| Driving distance (km) | 17 | 4 | 7 | 27 |

**Table 7.** Truncated normal distributions applied to estimate EV energy demand.

### 4.3.1.2 Load and DER Dynamics

In order to achieve realistic system behaviour, all the demand and generation profiles are based on different data sources. Due to the system size, one cannot obtain meaningful results without realistic dynamics. For that reason, we decide to collect deterministic data and trustworthy estimated profiles which represent the behaviour of the resources that are connected to the electrical system. The variety of loads included in this work are household, commercial, industrial, school and office loads. Alternatively, the generation profiles are either calculated with the formulas expressed in the previous Section 3 with some weather forecasts or real measurements. The time resolution varies depending on the data and hence, they are interpolated to reach the required resolution. Table 8 presents the information with regards to the data type, time resolution, date of measuring and the sources.

First, six different household loads, 3 industrial loads, a school load and hourly weather measures were extracted from the open power system data platform [49, 48, 56]. All the measures were taken in central Europe. Second, a set of 200 household randomly selected among the ones available in the 2009 RECS data set for the Midwest region of the United States is included. The profiles have been generated using the modelling proposed by Muratori et al. [57] that produces realistic patterns of residential power consumption, validated using metered data, with a resolution of 10 minutes [50]. Third, authors in [51] provided representative electrical load profiles of residential buildings in Germany with a temporal resolution of one second. These data include reactive household power consumption. Fourth, the tool [52] was used to reproduce 16 representative household profiles. Fifth, a set of industrial, commercial, office demand and generation profiles was extracted from the TERNI trial in the context of FINESCE [53, 54]. These profiles correspond to different customer types (e.g. industrial, commercial, offices) in Terni, Italy. Finally, the standard load profile for consumption in Germany was included to increase the heterogeneity, which corresponds to the representative power profile for a German household with $1\ MWh$ annual energy consumption. In summary, the whole set consist of: a pool of 297 household loads, 5 industrial loads, 2 commercial loads, 2 office loads, 1 PV industrial generation and 39 weather profiles.

| Type | Resolution (min) | Year | Source |
|---|---|---|---|
| Weather | 60 | 16-17 | OPS [48] |
| School | 1 | 16-17 | OPS [49] |
| Industrial load 1 | 1 | 16-17 | OPS [49] |
| Industrial load 2 | 1 | 16-17 | OPS [49] |
| Industrial load 3 | 1 | 16-17 | OPS [49] |
| Household GE 1 | 1 | 16-17 | OPS [49] |
| Household GE 2 | 1 | 16-17 | OPS [49] |
| Household GE 3 | 1 | 16-17 | OPS [49] |
| Household GE 4 | 1 | 16-17 | OPS [49] |
| Household GE 5 | 1 | 16-17 | OPS [49] |
| Household GE 6 | 1 | 16-17 | OPS [49] |
| 200 Households USA | 10 | 10 | [50] |
| 74 Households GE | 1 | 10 | [51] |
| CREST tool 16 H | 1 | - | [52] |
| Commercial Load 1 | 15 | 15 | FIWARE Lab Terna [53, 54] |
| Commercial Load 2 | 5 | 14-15 | FIWARE Lab Terna [53, 54] |
| Industrial Load 4 | 5 | 14-15 | FIWARE Lab Terna [53, 54] |
| Industrial Load 5 | 5 | 14-15 | FIWARE Lab Terna [53, 54] |
| Industrial Generation 2 | 5 | 14-15 | FIWARE Lab Terna [53, 54] |
| Office Load 1 | 5 | 14-15 | FIWARE Lab Terna [53, 54] |
| Office Load 2 | 5 | 14-15 | FIWARE Lab Terna [53, 54] |
| SLP | 15 | 14-15 | [55] |

**Table 8.** Input data sources: load, generation and weather time-series.

In the case the data do not include reactive power consumption for load, a random power factor ranged between two typical values from the literature has been assumed. Note that the probability of having inductive loads in the industry due to machinery is higher than in other schemes, for that reason lower power factors have been considered. On the other hand, the generation sources adopt a unity power factor in this work. Table 9 presents the power factor values according to the source type.

| Load Type | PF min | PF max |
|---|---|---|
| Household, School, Commercial and Office | 0.85 | 0.98 |
| Industrial | 0.75 | 0.95 |
| Wind and PV | 1 | 1 |

**Table 9.** Maximum and minimum Power Factors(PF) accordingly to the source.

Since the time granularity is not constant, all profiles were interpolated to reach one minute time resolution. Depending on the scenario, this granularity may be modified to values greater than one minute. Since the dynamics yield for distinct years, a representative day of winter is set as reference. Then, according to the scenario different loads can be aggregated per node. To produce representative household load profiles, a pack of 50 randomly selected profiles from the 293 household pool is aggregated. Thus, realistic household behaviours can be performed. Then, these profiles plus the standardized German profile are scaled depending on the number of households connected to the node. Alternatively, the other load types are uniquely scaled to the desired power rate and, in some cases, combined. The generation profiles that have been calculated according to Section 3 are scaled depending on the number of turbines or PV installation surface considered. Figure 16 presents the power demand profiles, whereas Figures 17 and 18 depict the wind and PV power profiles calculated accordingly to Section 3. Additionally, Table 10 presents the minimum, mean and maximum power values for the two day period analysed in this work.

The symbols regarding each kind of resource that can be connected to each node of the system are presented in Figure 19. These figures represent the different technologies that can be combined to define the customer behaviour that will be connected at each bus of the system. Moreover, the charging station symbol is included.

| Load Type | P min (kW) | P mean (kW) | P max (kW) |
|---|---|---|---|
| Household (H) | - | 50* | - |
| Industrial (I1) | 12.18 | 25.26 | 52.5 |
| Industrial (I2) | 1.14 | 3.8 | 11.46 |
| Industrial (I3) | 45 | 98.17 | 195 |
| Industrial (I4) | 22 | 194.97 | 861 |
| Industrial (I5) | 0 | 0.4 | 12 |
| Commercial (C1) | 378 | 4.07e+3 | 1.34e+4 |
| Commercial (C2) | 10 | 35.6 | 154 |
| Office (O1) | 16 | 117.78 | 563.43 |
| Office (O2) | 21 | 111.51 | 654 |
| School (Sc) | 16.02 | 88.18 | 189 |

**Table 10.** Minimum, Mean and Maximum power values of the representative loads. * This value corresponds to a set of 50 households.
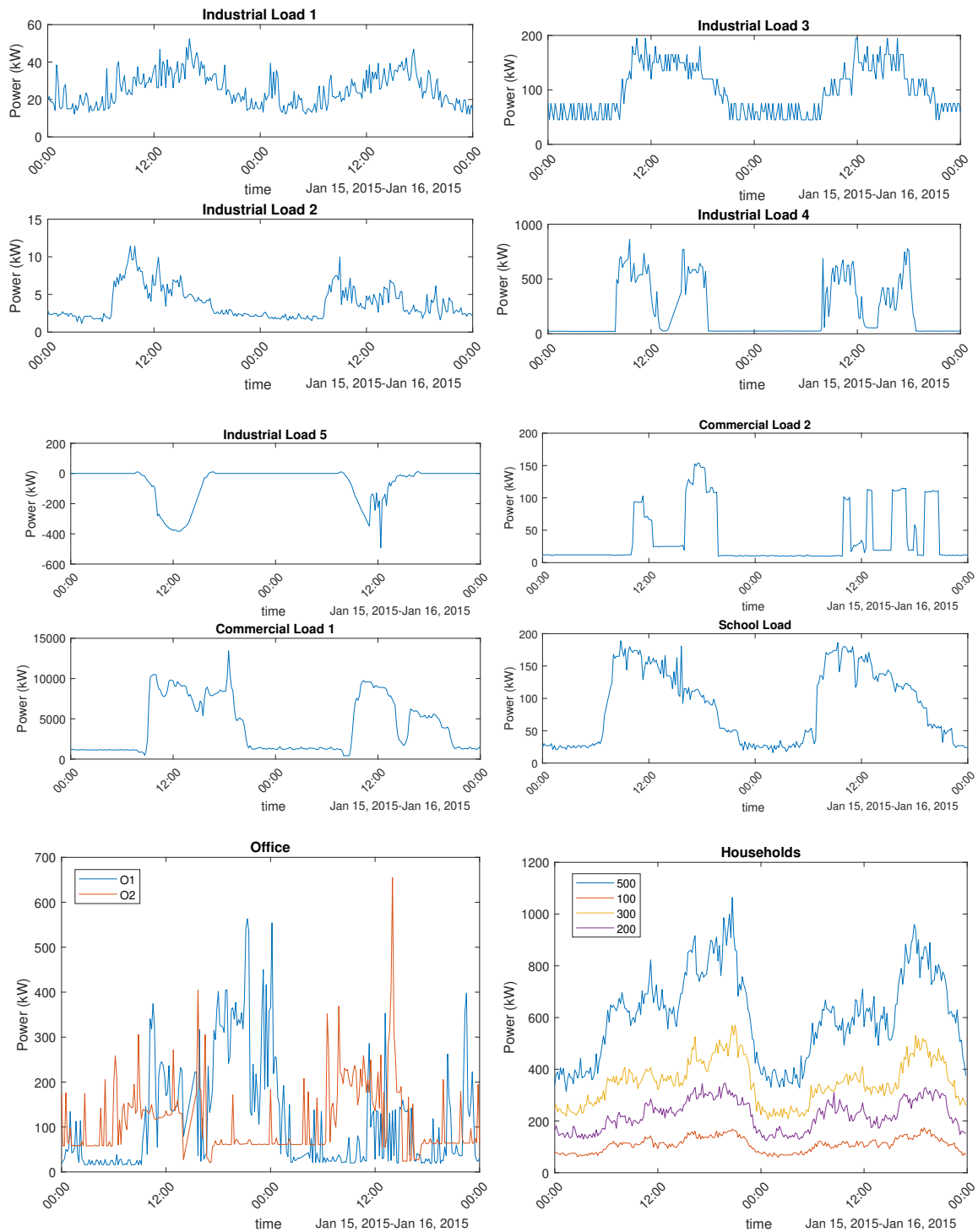
**Figure 16.** Representative power profiles (kW).

**Set of 39 wind profiles**
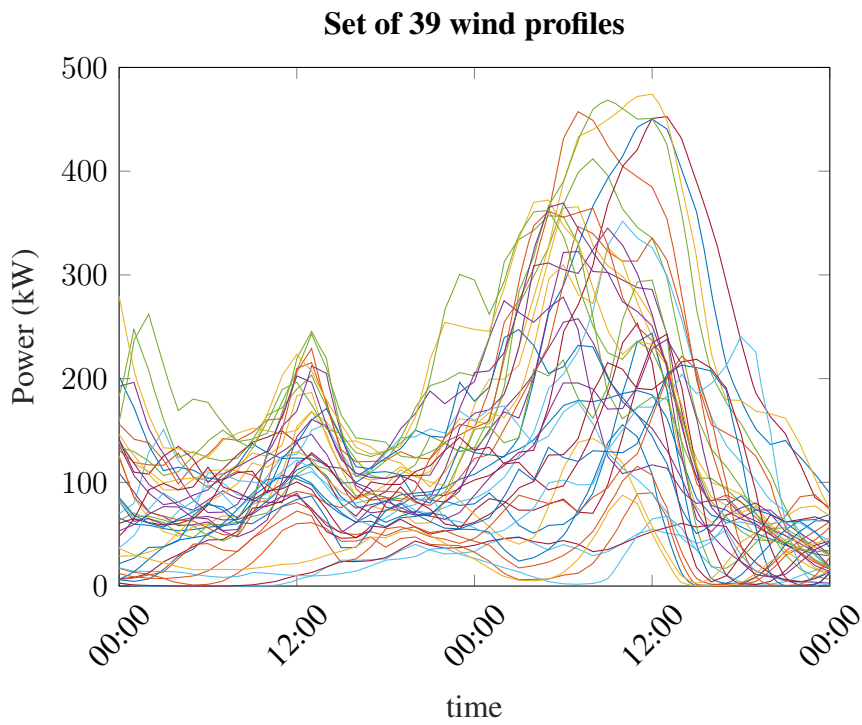


**Figure 17.** E40/500 operating at 39 different weather conditions.

**Set of 39 PV profiles**
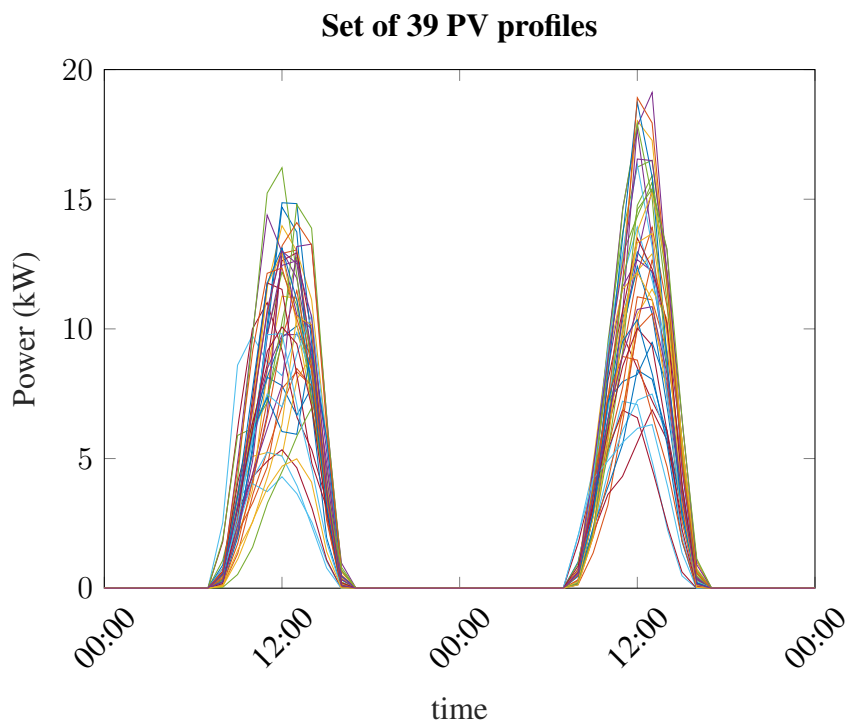


**Figure 18.** 39 distinct PV generation profiles according to (56) for a 200 $m^2$ surface.

Residential load

Industrial load

School load

Office Load

Commercial load

Wind generation

PV generation

Charging station (EVSE)
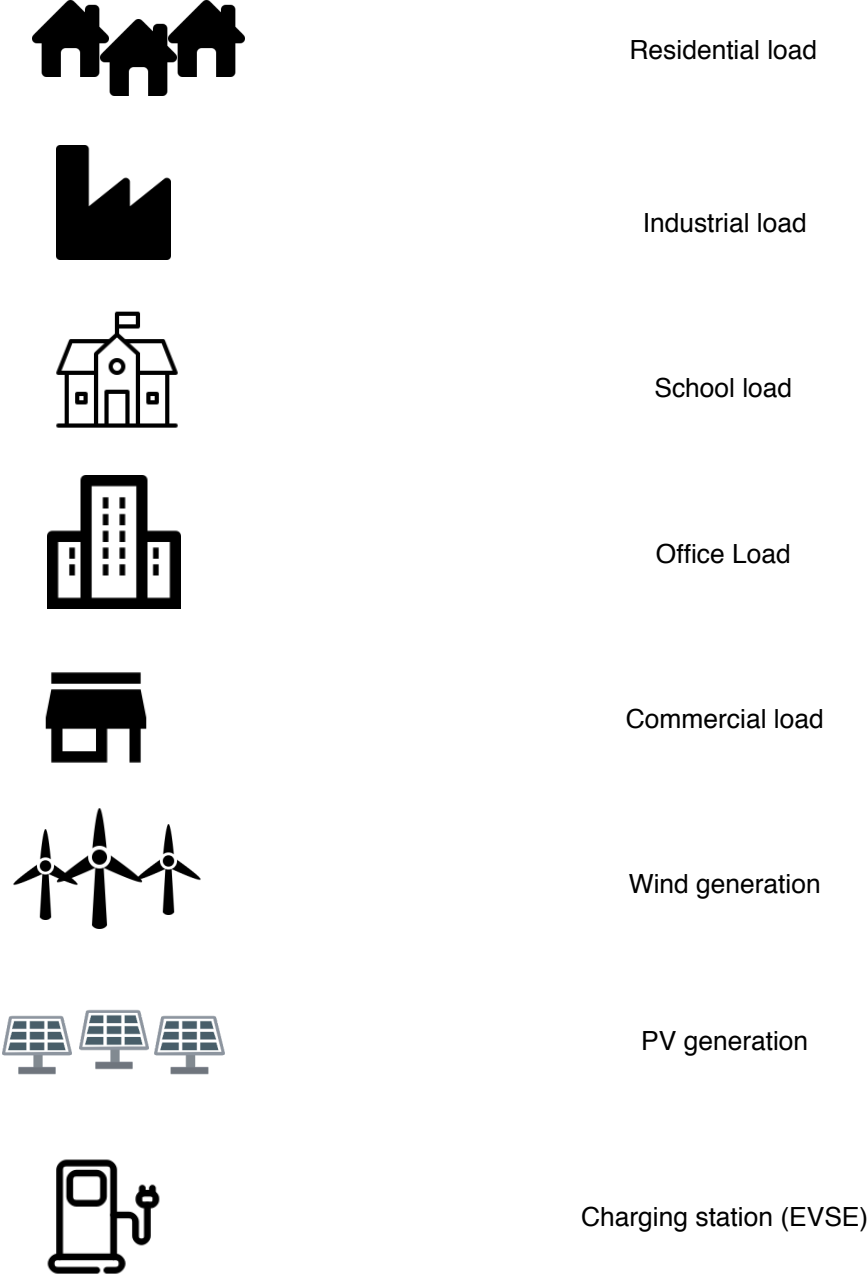
**Figure 19.** Type of customers or energy resources connected to the distribution system.

## 4.3.2   Grid Topologies

This section defines the different grid topologies studied and the resources connected at each node of the system. The grid parameters are directly obtained from the MATPOWER library [9]. The load, generation and EV demand is calculated as explained in previous chapters. The voltage limits are set similarly to the ones provided by MATPOWER (0.9 - 1.1 p.u.). For the sake of simplicity, the line thermal boundaries are set 30% greater than the maximal line current rates for each scenario without EV demand. Finally, the system bases for both scenarios are presented in the following Table 11.

| $S_{BASE}$ (MVA) | $U_{BASE}$ (kV) | $Z_{BASE}$ (Ohms) |
|:---:|:---:|:---:|
| 1 | 12,5 | 156,25 |

**Table 11.** Power system bases used in this work.

### 4.3.2.1   18-bus IEEE Case

The information regarding the original bus IEEE topology can be found in [58]. However, our system is slightly different to the one depicted in [58], since the grid parameters were extracted from MATPOWER library and they neglect the HV/MV transformer. In Figure 20, the original system is presented. This case was implemented in order to analyse the impact of voltage harmonics on a power system by using active filters to inject distortion-cancelling currents. The grid includes nodal capacitative elements and line admittances that are removed for our case, since we neglect them in our model.

Now, taking into account the power levels given in [58] for a single large distorting load (voltages between 1 - 0.85 p.u.), we define a realistic scenario for this system. Figure 21 and Table 12 presents all the resources connected per node and the nominal values respectively. The power values have been adapted to the ones given by the original system, so that ensure a realistic operation state.

The grid parameters are provided in the appendix of this thesis. As stated before, the line thermal boundaries are estimated assuming that each line is able to stand a current rate 30% greater than the one provided by the base case. Note that these values can be changed according to user requirements.
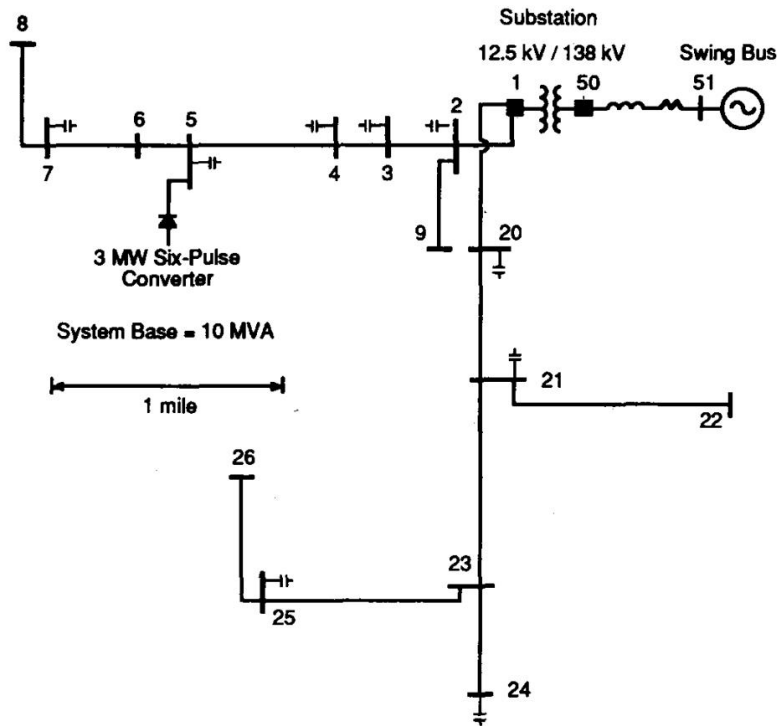
**Figure 20.** Original 18-bus IEEE system [58].

| Node | Customers | Nr. Houses | Load scale factor | Generation |
|:---:|:---:|:---:|:---:|:---:|
| 1 | - | - | - | - |
| 2 | - | - | - | - |
| 3 | - | - | - | - |
| 4 | H | 200 | - | - |
| 5 | H | 400 | - | - |
| 6 | H, C2 | 200 | 7 | - |
| 7 | C1 | - | 0.3333 | - |
| 8 | H, I1, I2 | 600 | 2 | PV I2 |
| 9 | H | 200 | - | - |
| 10 | O1 | - | 2 | - |
| 11 | H | 500 | - | - |
| 12 | H, C2 | 100 | 8 | - |
| 13 | H | 300 | - | Wind 4T |
| 14 | H | 200 | - | - |
| 15 | H,O2 | 250 | 1 | - |
| 16 | H | 450 | - | - |
| 17 | I3, I4, I5 | - | 1 | - |
| 18 | H, Sc | 150 | 1 | - |

**Table 12.** Type of customer and scale factors per node in the 18-bus IEEE system.
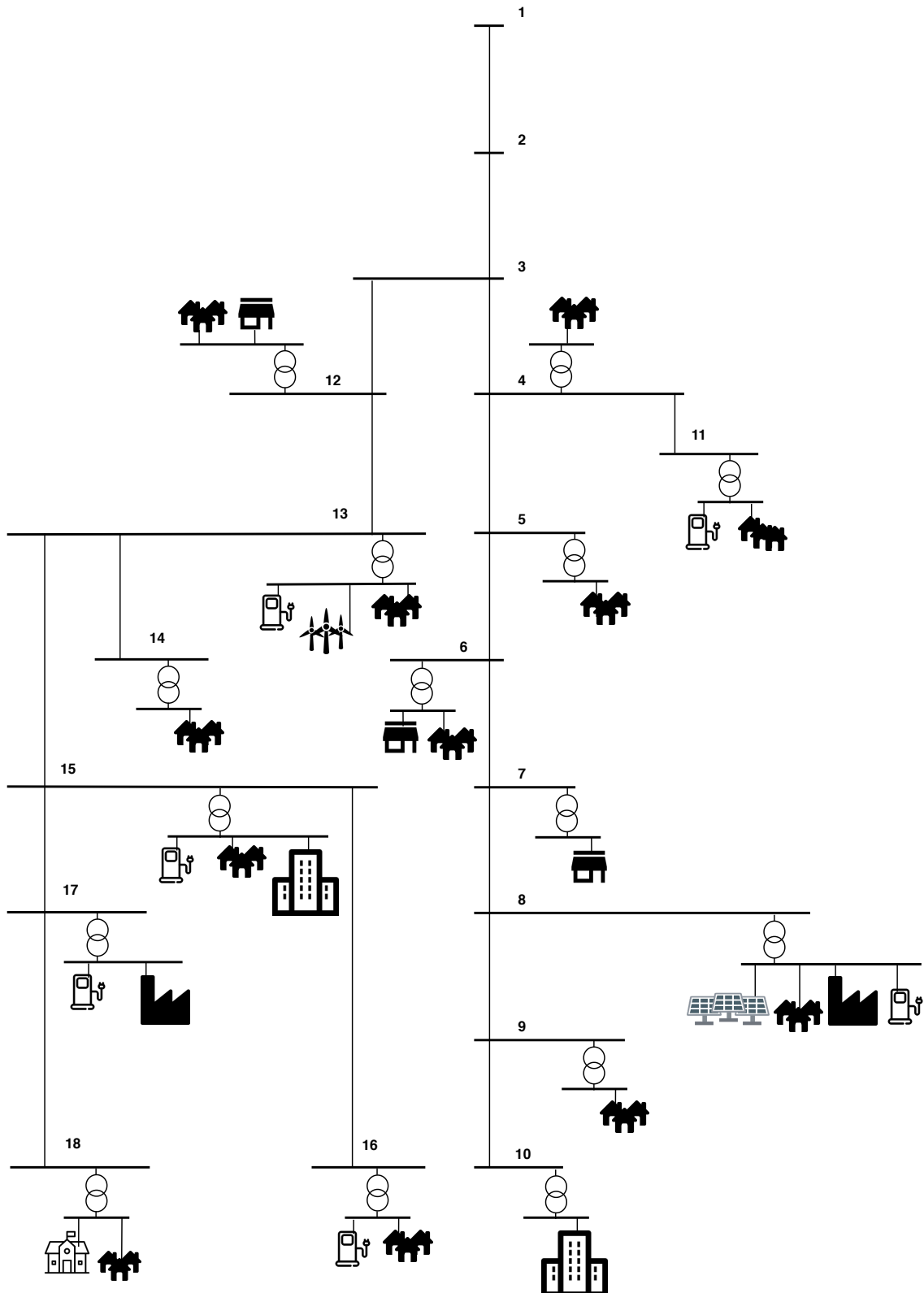
**Figure 21.** 18-bus IEEE grid topology with energy resources connected.

## 4.3.2.2 141-bus IEEE Case

This scenario consist of a radial distribution system in the metropolitan area of Caracas served by AES Corporation in Venezuela. The original case contains 231 nodes including sectioning, transformation and switching of the lateral. However, it was reduced to 141 eliminating the sectioning devices to accelerate calculations. All the information regarding the modified 231 or 141-bus IEEE topology is presented in [59]. The case was used to analyse the optimal location and sizing of static and switched shunt capacitors in radial distribution systems. Again, as in previous cases, the system dynamics will be set according to the values given in [59] for a normal operation state. Table 13 represents the type of customers and the scale factors used to build the scenario dynamics. Additionally, Figure 22 shows the grid topology scheme, but in this case only the charging stations and DER are depicted due to the case size. The grid parameters and the maximum current flow for the base case are provided in the appendix of this thesis.

| Node | Customers | Nr. Houses | Load Scale Factor | Generation |
|------|-----------|------------|-------------------|------------|
| 1  | -    | -  | - | - |
| 2  | -    | -  | - | - |
| 3  | -    | -  | - | - |
| 4  | -    | -  | - | - |
| 5  | -    | -  | - | - |
| 6  | -    | -  | - | - |
| 7  | -    | -  | - | - |
| 8  | H    | 60 | - | - |
| 9  | H    | 20 | - | - |
| 10 | -    | -  | - | - |
| 11 | -    | -  | - | - |
| 12 | H    | 30 | - | - |
| 13 | H    | 60 | - | - |
| 14 | -    | -  | - | - |
| 15 | -    | -  | - | - |
| 16 | -    | -  | - | - |
| 17 | C2,H | 50 | 1 | - |
| 18 | -    | -  | - | - |
| 19 | -    | -  | - | - |
| 20 | H    | 60 | - | - |
| 21 | H    | 60 | - | - |
| 22 | -    | -  | - | - |
| 23 | H    | 60 | - | - |
| 24 | -    | -  | - | - |
| 25 | -    | -  | - | - |

| Node | Customers | Nr. Houses | Load Scale Factor | Generation |
|------|-----------|------------|-------------------|------------|
| 26 | H,I1 | 50 | 2 | - |
| 27 | H | 60 | - | - |
| 28 | - | - | - | - |
| 29 | H | 60 | - | - |
| 30 | - | - | - | - |
| 31 | - | - | - | - |
| 32 | H,I3 | 50 | 1 | - |
| 33 | - | - | - | - |
| 34 | I4 | - | 1 | - |
| 35 | H,I5 | 200 | 10 | - |
| 36 | H,Sc | 50 | 1 | - |
| 37 | H | 50 | - | - |
| 38 | - | - | - | - |
| 39 | H | 40 | - | - |
| 40 | - | - | - | - |
| 41 | H | 60 | - | - |
| 42 | - | - | - | - |
| 43 | - | - | - | - |
| 44 | H | 50 | - | - |
| 45 | - | - | - | - |
| 46 | - | - | - | - |
| 47 | - | - | - | - |
| 48 | O2,H | 50 | 0,2 | - |
| 49 | H,C1 | 50 | 0,01 | - |
| 50 | - | - | - | - |
| 51 | H,I5 | 40 | 8 | - |
| 52 | H | 60 | - | - |
| 53 | H | 50 | - | - |
| 54 | - | - | - | - |
| 55 | - | - | - | - |
| 56 | H | 50 | - | - |
| 57 | - | - | - | - |
| 58 | I1,I3 | - | 1,5 | - |
| 59 | C2 | - | 1 | - |
| 60 | - | - | - | - |
| 61 | O1,H | 50 | 0,5 | - |
| 62 | H,O2 | 100 | 0,3 | - |
| 63 | - | - | - | - |
| 64 | H,C2 | 20 | 1,5 | - |

| Node | Customers | Nr. Houses | Load Scale Factor | Generation |
|------|-----------|------------|-------------------|------------|
| 65 | H | 150 | - | - |
| 66 | H,O1 | 200 | 0,1 | - |
| 67 | H | 50 | - | - |
| 68 | H | 80 | - | - |
| 69 | I1,I5,C2 | - | 2 | - |
| 70 | - | - | - | - |
| 71 | I4 | - | 0,4 | - |
| 72 | H,I5 | 200 | 2 | - |
| 73 | O2,O1 | - | 0,3 | - |
| 74 | H,C2 | 150 | 1 | - |
| 75 | H | 40 | - | - |
| 76 | H | 70 | - | - |
| 77 | O1 | - | 0,35 | - |
| 78 | - | - | - | - |
| 79 | I4 | - | 0,5 | - |
| 80 | O1,O2 | - | 0,6 | - |
| 81 | - | - | - | - |
| 82 | H | 150 | - | - |
| 83 | H | 60 | - | - |
| 84 | H,I1 | 150 | 2 | - |
| 85 | - | - | - | - |
| 86 | O1,I1,Sc | - | 2 (I1) , 0.5 (O1) | - |
| 87 | I5,I1,H | 50 | 2 | - |
| 88 | H | 60 | - | - |
| 89 | H | 50 | - | - |
| 90 | - | - | - | - |
| 91 | - | - | - | - |
| 92 | - | - | - | - |
| 93 | - | - | - | - |
| 94 | GEN | - | - | PV I2 |
| 95 | - | - | - | - |
| 96 | H | 150 | - | - |
| 97 | - | - | - | - |
| 98 | O1,H | 150 | 0,3 | - |
| 99 | - | - | - | - |
| 100 | O2,H | 150 | 0,33 | - |
| 101 | H | 10 | - | - |
| 102 | - | - | - | - |
| 103 | H | 100 | - | - |
| 104 | - | - | - | - |

| Node | Customers | Nr. Houses | Load Scale Factor | Generation |
|------|-----------|------------|-------------------|------------|
| 105 | I3 | - | 2 | - |
| 106 | Sc,H | 70 | 1 | - |
| 107 | C1 | - | 0,04 | - |
| 108 | - | - | - | - |
| 109 | C2 | - | 4 | - |
| 110 | O2 | - | 1 | - |
| 111 | H | 50 | - | - |
| 112 | O1 | - | 1 | - |
| 113 | GEN | - | - | Wind 7T + PV |
| 114 | - | - | - | - |
| 115 | - | - | - | - |
| 116 | I1,I5,C2 | - | 2 (I1,I5), 1 (C2) | - |
| 117 | H | 50 | - | - |
| 118 | - | - | - | - |
| 119 | H | 90 | - | - |
| 120 | - | - | - | - |
| 121 | - | - | - | - |
| 122 | - | - | - | - |
| 123 | GEN | - | - | Wind 10T |
| 124 | Sc | - | 1 | - |
| 125 | - | - | - | - |
| 126 | - | - | - | - |
| 127 | H | 60 | - | - |
| 128 | H | 60 | - | - |
| 129 | H | 90 | - | - |
| 130 | H | 90 | - | - |
| 131 | - | - | - | - |
| 132 | GEN | - | - | Wind 5T |
| 133 | H,I5 | 100 | 1 | - |
| 134 | O1,H | 30 | 0,01 | - |
| 135 | H | 20 | - | - |
| 136 | H | 60 | - | - |
| 137 | H | 50 | - | - |
| 138 | H | 50 | - | - |
| 139 | H | 50 | - | - |
| 140 | H | 150 | - | - |
| 141 | H | 70 | - | - |

**Table 13.** Type of customer and scale factors per node in the 141-bus IEEE system.
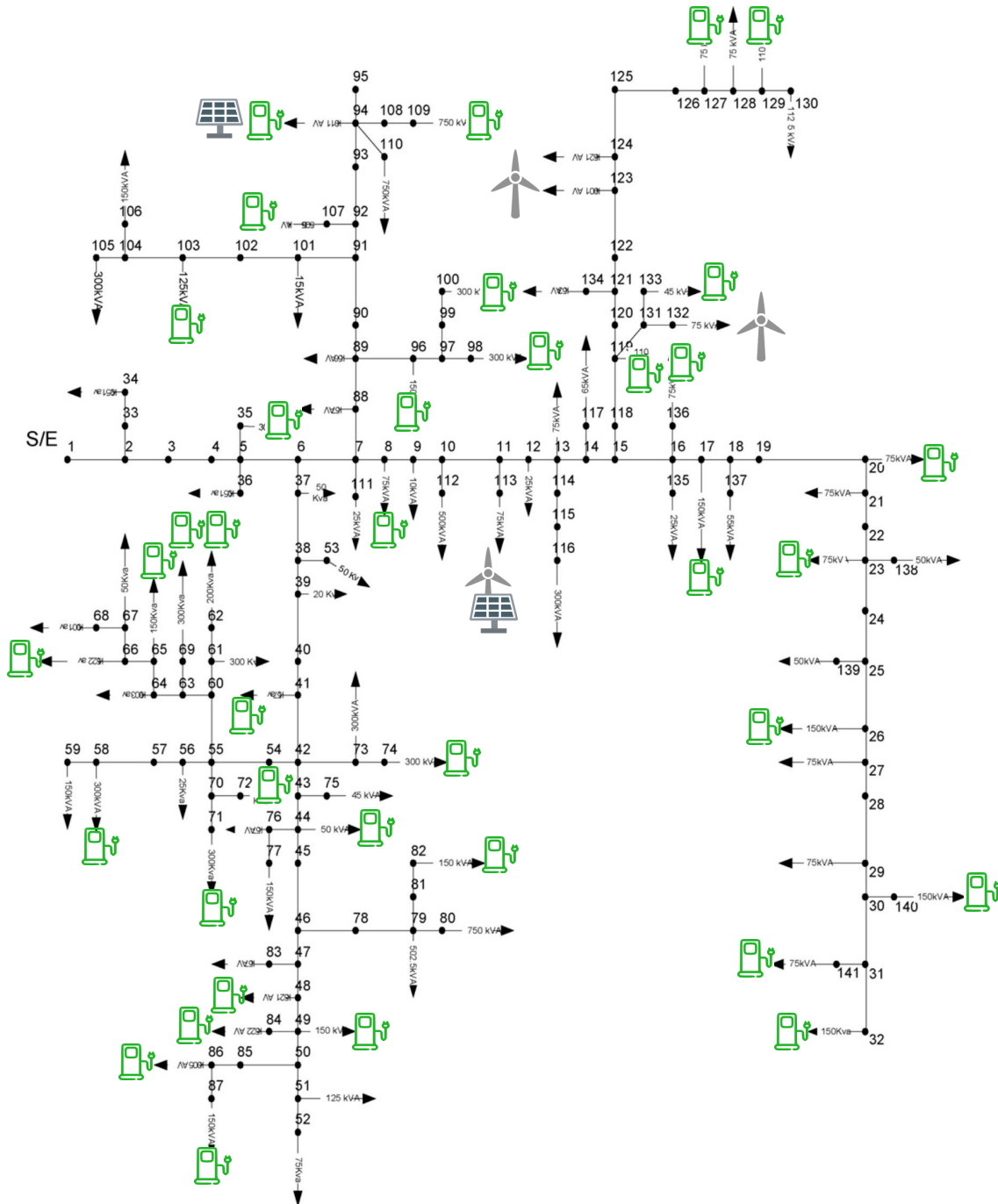
**Figure 22.** 141-bus IEEE grid topology only with Charging Stations and DER connected.

# Chapter 5

# Evaluation

This chapter aims at evaluating the algorithm performance. First, the power flow models are compared, and the convexified BFM is proved to be the best candidate for real-time applications. Second, the control is implemented in a low EV penetration scheme (4%-6% of total system demand). Third, the EV energy demand is increased to simulate a high demand scheme (13%-15% of total system demand). Both cases are applied to each scenario defined in the previous Chapter 4. The distribution of EV demand among the different nodes of the system for each scenario and case is provided in the appendix of this work. The simulation length is set approximately to one day and a half including two night and one-day charging schemes. The simulation starts at 7 p.m in the first day and ends at 9 a.m in the third day when the last EV is fully charged. The control is implemented with and without EV arrival forecast. The EV user is supposed to leave after or at the departure time, but never earlier. Finally, the results are compared to the base case without EV demand and to an uncoordinated charging scheme assuming that the EVs charge once connected to the system.

Note that the control horizon and prediction horizon is set to 6 hours since it presents positive results with relatively low computation burden as presented in Section 5.3. The time step is set to 10 minutes, to avoid abrupt changes on the curves generated by the EV aggregate model presented in Section 4.2.1. Optimization was performed on a PC with an Intel(R) Core(TM) i7-7500, 2.7 GHz CPU 8 GB RAM.

## 5.1   Power Flow Model Performance Comparison

The comparison is performed on the 18-bus IEEE scenario including EV arrival forecast and for a low EV demand scheme (see next section for further details). The power flow results are compared to the ones obtained by MATPOWER for the same system conditions. The errors are calculated according to the deviation to MATPOWER's results.

Table 14 presents the performance of the optimal power flow algorithms for a time horizon of 38 hours starting at 19.00 and for each power flow model. The results of the convexified BFM are exact, whereas the ACPF and DCPF include considerable errors on the line values. This error is due to the approximation of the line current to the active power (DCPF) and apparent power (LACPF) in the line. The voltage results of the LACPF are better with regards to the DCPF, in which the maximum voltage error increases notably. On the other hand, the optimization outputs are similar for the three approaches. The c-BFM ensures optimal global, while the other approximations stay nearby. Figure 23 depicts the total EV power demand for the first 6 hours.

| 18-IEEE | c-BFM | LACPF | DCPF |
|---|---|---|---|
| OPF model losses (MWh) | 3,366 | 3,473 | 2,731 |
| Losses - MATPOWER (MWh) | 3,366 | 3,367 | 3,368 |
| Losses deviation (%) | 0% | 3,50% | -18,86% |
| Avg. Current deviation (%) | 0% | 2,32% | 7,97% |
| Max. Current deviation (%) | 0% | 62,09% | 129,47% |
| Avg. voltage deviation (%) | 0% | 0,26% | 2,29% |
| Max. voltage deviation (%) | 0% | 1,23% | 5,69% |

**Table 14.** Power flow performance comparison with regards to the optimization model.
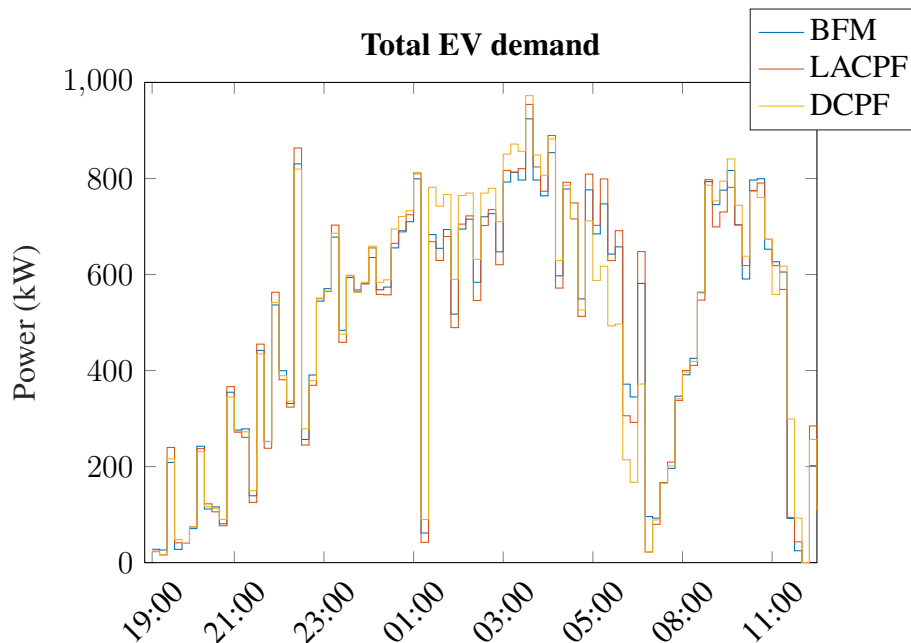


**Figure 23.** Power flow performance comparison with regards to the optimization model.

As shown in Figure 23, the linearised approaches differ from the optimal solution. However, as presented in Table 14 the exact value of the total system losses (Losses - MATPOWER) is similar for the three approaches. The LACOPF has an error of 0.0463% and the DCPF of 0.0524% compared to the global optimal. As expected, the LACPF loss approximation presents a better performance with regards to the DCPF approximation.

Figure 24 includes all the voltage linearisation errors of the LACPF for the simulation horizon. As seen in the Figure, the voltage error increases as the system voltage level strays away from the reference value of the slack (1.05 in this case). Note that the gap between 1.05 p.u. and 1.04 p.u. is due to the resistance value of line 2. The resistance of line 2 is approximately 10 times bigger than the one from line 1.
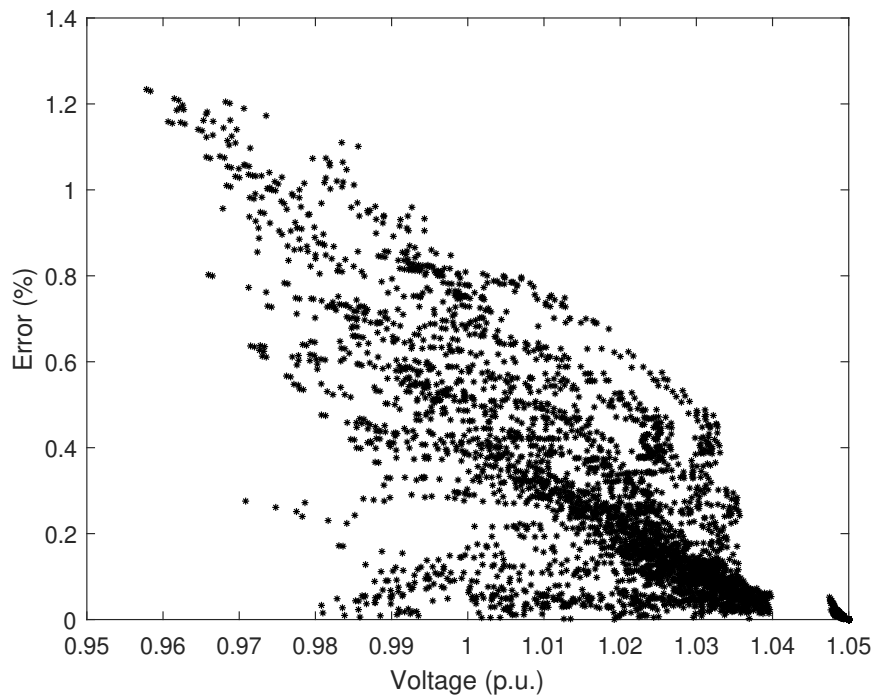


**Figure 24.** LACPF voltage linearisation error for the whole simulation horizon.

In conclusion, the DCPF would not be a suitable model for real-time application as expected since the error on lines and voltages is not acceptable. On the other hand, the LACPF presents a better performance for calculating the voltage magnitudes, but the line current approximation is still unacceptable. Thus, future works could include trust-region and sequential optimization techniques as in [33] to improve the performance of the linearised ACPF model. Using this approach may lead to considerable increasing computational efforts. However, in this work, the convexified BFM is set as the default power flow model, since its performance is exact and hence, the line currents and nodal voltages can be accurately monitored.

## 5.2   Scenario Analysis

### 5.2.1   Case 1: Low EV Demand

#### 5.2.1.1   18-bus IEEE Scenario

In this scenario, six charging stations are established in the nodes 8, 11, 13, 15, 16, and 17 as depicted in Figure 21. The EV fleet consists of 1000 vehicles, and the total EV energy demand represents the $4.26\%$ of the total system demand for the given simulation period. For this number of EVs, one out of three houses owns an EV. Table 15 shows the system losses for the given time frame according to each charging strategy. Note that the loss reduction percentage presents the decrease of total system losses if the optimal charging scheduling is applied instead of the uncoordinated scheme.

| Losses (MWh) | Base | Unc | wF | F |
|---|---|---|---|---|
| TOTAL | 3,06 | 3,58 | 3,37 | 3,36 |
| $KPI_{losses}$ | - | - | 5,84% | 6,02% |

**Table 15.** 18-bus IEEE Low EV demand case - System losses.

According to Table 15, the system losses decrease around 6% for both coordinated schemes compared to the uncoordinated strategy. Using arrival forecast may reduce up to 10 kWh in comparison with the strategy without forecasts. Thus, the improvement, in this case, is not noteworthy.

Table 16 presents the number of line constraint violations for the bounds defined in Section 4.3. It shows that the algorithm avoids system congestions while the uncoordinated scheme exceeds the line thermal limits 6 times. The uncoordinated strategy congests any line as it does not consider the network state. In contrast, both coordinated schemes include thermal line boundaries. Thus, it never exceeds any line limit. Moreover, it tries to reduce congestions as an effect of minimizing losses. The control tries to keep the current at its minimum rate as the losses increase quadratically with the current magnitude.

| Line Congestion | Unc. | wF | F |
|---|---|---|---|
| **1.3 x** $I_{BaseCase}^{MAX}$ | 6 | 0 | 0 |

**Table 16.** 18-bus IEEE Low EV demand case - Line congestions

On the other hand, the line current flow variability decreases in the coordinated scheme for all the lines connected downstream to a charging station. As depicted in Figure 25, this effect is notably noticed in the lines where the EV demand represents a significant percentage of the

power flow, such as lines 10 and 15 where 12.47% and 12,87% of the energy flow is EV demand respectively. Nonetheless, this effect is reduced in the lines where the EV demand is a lower portion of the power flow, such as lines 1 or 2 with a portion of 4,2% of EV energy demand. The lines that are not connected downstream to a charging station remain constant. Similarly, the voltage variations are decreased in the coordinated schemes. In Table 17, the average line current, and voltage variability are presented for each charging strategy. Additionally, Figure 26 and Table 18 present the voltage curve and variability of the most representative node with maximum variability for each case.

| Average Variability | Base | Unc. | wF | F |
|---|---|---|---|---|
| $KPI_{CV}$ Current | 48,81% | 50,93% | 44,42% | 44,22% |
| $KPI_{CV}$ Voltage | 1.506% | 1.5544 % | 1.47% | 1.464% |

**Table 17.** 18-bus IEEE Low EV demand case - Line current variability.

| Maximum Variability | Base | Unc. | wF | F |
|---|---|---|---|---|
| Node 18 | 2,19% | 2,32% | 2,11% | 2,10% |

**Table 18.** 18-bus IEEE Low EV demand case - Bus with maximum voltage variation.
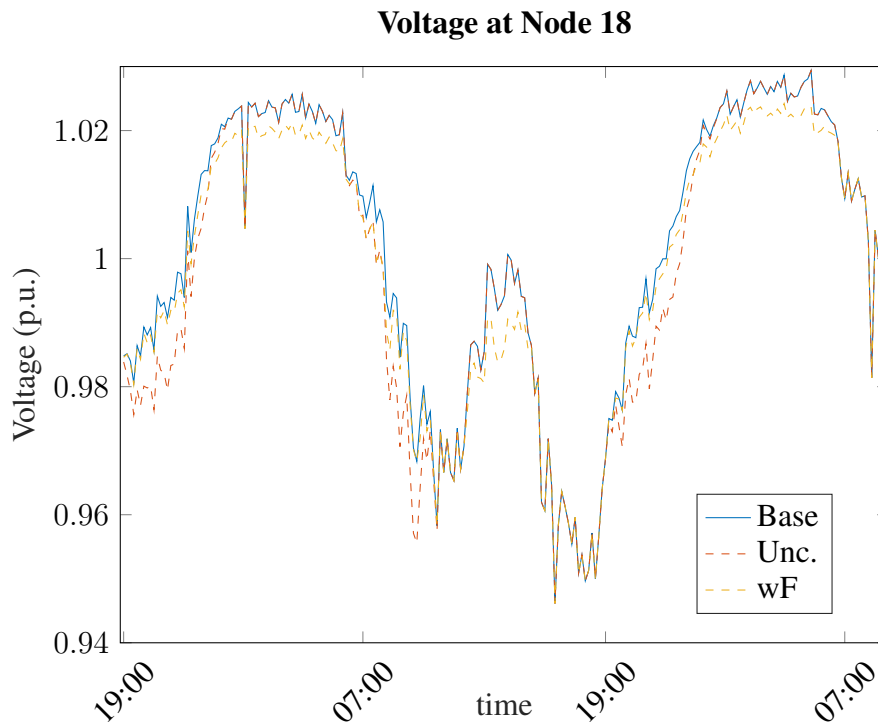
### Voltage at Node 18



**Figure 26.** 18-bus IEEE Low EV demand case - Voltage profile of node 18.
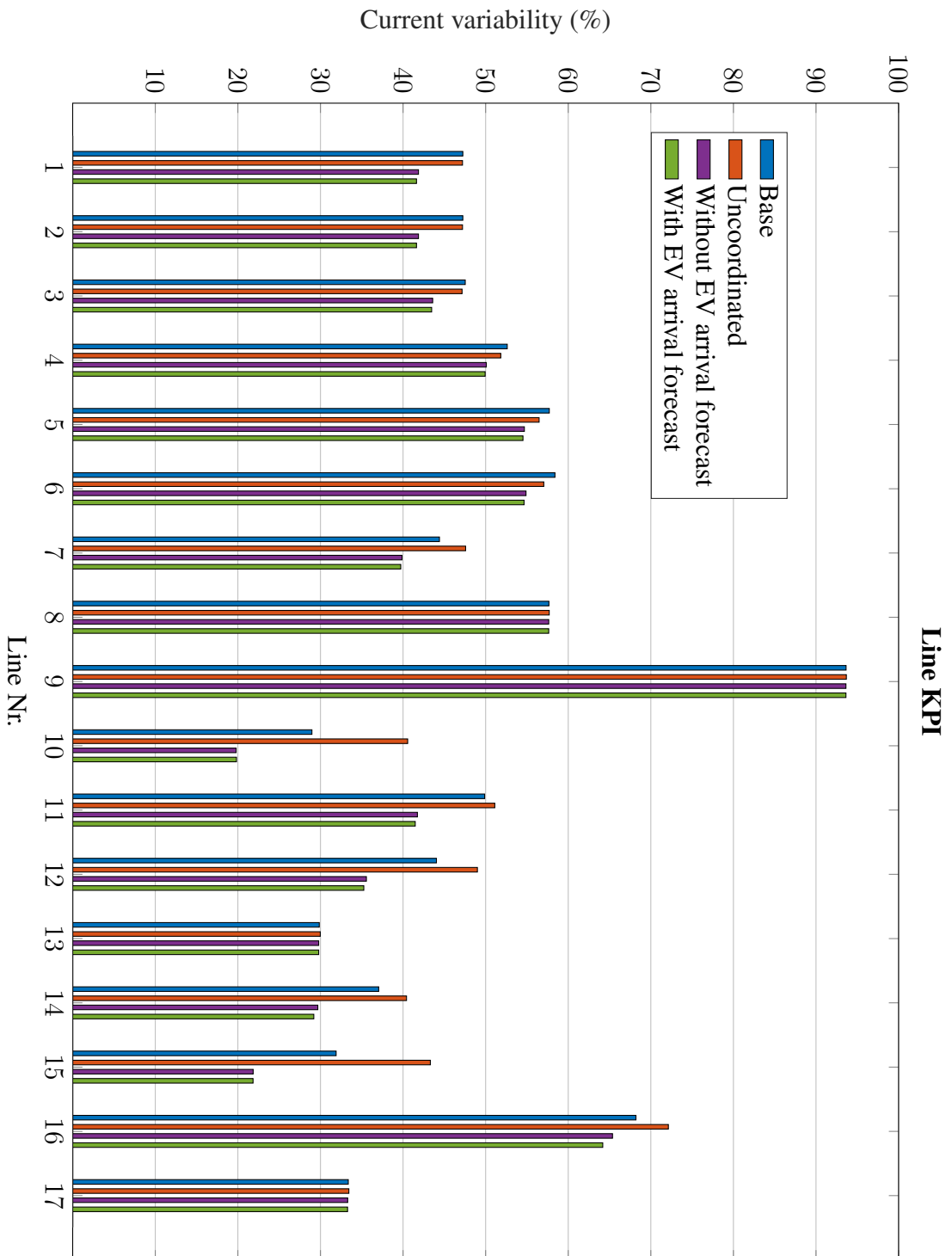
**Figure 25.** 18-bus IEEE Low EV demand case - Line current variability.

Another effect of minimizing losses in a radial system is the remarkable peak shaving[1] in the slack bus as presented in Figures 27 and 28. In this case, the parent line (Line 1) reaches the highest power flow levels since most of the energy demand must flow through it. Thus, the control avoids increasing the current flow during peak demand hours. On the contrary, the uncoordinated scheme increases the system demand peaks as expected from previous works. Therefore, the algorithm reduces the imported power variability up to 8% compared to the uncoordinated scheme and around 7% to the base case. This reduction is a positive effect that diminishes the overloads of the transformer that connects the distribution system to the upper grid. However, this effect depends strongly on the percentage of RES of the system. Then, if the parent lines do not provide most of the total system energy the effect might be mitigated.



**Figure 27.** 18-bus IEEE Low EV demand case - Power imported in the reference bus (kW).

---

[1]In the energy industry, peak shaving refers to leveling out peaks in electricity use by industrial and commercial power consumers. [60].
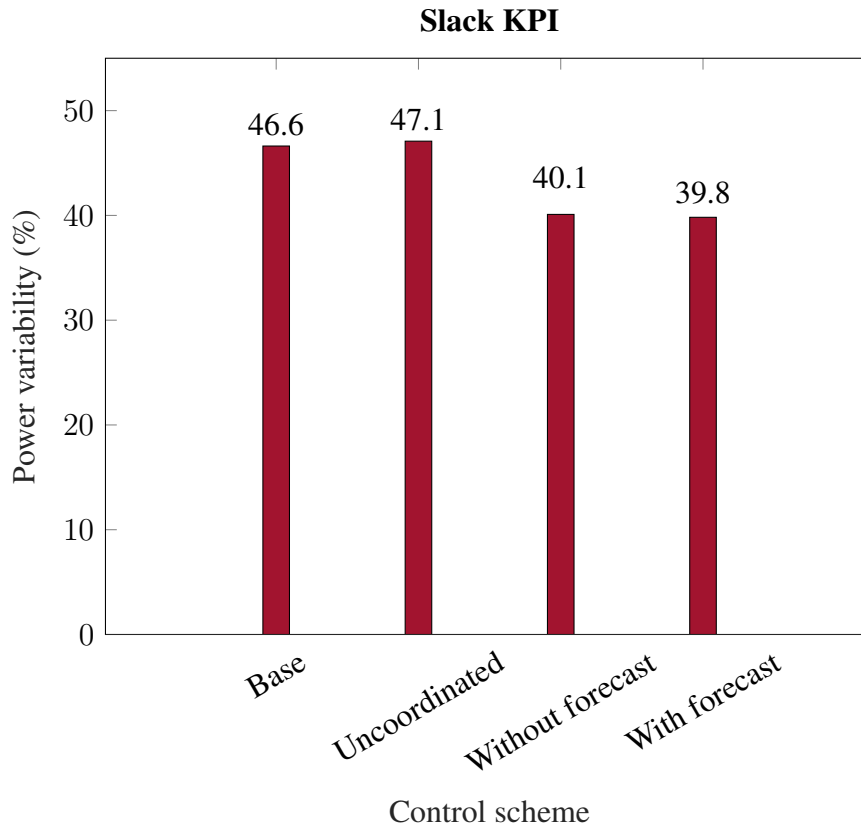
**Figure 28.** 18-bus IEEE Low EV demand case - Power imported variability at slack.

Furthermore, one can observe in Figure 27 that the algorithm does not entirely apply valley filling[2] at the slack bus. All the charging stations must cha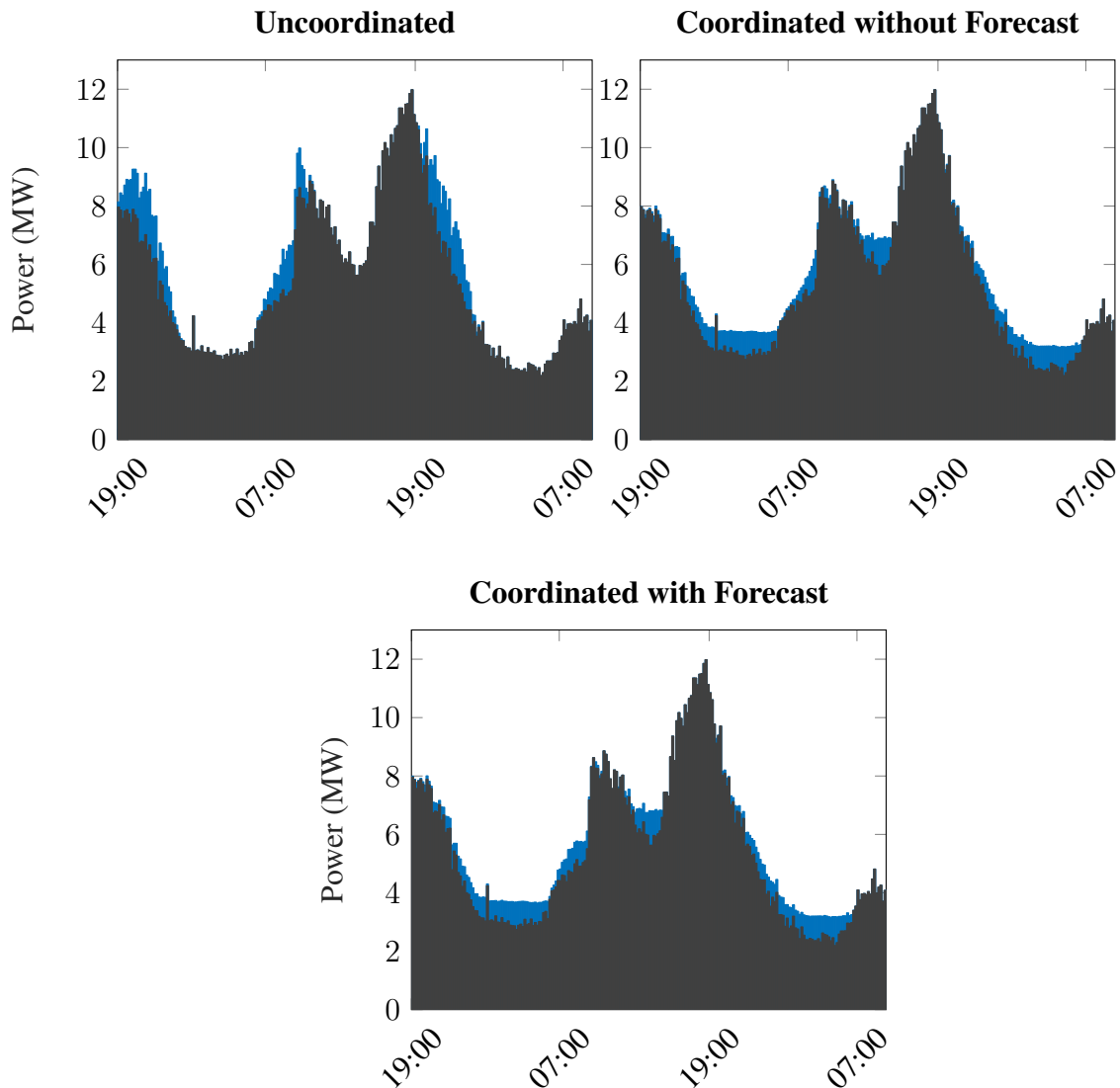rge at least at the minimum rate to fulfil the minimum EV accumulative energy constraint. Thus, a full valley filling cannot be achieved.

In the same Figure 27, looking at around 1.00 a.m, the charging station number 11 decides to charge while the rest of the charging stations avoid charging. Note that the overall system reaches a demand peak by this time. On the one hand, the minimum EV accumulative energy constraint forces the algorithm charging to avoid a constraint violation. On the other hand, even though charging station number 11 could charge before, it did not. In this particular case, during that time step, the overall system demand increases, whereas the demand at node 11 decreases. Thus, from the line number 10 perspective is more optimal to charge with the minimum power rate at 1.00 a.m than when the line is more loaded. In the end, the decision of charging is affected by the overall system state. Figure 29 presents the power profile at slack, increasing the peak at 1.00 a.m two times. As shown in the Figure, the bigger the peak, the more the decision of charging is affected. Now charging station 11 does not charge during this period, because it would considerably increase the total system losses. Figure 30 depicts the power flow in line 10 for both cases.

---

[2]A form of load management that involves building off-peak loads [61].

**Imported Power at slack**
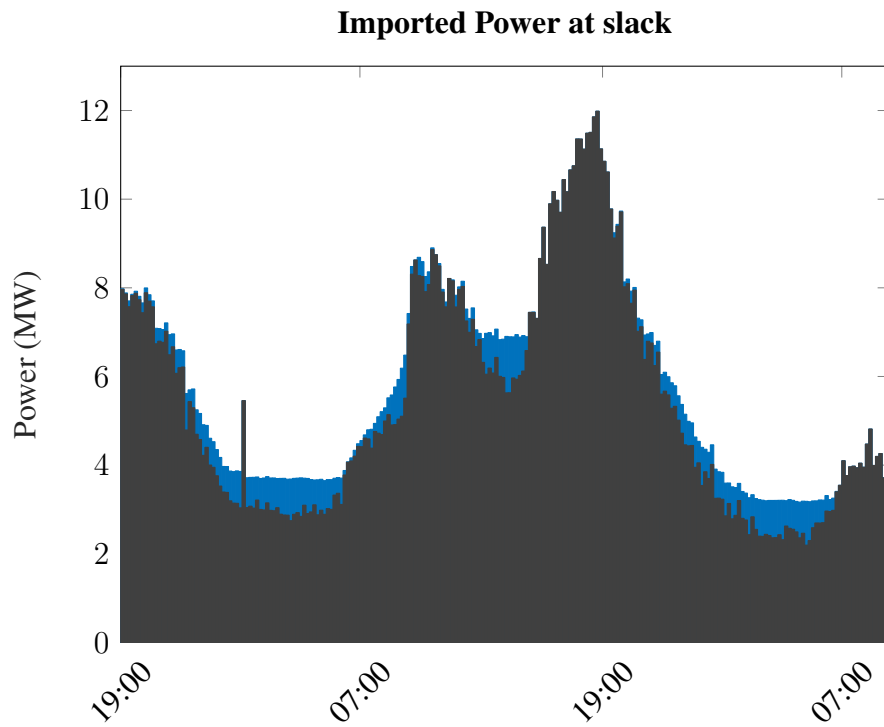


**Figure 29.** 18-bus IEEE Low EV demand case - Power imported in the reference bus (kW) increasing two times the demand peak at 1.00 a.m.
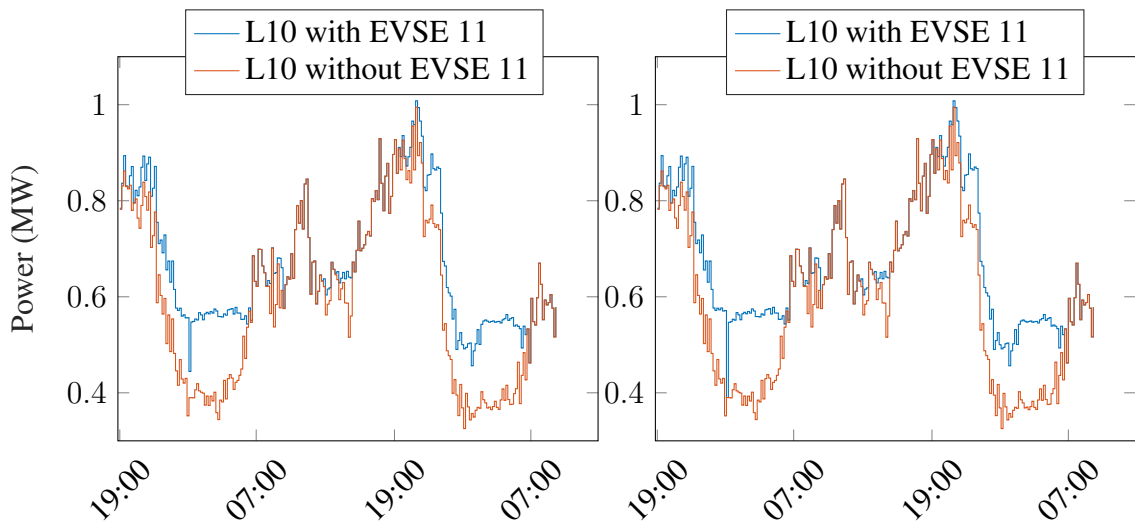


**Figure 30.** 18-bus IEEE Low EV demand case - Power flow of line 10 with and without EVSE demand. On the left, the power flows for the normal scenario. On the right, the power flows for the increased peak at 1.00 a.m.

Moreover, one cannot ensure peak shaving in all the nodes of the system. As mentioned before, the objective of loss minimization tends to allocate EV demand to reduce line current flow peaks. Thus, depending on the dynamics and magnitudes of the nodal loads, the algorithm focuses on the lossy lines adapting the flexible demand according to them. Figures 31 and 32 present a clear example of this effect. Nodes 8, 9 and 10 present a small percentage of demand compared to node 7, which consists of a big commercial load. Since node 8 includes PV generation, the daily net demand is reduced noticeable compared to the daily demand of node 7. Then, if there were nodal Peak Shaving, the control would charge when the generation surplus happens. However, from a line perspective is better to charge before the commercial load reaches the huge peak of 5 MW avoiding in this way overloading line 6. Therefore, the control applies peak shaving on the nodes where the charging stations are complemented with big loads, whereas in nodes with smaller loads are allocated according to these representative nodes of the system.
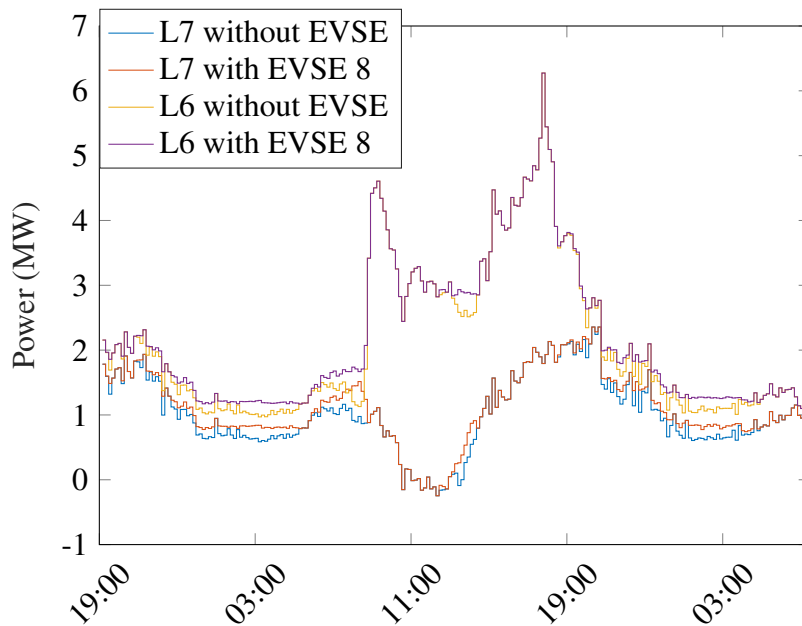


**Figure 31.** 18-bus IEEE Low EV demand case - Power flow of lines 6 and 7 with and without EVSE demand.
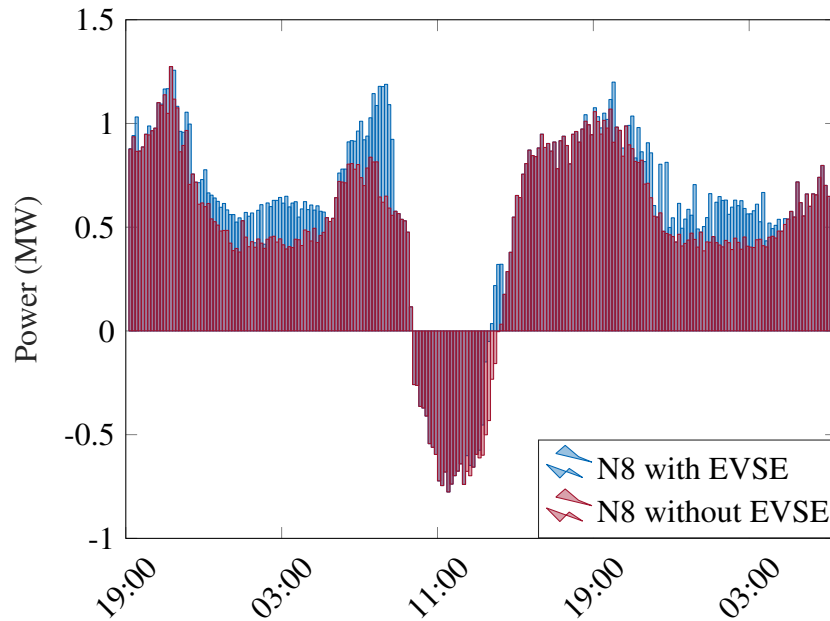
**Figure 32.** 18-bus IEEE Low EV demand case - Nodal power of node 8 with and without EVSE demand.

Last but not least, Table 19 presents the time performance of this case. There is a minor variation between the strategy with and without forecasts. The time performance is quite suitable for this real-time application since the response takes less than 1 second.

| Time (sec) | Max. | Min. | Avg. |
|---|---|---|---|
| Without Forecast | 0,433 | 0,175 | 0,252 |
| With Forecast | 0,594 | 0,219 | 0,292 |

**Table 19.** Control time performance for the 18-bus IEEE Low EV demand case with 6 charging stations.

### 5.2.1.2 141-bus IEEE Scenario

In this case, the scenario is compounded by 37 charging stations distributed in the nodes 8, 17, 20, 23, 26, 32, 35, 41, 44, 48, 49, 58, 62, 65, 66, 69, 71, 72, 74, 82, 84, 86, 87, 94, 96, 98, 100, 103, 107, 109, 119, 127, 129, 133, 136, 140 and 141 according to Figure 22. The EV fleet consists of 1790 EVs and the total EV energy demand represents the 6,24% of the total system demand for the given simulation period. Again as in the previous case, approximately one out of three households owns an EV. Table 20 shows the system losses for each charging strategy.

In the same way as before, the losses decrease for the coordinated schemes. The system size has increased to 141 nodes and 140 lines. As a result, the total losses are more significant than the previous scenario, even though the EV demand percentage is similar.

| Losses (MWh) | Base | Unc. | wF | F |
|---|---|---|---|---|
| TOTAL | 5,70 | 7,08 | 6,48 | 6,47 |
| $KPI_{losses}$ | - | - | 8,59% | 8,69% |

**Table 20.** 141-bus IEEE Low EV demand case - System losses.

On the other hand, Table 21 presents the number of line constraint violations. Both coordinated schemes keep the line flows under the thermal boundaries avoiding constraint violations. In contrast, the other approach exceed the line thermal limits 209 times, which can have negative impacts on the system.

| Line Congestion | Unc. | wF | F |
|---|---|---|---|
| **1.3 x** $I^{MAX}_{BaseCase}$ | 209 | 0 | 0 |

**Table 21.** 141-bus IEEE Low EV demand case - Line congestions

As a consequence of the voltage and line flow variability decrease presented in Table 22, the charging stations charge in the periods when the voltage tends to increase. Thus, the control tends to reduce over-voltages. Figure 33 and Table 23 present the voltage curve and variability of the most representative node with maximum variability for each case.

| Average Variability | Base | Unc. | wF | F |
|---|---|---|---|---|
| $KPI_{CV}$ Current | 45,06% | 48,59% | 41,21% | 40,96% |
| $KPI_{CV}$ Voltage | 0.941% | 1.097% | 0.857% | 0.853% |

**Table 22.** 141-bus IEEE Low demand case - Line current and voltage variability.

| Maximum Variability | Base | Unc. | wF | F |
|:---:|:---:|:---:|:---:|:---:|
| Node 52 | 1,22% | 1,42% | 1,11% | 1,10% |

**Table 23.** 141-bus IEEE Low EV demand case - Bus with maximum voltage variation.
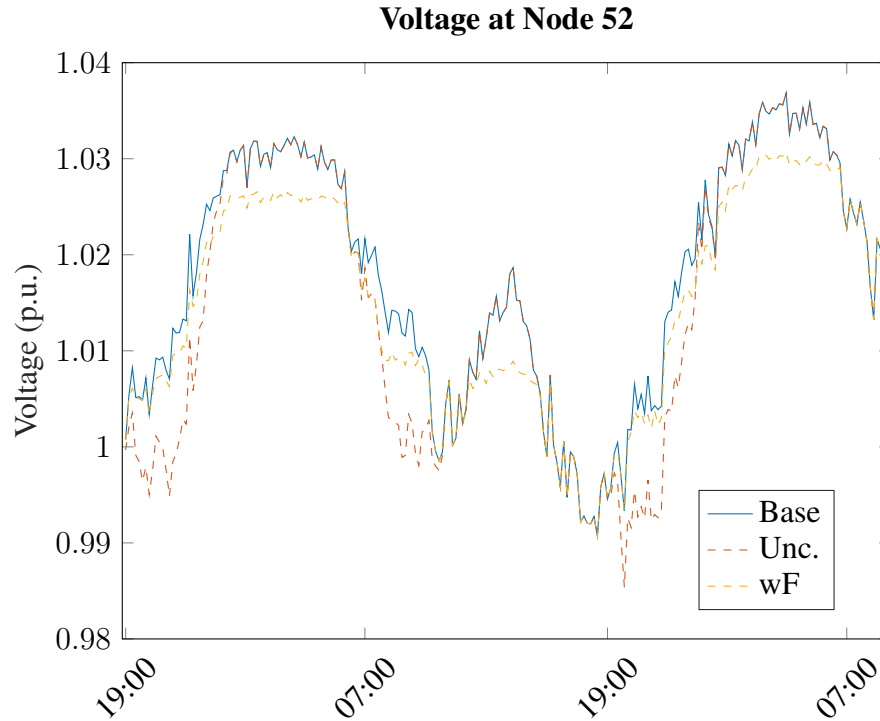


**Figure 33.** 141-bus IEEE Low EV demand case - - Voltage profile of node 52.

Regarding the Peak Shaving effect in the slack bus, in this case, the algorithm presents an improvement up to 12% including forecast and 11% without forecasts. Figures 34 and 35 present clear evidence of the expected effect on the overall distribution system demand. Around 22.00 on the second day, the uncoordinated scheme increases the system peak notably whereas the coordinated schemes avoid this time to charge.

**Uncoordinated**

**Coordinated without Forecast**

**Coordinated with Forecast**
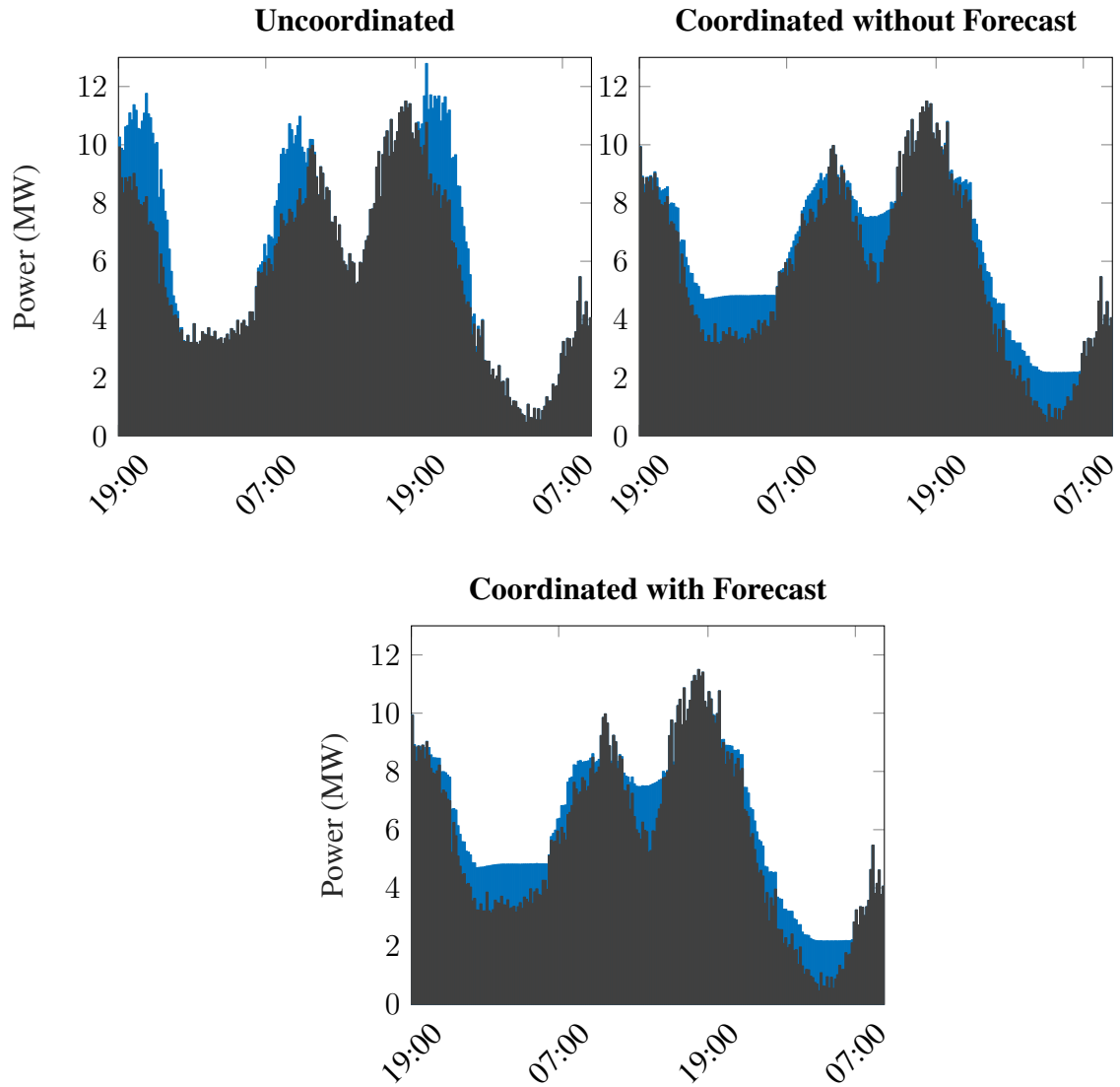
**Figure 34.** 141-bus IEEE Low EV demand case - Power imported in the reference bus (kW).

**Slack KPI**
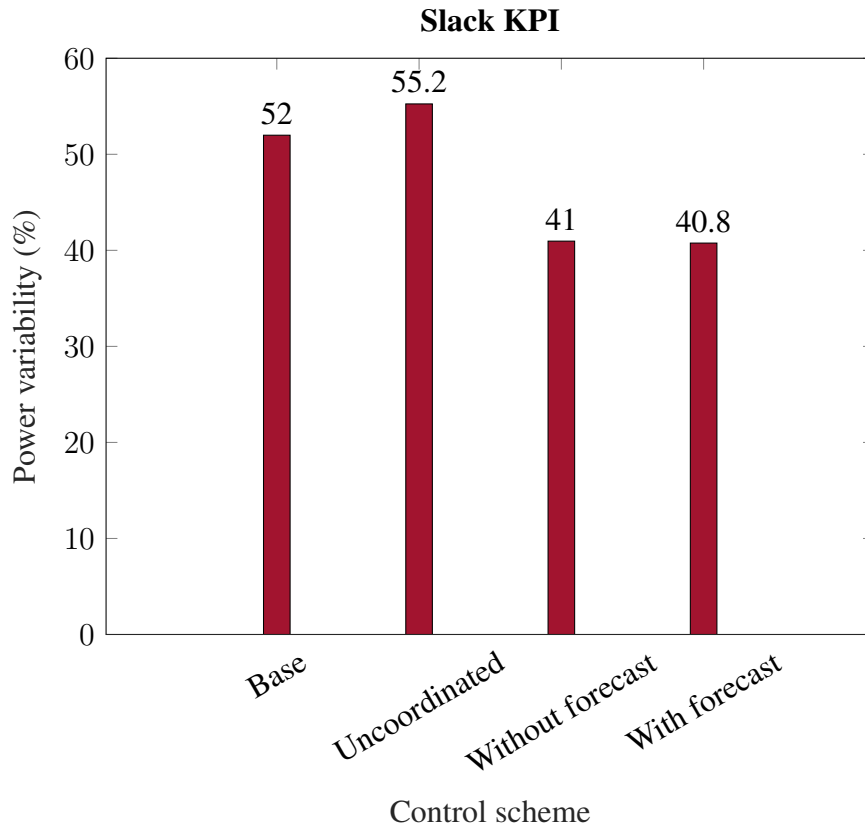


**Figure 35.** 141-bus IEEE Low EV demand case - Power imported variability at slack.

Finally, Table 24 shows the time performance for this scheme.

| Time (sec) | Max. | Min. | Avg. |
|---|---|---|---|
| Without Forecast | 23,536 | 11,403 | 14,906 |
| With Forecast | 22,934 | 10,888 | 15,249 |

**Table 24.** Control time performance for the 141-bus IEEE Low demand case with 37 charging stations.

## 5.2.2 Case 2: High EV Demand

### 5.2.2.1 18-bus IEEE Scenario

In this case, all the demand nodes from node 3 to node 18 include a charging station. The EV fleet consists of 3550 EVs distributed among the 15 charging stations. The EV demand represents 13,8% of the total system demand for the given simulation period. For this number of EVs, each household owns an EV. The results of this high EV demand scheme are presented below. According to Table 25, the losses for the coordinated schemes are reduced by 16% compared to the uncoordinated scheme.

| Losses (MWh) | Base | Unc. | wF | F |
|---|---|---|---|---|
| TOTAL | 3,06 | 4,96 | 4,16 | 4,13 |
| $KPI_{losses}$ | - | - | 16,20% | 16,81% |

**Table 25.** 18-bus IEEE High EV demand case - System losses.

The number of constraint violations has increased about 25 times compared to the previous low EV demand case as presented in Table 26.

| Line Congestion | Unc. | wF | F |
|---|---|---|---|
| **1.3 x** $I_{BaseCase}^{MAX}$ | 157 | 0 | 0 |

**Table 26.** 18-bus IEEE High EV demand case - Line congestions

The current and voltage variability has improved as expected according to Table 27. As shown in Figure 36, the minimum voltage level for the coordinated schemes remains constant and similar to the one of the base case ($0,9462\ p.u.$), while in the uncoordinated strategy falls to $0,9351\ p.u.$. Table 28 presents the voltage variability of the most representative bus.

| Average Variability | Base | Unc. | wF | F |
|---|---|---|---|---|
| $KPI_{CV}$ Current | 48,81% | 57,17% | 35,36% | 34,36% |
| $KPI_{CV}$ Voltage | 1,51% | 1,72% | 1,42% | 1,39% |

**Table 27.** 18-bus IEEE High EV demand case - Line current and voltage variability.

| Maximum Variability | Base | Unc. | wF | F |
|:---:|:---:|:---:|:---:|:---:|
| Node 18 | 2,19% | 2,67% | 2,03% | 1,98% |

**Table 28.** 18-bus IEEE High EV demand case - Bus with maximum voltage variation.

**Voltage at Node 18**



**Figure 36.** 18-bus IEEE High EV demand case - Voltage profile of node 18.

The peak shaving increases notably reducing around 20% of the imported power variations compared to the base case and 26% compared to the uncoordinated strategy (see Figures 37 and 38).

**Imported Power at slack**

**Coordinated without Forecast**

**Coordinated with Forecast**
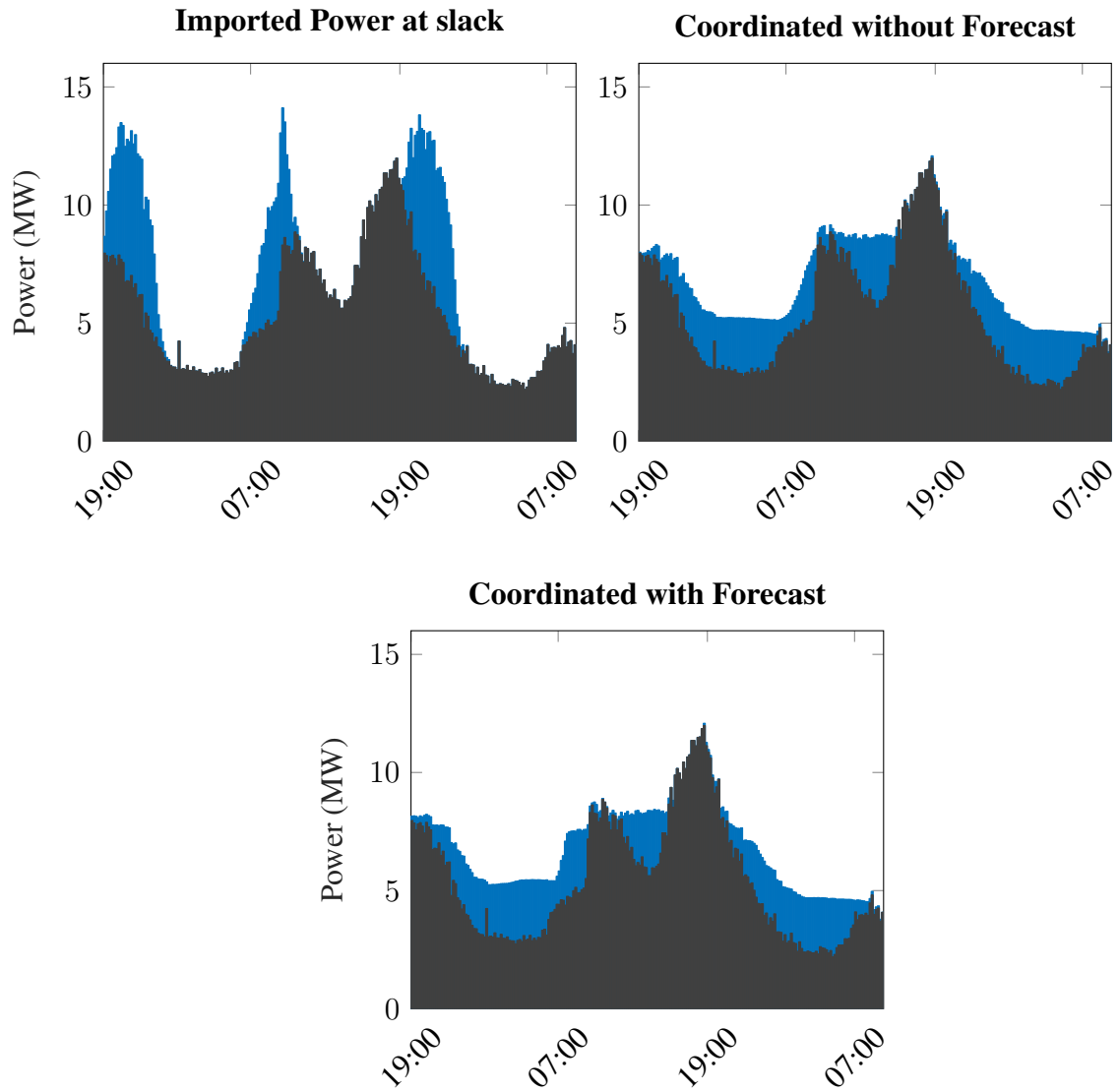
**Figure 37.** 18-bus IEEE High EV demand case - Power imported in the reference bus (kW).

**Node 1**



**Figure 38.** 18-bus IEEE High EV demand case - Power imported variability at slack.

Finally, the time performance remains under 1 second as presented in 29.

| Time (sec) | Max. | Min. | Avg. |
|---|---|---|---|
| Without Forecast | 0,639 | 0,194 | 0,350 |
| With Forecast | 0,568 | 0,193 | 0,354 |

**Table 29.** Control time performance for the 18-bus IEEE High EV demand case with 6 charging stations.

## 5.2.2.2 141-bus IEEE Scenario

In this case, there are 82 charging stations distributed among all the demand nodes. The EV fleet consists of 4700 EVs, and the EV demand represents the 14,96% of the total system demand for the given simulation period. For this number of EVs, each household owns an EV. The results of this high EV demand scheme are presented below. According to Table 30, the losses for the coordinated schemes are reduced by 21% compared to the uncoordinated scheme.

| Losses (MWh) | Base | Unc. | wF | F |
|---|---|---|---|---|
| TOTAL | 5,70 | 10,22 | 8,06 | 8,03 |
| $KPI_{losses}$ | - | - | 21,15% | 21,47% |

**Table 30.** 141-bus IEEE High EV demand case - System losses.

The number of constraint violations has increased notably for this case as presented in Table 31.

| Line Congestion | Unc. | wF | F |
|---|---|---|---|
| **1.3 x** $I^{MAX}_{BaseCase}$ | 2584 | 0 | 0 |

**Table 31.** 141-bus IEEE High EV demand case - Line congestions

The current and voltage variability has improved as expected according to Table 32. Table 33 presents the voltage variability of the most representative node of the system and Figure 39 depicts the voltage curves for the simulation horizon for each charging scheme. As seen in the Figure 39, the minimum voltage level for the coordinated scheme remains constant and similar to the one of the base case ($0,9907\ p.u.$), while in the uncoordinated strategy falls to $0,9692\ p.u.$.

| Average Variability | Base | Unc. | wF | F |
|---|---|---|---|---|
| $KPI_{CV}$ Current | 45,06% | 59,13% | 36,02% | 35,39% |
| $KPI_{CV}$ Voltage | 0,94% | 1,48% | 0,76% | 0,75% |

**Table 32.** 141-bus IEEE High EV demand case - Line current and voltage variability.

| Maximum Variability | Base | Unc. | wF | F |
|---|---|---|---|---|
| Node 52 | 1,22% | 1,93% | 0,99% | 0,96% |

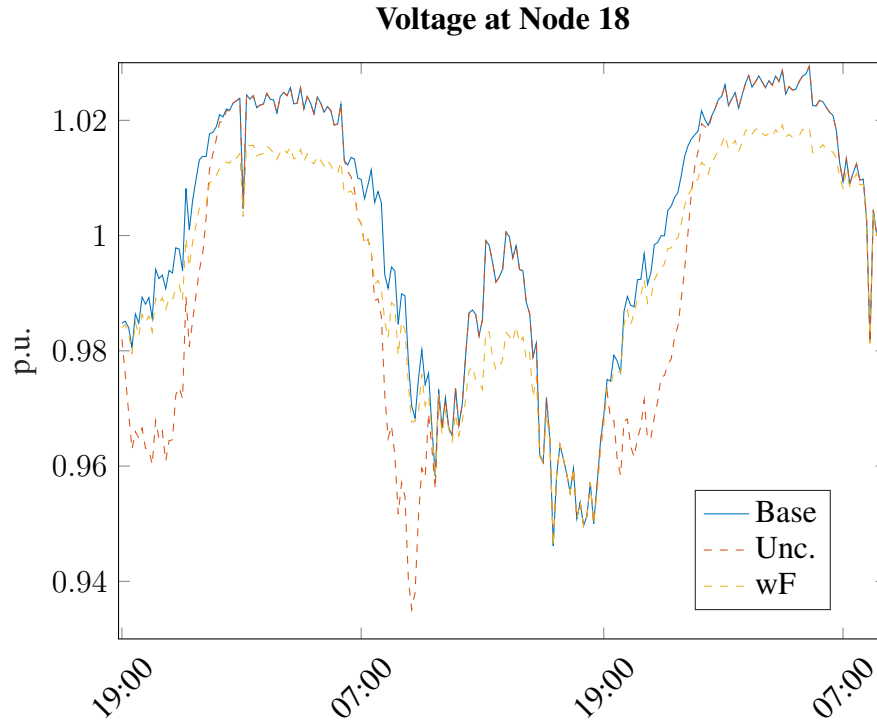**Table 33.** 141-bus IEEE High EV demand case - Bus with maximum voltage variation.
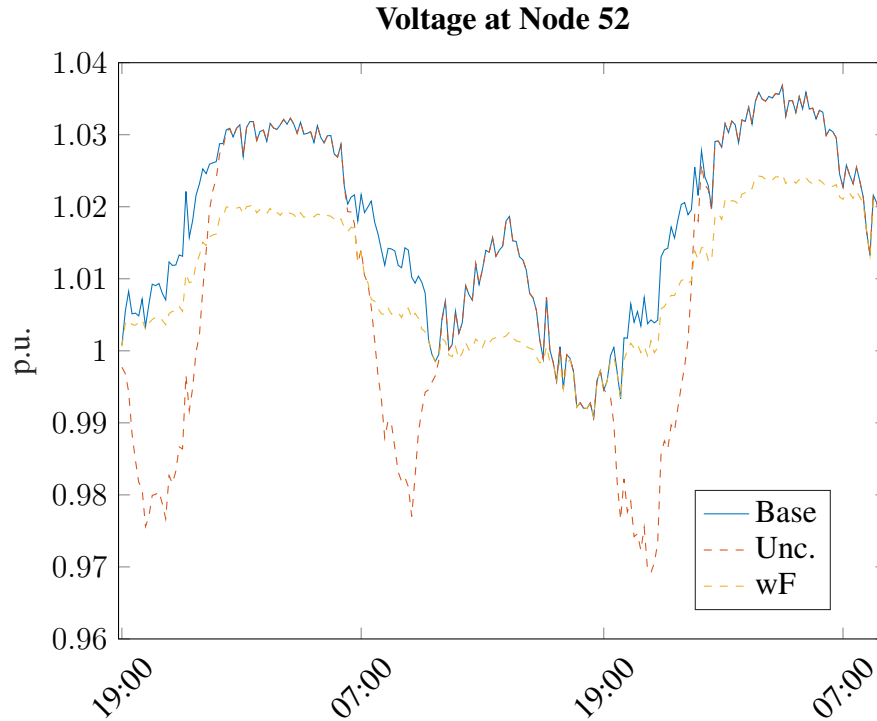


**Figure 39.** 141-bus IEEE High EV demand case - Voltage profile of node 52.

The peak shaving increases notably reducing around 22% the imported power variations compared to the base case and 35% compared to the uncoordinated strategy according to Figures 40 and 41.

**Uncoordinated**

**Coordinated without Forecast**

**Coordinated with Forecast**



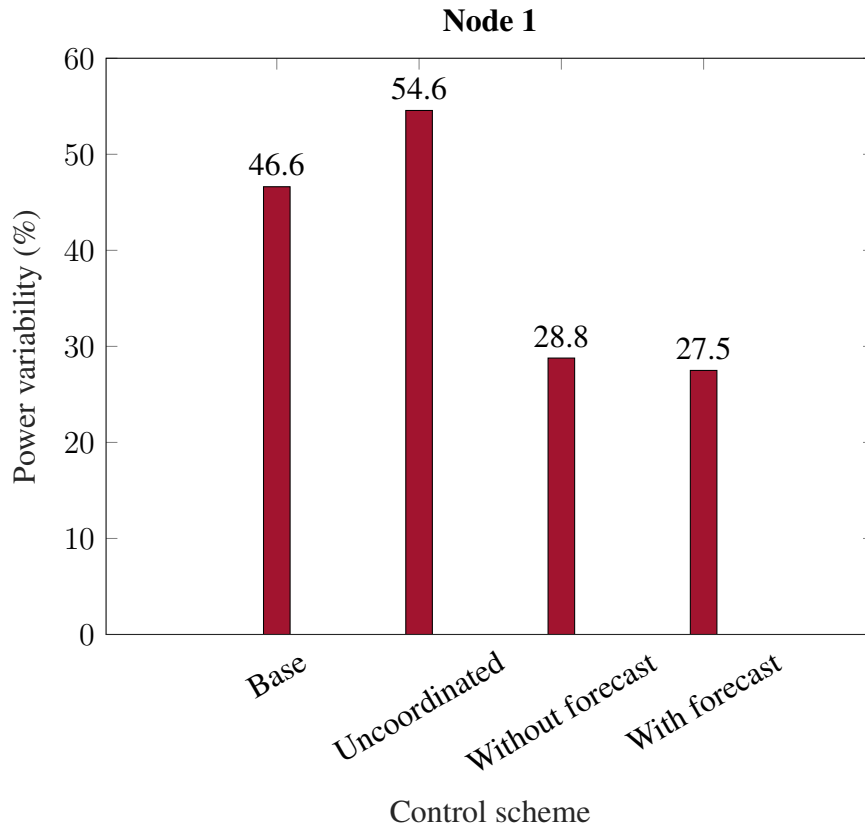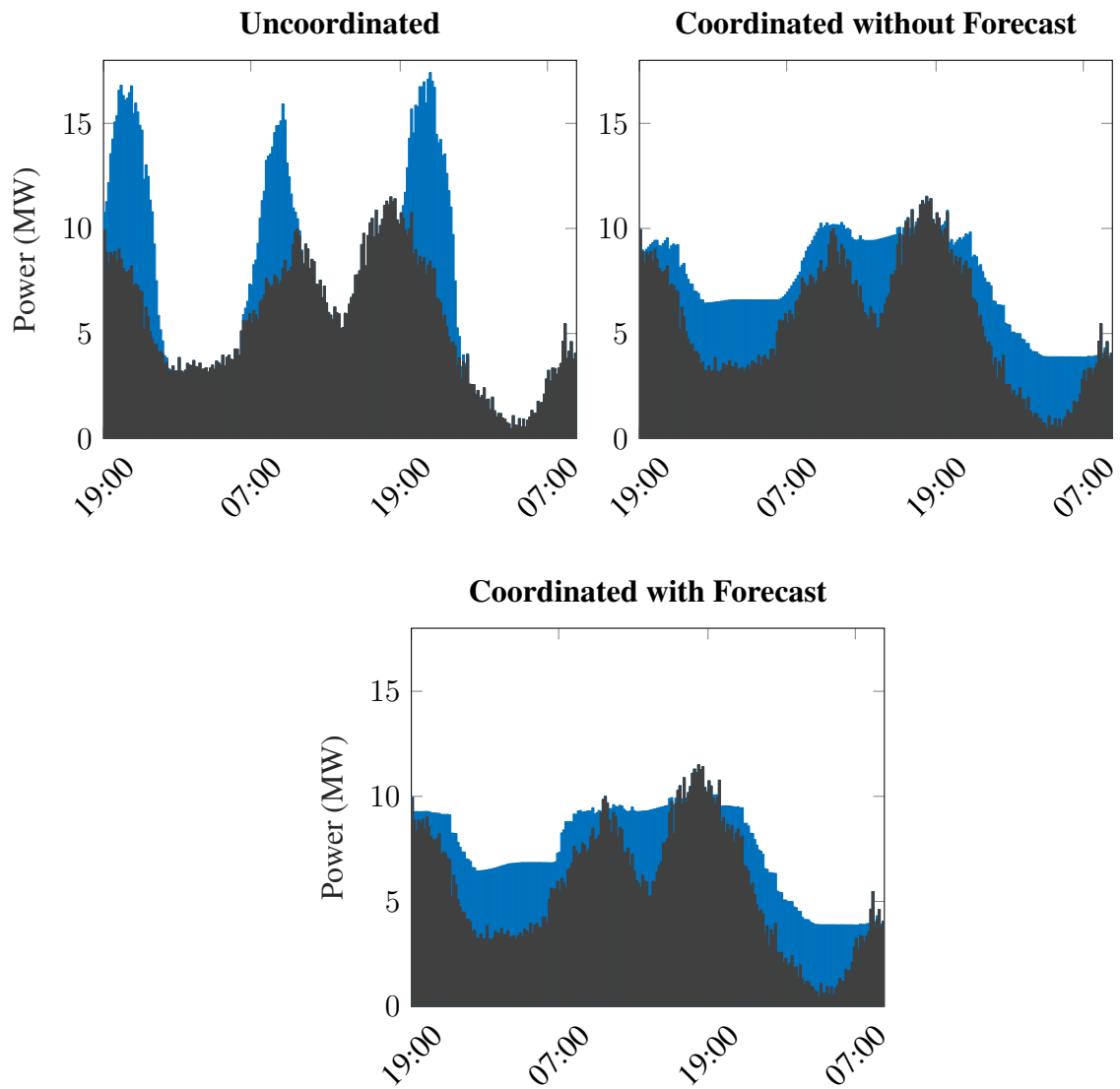**Figure 40.** 141-bus IEEE High EV demand case - Power imported in the reference bus (kW).

**Node 1**
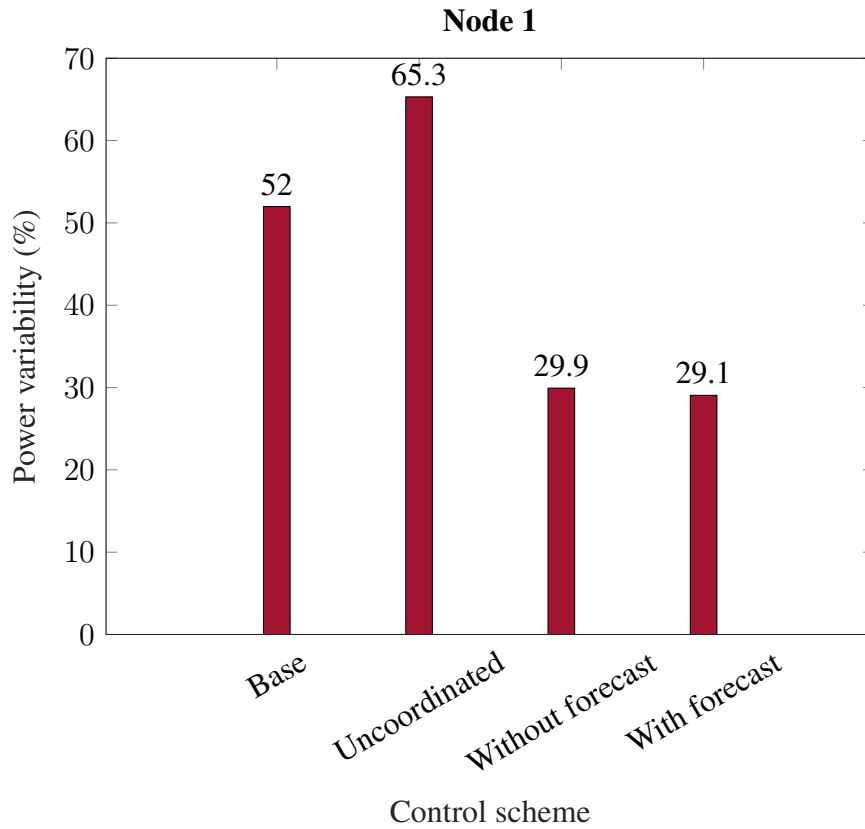


**Figure 41.** 141-bus IEEE High EV demand case - Power imported variability at slack.

Finally, the time performance can be still considered acceptable for this real-time application (Table 34).

| Time (sec) | Max. | Min. | Avg. |
|---|---|---|---|
| Without Forecast | 26,705 | 13,975 | 20,371 |
| With Forecast | 21,172 | 11,342 | 14,748 |

**Table 34.** Control time performance for the 141-bus IEEE High EV demand case with 82 charging stations.

## 5.3   Control Horizon Impact

Table 35 presents the algorithm performance for different control and prediction horizons. As shown in the table, larger prediction horizons improve the quality of the solution, but the computational burden and uncertainty increase. In this work, the forecast is assumed to be exact, and hence, the impact of uncertainties is not reflected in the solution. On the other hand, a shorter prediction horizon reduces the computational burden and uncertainty, but the solution deteriorates as the number of charging stations increases. Thus, a horizon of 6 hours yields a good balance between time burden and solution quality and is set as a default in our control set up.

| Horizon (hrs) | 3 | 6 | 12 |
|---|---|---|---|
| *Low EV demand* | | | |
| **Losses (kWh)** | 3,38 | 3,373 | 3,371 |
| **Max. time burden (s)** | 0,25 | 0,43 | 1,10 |
| **Min. time burden (s)** | 0,13 | 0,17 | 0,57 |
| **Avg. time burden (s)** | 0,09 | 0,25 | 0,76 |
| *High EV demand* | | | |
| **Losses (kWh)** | 4,17 | 4,157 | 4,153 |
| **Max. time burden (s)** | 0,55 | 0,63 | 2,60 |
| **Min. time burden (s)** | 0,11 | 0,19 | 0,64 |
| **Avg. time burden (s)** | 0,21 | 0,35 | 1,28 |

**Table 35.** 18-bus IEEE scenario - Algorithm performance for different time horizons.

## 5.4 Integration of Minimum Admissible Charging Bounds

Heretofore, each charging station was able to charge with any power rate lower than the upper charging power bound, since the lower limit was set to zero. However, in actual conditions, EVs have a minimum charging rate [62]. In the SOCP model, if we a minimum charging power bound, each charging station is forced to charge every time step with at least this value. For the sake of avoiding this, binary variables are required to activate and deactivate the charging power constraints. However, the optimization model complexity increases into a MISOCP, and some variations in the EV aggregate model must be adopted. Then, the expression (72) from the model introduced at Section 4.2.1 changes to (108) and additionally (109) is included.

$$b_{EVSE}(i_e, t) \cdot \underline{P}_{EVSE}(i_e, t) \leq P_{EVSE}^{supplied}(i_e, t) \leq b_{EVSE}(i_e, t) \cdot \overline{P}_{EVSE}(i_e, t) \tag{108}$$

$$b_{EVSE}(i_e, t) \leq 1 \tag{109}$$

Although using previous expressions solves the problem of charging at a minimum rate, the computational burden is also increased. Tables 36 and 37 compare the SOCP and MISOCP model performance for both scenarios. The lower bound is set to the minimum charging power that an EV can charge [62]. Note that for the 141-bus IEEE scenario the losses comparison is not included since the MISOCP simulation times were excessively high.

| 18 IEEE | MISOCP | SOCP |
|---|---|---|
| *Low EV demand* | | |
| **Total system losses (MWh)** | 3,3727 | 3,3725 |
| **Max. time burden (s)** | 6,18 | 0,43 |
| **Min. time burden (s)** | 0,73 | 0,18 |
| **Avg. time burden (s)** | 2,39 | 0,25 |
| High EV demand | | |
| **Total system losses (MWh)** | 4,1576 | 4,1573 |
| **Max. time burden (s)** | 55,20 | 0,64 |
| **Min. time burden (s)** | 0,59 | 0,19 |
| **Avg. time burden (s)** | 6,46 | 0,35 |

**Table 36.** 18-bus IEEE scenario - MISOCP and SOCP comparison.

Introducing binary variables have a remarkable impact on a high number of charging stations. In the 141-bus IEEE scenario, the time burden increases considerably compared to the SOCP approach. For that reason, a centralized MISOCP is not suitable for large systems. Alternatively, as shown in Table 38, rounding up the solution for those values below the lower charging bounds may introduce considerable errors on the lines where EVs have an essential impact. Even though the algorithm tends to charge during low congested periods, this could lead to an infeasibility.

| 141 IEEE | MISOCP | SOCP |
|---|---|---|
| *Low EV demand* | | |
| **Max. time burden (s)** | 3624,3 | 23,5 |
| **Min. time burden (s)** | 70,2514 | 11,4 |
| **Avg. time burden (s)** | 1108,6 | 14,9 |
| High EV demand | | |
| **Max. time burden (s)** | 5560,3 | 26,7 |
| **Min. time burden (s)** | 355,2 | 14,0 |
| **Avg. time burden (s)** | 1593,7 | 20,4 |

**Table 37.** 141-bus IEEE scenario - MISOCP and SOCP comparison.

| | 18 IEEE | 141 IEEE |
|---|---|---|
| *Low EV demand* | | |
| **Loss increase (kWh)** | 0,0021% (3,3726) | 0,014% (6,4760) |
| **max % Current deviation** | 0,23% | 1,63% |
| **max % Voltage deviation** | 0,002% | 0,004% |
| *High EV demand* | | |
| **Loss increase (kWh)** | 0,0021% (4,1574) | 0,0294% (8,0594) |
| **max % Current deviation** | 0,39% | 10,57% |
| **max % Voltage deviation** | 0,002% | 0,011% |

**Table 38.** Rounding error forcing EVSE to charge with $P_{min}$ when $P < P_{min}$.

On the other hand, assuming that EVs do not charge with values below the minimum admissible may not have a significant impact on the overall system performance. Since the centralized control is running at relatively small time steps (10 minutes), each local control adjusts at every iteration the lower energy curve. Then, if in one time step an EVSE does not charge, the minimum curve will increase its slope for the next iteration. However, this analysis is out of the scope of this thesis, and it is proposed as future work.

# Chapter 6

# Conclusion

The non-convexity of the power flow equations is efficiently solved by the convex relaxation proposed in [35]. Even though there are other approaches, this has been proved to be appropriate for demand-side response applications on distribution systems. The DCPF approach cannot be applied to real-time applications on a distribution level since the voltage, and current approximations are not acceptable. Nevertheless, the LACPF presented in this work shows excellent performance for voltage estimation, but the line approximation is rather weak and an iterative process to reduce the error would be necessary.

Uncoordinated charging schemes may cause high demand peaks in an electrical system congesting lines and deteriorating the voltage quality. One unnecessary expensive solution would be increasing the total system capacity. This master thesis proposes an optimal charging strategy which minimizes the impact of EVs in the electrical network. The proposed centralized control has been validated for two different scenarios showing optimal operation. The strategy can reduce up to 8% of the system losses compared to an uncoordinated scheme for an EV energy demand of 6% of the total system demand. Thus, saving considerable operation costs.

Furthermore, the uncoordinated charging scheme may violate line constraints, whereas the proposed control avoids overloading them. The exactness of the convexified BFM allows the control to monitor the real voltage and current values preventing from constraint violations. Since the algorithm aims at minimizing losses, EVs will charge when the lines are at the minimal current level reducing the current variability in lines. A decrease in the line current flow variability leads to a decrease in the voltage variability. The algorithm tends to charge at the periods where the voltage is higher and avoids charging at its minimum values. Therefore, this algorithm contributes positively to power quality.

The scheduled power profiles perform Peak Shaving at the High Voltage (HV) - Medium Voltage (MV) substation level reducing congestions on the main transformer. The power variations are decreased notably compared to the case without EV demand by 5% for an 18-bus system and by 12% for a 141-bus case and a demand of 4-6% of the total system demand. Assuming a

similar demand pattern in the whole electrical system, this control allocates charging events in the periods where the energy price is lower. Then, contributing to reduce the operation costs of the system. However, one cannot ensure that the same effect happens at each node of the system. The nodes with higher demand are the most representative nodes, and the charging profiles will depend primarily on them since they are the primary source of line congestion. Additionally, this effect has been proved for radial system where the slack bus supplies most of the energy demanded by the system ($\approx 80\%$).

On the other hand, the control algorithm guarantees that the solution at each iteration is globally optimal, and the computational burden remains under 1 second for a 18-bus system and 30 seconds for a 141-bus system. The performance can be considered acceptable for this real-time application, where the control operates every 10 minutes. Moreover, including EV arrival forecasts would not influence the algorithm performance significantly, but the accuracy of the forecasts may affect the optimality of the solution. Thus, it can be concluded that the arrival forecasts can be retrieved from the model since the improvement in the overall system objective is negligible.

The model complexity increases when including binary variables to force each charging station to charge with a minimum power rate. The MISOCP model presents extremely high computation times with regards to the SOCP model (up to 1 hour). Thus, the MISOCP cannot be implemented in large systems, and other alternatives would be necessary to address this problem.

Last but not least, this developed tool can be used for design purposes, such as analyzing the impact of connecting charging stations in different nodes of a distribution system. The work can be deployed to see which nodes are more appropriate to include charging stations according to a radial system topology.

# Chapter 7

# Future Work

Future work of this thesis might include a more realistic EV behavior model. This study estimates the arrivals and departures with truncated normal distributions, which does not include casual events, such as sudden or brief stays. Moreover, the model considers that the user charges either at home or work neglecting other schemes.

As introduced in the result analysis, the departure of EV users is known once they arrived. Furthermore, they do not leave before the expected time, excluding such uncertainty. Implementation of stochastic parameters to model sudden leave of EVs is proposed as a future step for improving the algorithm.

Another possible future direction of this work can be the analysis of a distributed control. As seen in evaluation, the centralized MISOCP requires unacceptable computation times to reach the global optimal. Then, the performance of a distributed approach can be compared to the centralized control developed in this thesis. An interesting starting point might be the work proposed at [13].

This study has focused on the upper control level neglecting the interaction with the charging station level. The combination of the proposed method with local controls and its analysis is also included as future work.

Finally, the V2G scheme can be also incorporated in the algorithm. Thus, driving an analysis of the impact of providing ancillary services. Additionally, the charging stations may be also complemented with other technologies, such as battery storage systems. The integration and interaction of different agents is also proposed as future work of this thesis.

# Bibliography

[1] T. G. San Román, I. Momber, M. R. Abbad, and Á. Sánchez Miralles, "Regulatory framework and business models for charging plug-in electric vehicles: Infrastructure, agents, and commercial relationships," Energy Policy, vol. 39, no. 10, pp. 6360–6375, 2011.

[2] Carlos Montes Portela,Paul Klapwijk, Lennart Verheijen,Hans de Boer,Han Slootweg,Marko Van Eekelen, "Oscp - an open protocol for smart charging of electric vehicles," CIRED 23rd International Conference on Electricity Distribution, no. 15-18, pp. 1–5, June 2015.

[3] Statista, "Europe: number of electric vehicle charging stations 2018 | statistic."

[4] Fereidoon Sioshansi, "The impact of electric vehicles on electricity demand - energy post," November 2018.

[5] Hauke Engel,Russell Hensley,Stefan Knupfer,Shivika Sahdev, "The potential impact of electric vehicles on global energy systems," August 2018.

[6] Z. Ma, D. S. Callaway, and I. A. Hiskens, "Decentralized charging control of large populations of plug-in electric vehicles," IEEE Transactions on Control Systems Technology, vol. 21, no. 1, pp. 67–78, 2013.

[7] A. Bosovic, M. Music, and S. Sadovic, "Analysis of the impacts of plug-in electric vehicle charging on the part of a real medium voltage distribution network," in IEEE PES Innovative Smart Grid Technologies, Europe, pp. 1–7, IEEE, 12/10/2014 - 15/10/2014.

[8] Ahmed R. Abul'Wafa, Aboul'fotouh El'Garably, and Wael A.Fatah Mohamed, "Uncoordinated vs coordinated charging of electric vehicles in distribution systems performance," International Journal of Engineering and Information Systems (IJEAIS), vol. 1, no. 6, pp. 54–65, 2017.

[9] R. D. Zimmerman, C. E. Murillo-Sanchez, and R. J. Thomas, "Matpower: Steady-state operations, planning, and analysis tools for power systems research and education," IEEE Transactions on Power Systems, vol. 26, no. 1, pp. 12–19, 2011.

[10] J. Lofberg, "Yalmip : A toolbox for modeling and optimization in matlab," In Proceedings of the CACSD Conference, Taipei, Taiwan 2004.

[11] L. L. Gurobi Optimization, "Gurobi optimizer reference manual," 2018.

[12] G.. Pasaoglu, D. Fiorello, A. Martino, G. Scarcella, A. Alemanno, A. Zubaryeva, C. Thiel, "Driving and parking patterns of european car drivers - a mobility survey," JRC Scientific and Policy Reports, vol. Report EUR 25627 EN, 2012.

[13] Y. Zheng, Y. Song, D. Hill, and K. Meng, "Online distributed mpc-based optimal scheduling for ev charging stations in distribution systems," IEEE Transactions on Industrial Informatics, p. 1, 2018.

[14] J. García-Villalobos, I. Zamora, J. I. San Martín, F. J. Asensio, and V. Aperribay, "Plug-in electric vehicles in electric distribution networks: A review of smart charging approaches," Renewable and Sustainable Energy Reviews, vol. 38, pp. 717–731, 2014.

[15] S. Kolen, C. Molitor, L. Wagner, and A. Monti, "Two-level agent-based scheduling for a cluster of heating systems," Sustainable Cities and Society, vol. 30, pp. 273–281, 2017.

[16] N. Liu, Q. Chen, J. Liu, X. Lu, P. Li, J. Lei, and J. Zhang, "A heuristic operation strategy for commercial building microgrids containing evs and pv system," IEEE Transactions on Industrial Electronics, vol. 62, no. 4, pp. 2560–2570, 2015.

[17] Rohit R. Deshmukh,Makarand S. Ballal, "An energy management scheme for grid connected evs charging stations," IEEE Transactions on Smart Grid, vol. 9, no. 5, pp. 4689–4701, 2018.

[18] Y. WU, A. Ravey, D. Chrenko, and A. Miraoui, "A real time energy management for ev charging station integrated with local generations and energy storage system," in 2018 IEEE Transportation Electrification Conference and Expo (ITEC), pp. 1–6, IEEE, 13/06/2018 - 15/06/2018.

[19] S. Gao, K. T. Chau, C. Liu, D. Wu, and C. C. Chan, "Integrated energy management of plug-in electric vehicles in power grid with renewables," IEEE Transactions on Vehicular Technology, vol. 63, no. 7, pp. 3019–3027, 2014.

[20] S. Khan, K. Mehmood, Z. Haider, S. Bukhari, S.-J. Lee, M. Rafique, and C.-H. Kim, "Energy management scheme for an ev smart charger v2g/g2v application with an ev power allocation technique and voltage regulation," Applied Sciences, vol. 8, no. 4, p. 648, 2018.

[21] D. Lauinger, F. Vuille, D. Kuhn, "A review of the state of research on vehicle-to-grid (v2g): Progress and barriers to deployment," European Battery, Hybrid and Fuel Cell Electric Vehicle Congress, Geneva, 14th - 16th March 2017.

[22] H. Ahmadi and M. P. Moghadam, "Effects of ev-parking lots on transmission lines congestion and price in the electricity market," in <u>CIRED 2012 Workshop: Integration of Renewables into the Distribution Grid</u>, p. 44, IET, 29-30 May 2012.

[23] Raffael La Fauci, <u>Management of PHEVs in Low Voltage Distribution Networks using BFS and ACS</u>. PhD thesis, Politecnico di Torino & Swiss Federal Institute of Technology (ETH) Zurich, 2010.

[24] S. Bracco, F. Delfino, F. Pampararo, M. Robba, and M. Rossi, "A dynamic optimization-based architecture for polygeneration microgrids with tri-generation, renewables, storage systems and electrical vehicles," <u>Energy Conversion and Management</u>, vol. 96, pp. 511–520, 2015.

[25] H. Yuan, F. Li, Y. Wei, and J. Zhu, "Novel linearized power flow and linearized opf models for active distribution networks with application in distribution lmp," <u>IEEE Transactions on Smart Grid</u>, vol. 9, no. 1, pp. 438–448, 2018.

[26] Y. Song, Y. Zheng, and D. Hill, "Optimal scheduling for ev charging stations in distribution networks: A convexified model," <u>IEEE Transactions on Power Systems</u>, p. 1, 2016.

[27] Hitoshi Yano, Koji Kudo, Takashi Ikegami, Hiroto Iguchi, Kazuto Kataoka, and Kazuhiko Ogimoto, <u>A Novel Charging-Time Control Method for Numerous EVs based on a Period Weighted Prescheduling for Power Supply and Demand Balancing: Conference] ; 16 - 20 Jan. 2012, Washington, DC, USA</u>. Piscataway, NJ: IEEE, 2012.

[28] T. Ishibashi, T. Shimakage, N. Takeuchi, T. Kikuchi, and M. Nonogaki, "Energy management using a quick charger with storage battery for electric vehicles," in <u>2015 IEEE International Telecommunications Energy Conference (INTELEC)</u>, pp. 1–4, IEEE, 18/10/2015 - 22/10/2015.

[29] I. ChargePoint, "Understanding ocpp," 2013.

[30] T. Niknam, M. r. Narimani, M. Jabbari, and A. R. Malekpour, "A modified shuffle frog leaping algorithm for multi-objective optimal power flow," <u>Energy</u>, vol. 36, no. 11, pp. 6420–6432, 2011.

[31] J. Zhu, <u>Optimization of power system operation</u>. IEEE Press series on power engineering, Hoboken, New Jersey and Piscataway, New Jersey and Piscataway, New Jersey: Wiley IEEE and IEEE Xplore, 2009.

[32] I. M. Nejdawi, K. A. Clements, and P. W. Davis, "An efficient interior point method for sequential quadratic programming based optimal power flow," <u>IEEE Transactions on Power Systems</u>, vol. 15, no. 4, pp. 1179–1183, 2000.

[33] K.-y. Liu, W. Sheng, and S. Cheng, "Optimal power flow algorithm and analysis in distribution system considering distributed generation," IET Generation, Transmission & Distribution, vol. 8, no. 2, pp. 261–272, 2014.

[34] M. Farivar and S. H. Low, "Branch flow model: Relaxations and convexification—part i," IEEE Transactions on Power Systems, vol. 28, no. 3, pp. 2554–2564, 2013.

[35] S. H. Low, "Convex relaxation of optimal power flow—part i: Formulations and equivalence," IEEE Transactions on Control of Network Systems, vol. 1, no. 1, pp. 15–27, 2014.

[36] D. Mildt, M. Cupelli, and R. Kubo, "Model predictive control for microgrid power management under forecast uncertainties.dvi," IEEJ Joint Technical Meeting on Systems and Smart Facilities, IEE Japan (2017).

[37] S. H. Low, "Convex relaxation of optimal power flow—part ii: Exactness," IEEE Transactions on Control of Network Systems, vol. 1, no. 2, pp. 177–189, 2014.

[38] Lingwen Gan, Na Li, Ufuk Topcu, and and Steven Low, "Branch flow model for radial networks: Convex relaxation," Division of Engineering and Applied Science.

[39] M. Farivar and S. H. Low, "Branch flow model: Relaxations and convexification—part i," IEEE Transactions on Power Systems, vol. 28, no. 3, pp. 2554–2564, 2013.

[40] K. Christakou, D.-C. Tomozei, J.-Y. Le Boudec, and M. Paolone, "Ac opf in radial distribution networks - part i: On the limits of the branch flow convexification and the alternating direction method of multipliers."

[41] Michael Pierrot, "The wind power e40/500 (enercon)."

[42] A. Yona, T. Senjyu, and T. Funabashi, 2nd IEEE/IFIP International Workshop on Broadband Convergence Networks, 2007: BcN '07 ; Munich, Germany, 21 May 2007. Piscataway, NJ: IEEE, 2007.

[43] The mobility house, "All relevant charging cable and plug types: An overview for everyone interested in electronic mobility."

[44] P. Zhang, K. Qian, C. Zhou, B. G. Stewart, and D. M. Hepburn, "A methodology for optimization of power systems demand due to electric vehicle charging load," IEEE Transactions on Power Systems, vol. 27, no. 3, pp. 1628–1636, 2012.

[45] Xiaochen Zhang and Santiago Grijalva, An Advanced Data Driven Model for Residential Electric Vehicle Charging Demand: Denver, Colorado, USA, 26 - 30 July 2015. Piscataway, NJ: IEEE, 2015.

[46] S. Götz, "Berufspendler: Deutsche pendeln im schnitt rund 17 kilometer zur arbeit,," 19-Sep-2017.

[47] M. Sedlak, "Verbrauch und reichweite von elektroautos,."

[48] S. Pfenninger and I. Staffell, "Open power system data. 2019. data package weather data. version 2019-04-09. (primary data from various sources, for a complete list see url)."

[49] A. Minde, "Household dataopen power system data. 2017. data package household data. version 2017-11-10. (primary data from various sources, for a complete list see url).."

[50] M. Muratori, "Impact of uncoordinated plug-in electric vehicle charging on residential power demand," Nature Energy, vol. 3, no. 3, pp. 193–201, 2018.

[51] Tjarko Tjaden, Joseph Bergner, Johannes Weniger, and Volker Quaschning, "Representative electrical load profiles of residential buildings in germany with a temporal resolution of one second."

[52] E. McKenna and M. Thomson, "High-resolution stochastic integrated thermal–electrical domestic demand model," Applied Energy, vol. 165, pp. 445–461, 2016.

[53] "Trial results. fi.ict-2011.1.8 finesce d4.7 v.0.1," September 30th 2015.

[54] David Lillienberg et al., "Consolidated trial description. fi.ict-2011.1.8 finesce d7.2," vol. Version 1.0, p. 39, April 14, 2014.

[55] BDEW, "Standardlastprofile strom," 23/04/2019.

[56] Open Power System Data, "Open power system data – a platform for open data of the european power system.."

[57] M. Muratori, M. C. Roberts, R. Sioshansi, V. Marano, and G. Rizzoni, "A highly resolved modeling technique to simulate residential power demand," Applied Energy, vol. 107, pp. 465–473, 2013.

[58] W. M. Grady, M. J. Samotyj, and A. H. Noyola, "The application of network objective functions for actively minimizing the impact of voltage harmonics in power systems," IEEE Transactions on Power Delivery, vol. 7, no. 3, pp. 1379–1386, 1992.

[59] H. M. Khodr, F. G. Olsina, P. D. O.-D. Jesus, and J. M. Yusta, "Maximum savings approach for location and sizing of capacitors in distribution systems," Electric Power Systems Research, vol. 78, no. 7, pp. 1192–1203, 2008.

[60] "Peak shaving."

[61] New York State Department of Public Service, "Glossary of terms used by utilities and their regulators. valley filling."

[62] PHOENIX CONTACT GmbH & Co. KG, "User manual um en ev-cc-ac1-m3-c," 27/05/2019.

# List of Figures

# List of Tables

# ANNEX A: Grid Parameters

The grid parameters of the scenarios studied are presented below. The line number 86 (N86-N87) from the case 141 has originally a null resistance value and a very low reactance. In this study, these values have been changed and fixed equal to the ones from line number 87 (N7-N88) to avoid matrix singularity.

| From | To | R (%) | X (%) | B (%) | $Z_{BASE}$ ($\Omega$) | $I_{BASEcase}^{MAX}$ |
|------|-----|-------|-------|-------|----------|----------|
| 1 | 2 | 0,005 | 0,035 | 0 | 156,25 | 13,44 |
| 2 | 3 | 0,031 | 0,675 | 0 | 156,25 | 13,44 |
| 3 | 4 | 0,043 | 0,120 | 0 | 156,25 | 9,92 |
| 4 | 5 | 0,060 | 0,167 | 0 | 156,25 | 8,97 |
| 5 | 6 | 0,031 | 0,088 | 0 | 156,25 | 8,36 |
| 6 | 7 | 0,089 | 0,250 | 0 | 156,25 | 7,29 |
| 7 | 8 | 0,029 | 0,082 | 0 | 156,25 | 2,67 |
| 8 | 9 | 0,172 | 0,212 | 0 | 156,25 | 1,61 |
| 9 | 10 | 0,407 | 0,305 | 0 | 156,25 | 1,28 |
| 4 | 11 | 0,170 | 0,220 | 0 | 156,25 | 0,99 |
| 3 | 12 | 0,291 | 0,376 | 0 | 156,25 | 4,57 |
| 12 | 13 | 0,222 | 0,287 | 0 | 156,25 | 3,41 |
| 13 | 14 | 0,480 | 0,621 | 0 | 156,25 | 0,37 |
| 13 | 15 | 0,398 | 0,516 | 0 | 156,25 | 2,97 |
| 15 | 16 | 0,291 | 0,376 | 0 | 156,25 | 1,02 |
| 15 | 17 | 0,372 | 0,459 | 0 | 156,25 | 1,64 |
| 17 | 18 | 0,110 | 0,136 | 0 | 156,25 | 0,43 |

**Table 39.** Modified parameters of 18-bus IEEE scenario imported from MATPOWER library. Line data.

| Bus Nr. | Node type | $G_S$ | $B_S$ | $V_N$ (kV) | $V_{max}$ (p.u.) | $V_{min}$ (p.u.) |
|---------|-----------|-------|-------|------------|------------------|------------------|
| 1 | Slack | 0 | 0 | 12,5 | 1,1 | 0,9 |
| 2 | PQ | 0 | 0 | 12,5 | 1,1 | 0,9 |
| 3 | PQ | 0 | 0 | 12,5 | 1,1 | 0,9 |
| 4 | PQ | 0 | 0 | 12,5 | 1,1 | 0,9 |
| 5 | PQ | 0 | 0 | 12,5 | 1,1 | 0,9 |
| 6 | PQ | 0 | 0 | 12,5 | 1,1 | 0,9 |
| 7 | PQ | 0 | 0 | 12,5 | 1,1 | 0,9 |
| 8 | PQ | 0 | 0 | 12,5 | 1,1 | 0,9 |
| 9 | PQ | 0 | 0 | 12,5 | 1,1 | 0,9 |
| 10 | PQ | 0 | 0 | 12,5 | 1,1 | 0,9 |
| 11 | PQ | 0 | 0 | 12,5 | 1,1 | 0,9 |
| 12 | PQ | 0 | 0 | 12,5 | 1,1 | 0,9 |
| 13 | PQ | 0 | 0 | 12,5 | 1,1 | 0,9 |
| 14 | PQ | 0 | 0 | 12,5 | 1,1 | 0,9 |
| 15 | PQ | 0 | 0 | 12,5 | 1,1 | 0,9 |
| 16 | PQ | 0 | 0 | 12,5 | 1,1 | 0,9 |
| 17 | PQ | 0 | 0 | 12,5 | 1,1 | 0,9 |
| 18 | PQ | 0 | 0 | 12,5 | 1,1 | 0,9 |

**Table 40.** Modified parameters of 18-bus IEEE scenario imported from MATPOWER library. Bus data.

| From | To | R (%) | X (%) | B (%) | $Z_{BASE}$ ($\Omega$) | $I^{MAX}_{BASEcase}$ |
|---|---|---|---|---|---|---|
| 1 | 2 | 0,0371 | 0,0263 | 0 | 156,25 | 12,94 |
| 2 | 3 | 0,1109 | 0,0786 | 0 | 156,25 | 12,19 |
| 3 | 4 | 0,0006 | 0,0004 | 0 | 156,25 | 12,19 |
| 4 | 5 | 0,0059 | 0,0042 | 0 | 156,25 | 12,19 |
| 5 | 6 | 0,0044 | 0,0032 | 0 | 156,25 | 11,72 |
| 6 | 7 | 0,0302 | 0,0402 | 0 | 156,25 | 6,16 |
| 7 | 8 | 0,0473 | 0,0631 | 0 | 156,25 | 3,44 |
| 8 | 9 | 0,0417 | 0,0295 | 0 | 156,25 | 3,39 |
| 9 | 10 | 0,0326 | 0,0231 | 0 | 156,25 | 3,36 |
| 10 | 11 | 0,0075 | 0,0053 | 0 | 156,25 | 2,93 |
| 11 | 12 | 0,0830 | 0,0587 | 0 | 156,25 | 2,93 |
| 12 | 13 | 0,0789 | 0,0557 | 0 | 156,25 | 2,89 |
| 13 | 14 | 0,0314 | 0,0222 | 0 | 156,25 | 2,59 |
| 14 | 15 | 0,0615 | 0,0435 | 0 | 156,25 | 2,52 |
| 15 | 16 | 0,0553 | 0,0392 | 0 | 156,25 | 1,92 |
| 16 | 17 | 0,0256 | 0,0181 | 0 | 156,25 | 1,80 |
| 17 | 18 | 0,0532 | 0,0364 | 0 | 156,25 | 1,61 |
| 18 | 19 | 0,0120 | 0,0085 | 0 | 156,25 | 1,50 |
| 19 | 20 | 0,0359 | 0,0254 | 0 | 156,25 | 1,50 |
| 20 | 21 | 0,0235 | 0,0158 | 0 | 156,25 | 1,41 |
| 21 | 22 | 0,0368 | 0,0197 | 0 | 156,25 | 1,30 |
| 22 | 23 | 0,0169 | 0,0123 | 0 | 156,25 | 1,30 |
| 23 | 24 | 0,0439 | 0,0320 | 0 | 156,25 | 1,10 |
| 24 | 25 | 0,0256 | 0,0181 | 0 | 156,25 | 1,10 |
| 25 | 26 | 0,0469 | 0,0341 | 0 | 156,25 | 1,00 |
| 26 | 27 | 0,0215 | 0,0157 | 0 | 156,25 | 0,84 |
| 27 | 28 | 0,0376 | 0,0266 | 0 | 156,25 | 0,73 |
| 28 | 29 | 0,0421 | 0,0298 | 0 | 156,25 | 0,73 |
| 29 | 30 | 0,0220 | 0,0159 | 0 | 156,25 | 0,64 |
| 30 | 31 | 0,0082 | 0,0059 | 0 | 156,25 | 0,41 |
| 31 | 32 | 0,0223 | 0,0158 | 0 | 156,25 | 0,32 |
| 2 | 33 | 0,0285 | 0,0202 | 0 | 156,25 | 0,98 |
| 33 | 34 | 0,0013 | 0,0006 | 0 | 156,25 | 0,98 |
| 5 | 35 | 0,1462 | 0,0356 | 0 | 156,25 | 0,45 |
| 5 | 36 | 0,0814 | 0,1006 | 0 | 156,25 | 0,24 |
| 6 | 37 | 0,0035 | 0,0047 | 0 | 156,25 | 5,69 |
| 37 | 38 | 0,1309 | 0,0926 | 0 | 156,25 | 5,62 |
| 38 | 39 | 0,0603 | 0,0426 | 0 | 156,25 | 5,54 |
| 39 | 40 | 0,0223 | 0,0158 | 0 | 156,25 | 5,48 |

| From | To | R (%) | X (%) | B (%) | $Z_{BASE}$ ($\Omega$) | $I_{BASEcase}^{MAX}$ |
|---|---|---|---|---|---|---|
| 40 | 41 | 0,0590 | 0,0418 | 0 | 156,25 | 5,48 |
| 41 | 42 | 0,1491 | 0,1055 | 0 | 156,25 | 5,39 |
| 42 | 43 | 0,0776 | 0,0549 | 0 | 156,25 | 2,60 |
| 43 | 44 | 0,0285 | 0,0202 | 0 | 156,25 | 2,54 |
| 44 | 45 | 0,0260 | 0,0185 | 0 | 156,25 | 1,52 |
| 45 | 46 | 0,0103 | 0,0082 | 0 | 156,25 | 1,52 |
| 46 | 47 | 0,0409 | 0,0289 | 0 | 156,25 | 1,42 |
| 47 | 48 | 0,0268 | 0,0190 | 0 | 156,25 | 1,32 |
| 48 | 49 | 0,0471 | 0,0328 | 0 | 156,25 | 1,23 |
| 49 | 50 | 0,0532 | 0,0358 | 0 | 156,25 | 0,68 |
| 50 | 51 | 0,0256 | 0,0181 | 0 | 156,25 | 0,25 |
| 51 | 52 | 0,0145 | 0,0102 | 0 | 156,25 | 0,11 |
| 38 | 53 | 0,0541 | 0,0383 | 0 | 156,25 | 0,09 |
| 42 | 54 | 0,0104 | 0,0073 | 0 | 156,25 | 2,81 |
| 54 | 55 | 0,0339 | 0,0240 | 0 | 156,25 | 2,81 |
| 55 | 56 | 0,0574 | 0,0406 | 0 | 156,25 | 0,53 |
| 56 | 57 | 0,0558 | 0,0394 | 0 | 156,25 | 0,46 |
| 57 | 58 | 0,0433 | 0,0307 | 0 | 156,25 | 0,46 |
| 58 | 59 | 0,0302 | 0,0214 | 0 | 156,25 | 0,17 |
| 55 | 60 | 0,0215 | 0,0152 | 0 | 156,25 | 1,75 |
| 60 | 61 | 0,0210 | 0,0149 | 0 | 156,25 | 0,55 |
| 61 | 62 | 0,0264 | 0,0187 | 0 | 156,25 | 0,24 |
| 60 | 63 | 0,0227 | 0,0161 | 0 | 156,25 | 1,31 |
| 63 | 64 | 0,0673 | 0,0477 | 0 | 156,25 | 1,12 |
| 64 | 65 | 0,0433 | 0,0307 | 0 | 156,25 | 0,90 |
| 65 | 66 | 0,0194 | 0,0138 | 0 | 156,25 | 0,62 |
| 66 | 67 | 0,0293 | 0,0208 | 0 | 156,25 | 0,25 |
| 67 | 68 | 0,0140 | 0,0099 | 0 | 156,25 | 0,16 |
| 63 | 69 | 0,0235 | 0,0167 | 0 | 156,25 | 0,25 |
| 55 | 70 | 0,0149 | 0,0105 | 0 | 156,25 | 0,69 |
| 70 | 71 | 0,0077 | 0,0019 | 0 | 156,25 | 0,41 |
| 70 | 72 | 0,0450 | 0,0318 | 0 | 156,25 | 0,38 |
| 42 | 73 | 0,0149 | 0,0105 | 0 | 156,25 | 0,58 |
| 73 | 74 | 0,0019 | 0,0041 | 0 | 156,25 | 0,45 |
| 43 | 75 | 0,0244 | 0,0172 | 0 | 156,25 | 0,08 |
| 44 | 76 | 0,0355 | 0,0251 | 0 | 156,25 | 1,06 |
| 46 | 77 | 0,0332 | 0,0280 | 0 | 156,25 | 0,22 |
| 76 | 78 | 0,0107 | 0,0071 | 0 | 156,25 | 0,96 |
| 78 | 79 | 0,0267 | 0,0065 | 0 | 156,25 | 0,96 |
| 79 | 80 | 0,0645 | 0,0157 | 0 | 156,25 | 0,42 |
| 79 | 81 | 0,0973 | 0,0238 | 0 | 156,25 | 0,26 |

| From | To | R (%) | X (%) | B (%) | $Z_{BASE}$ ($\Omega$) | $I^{MAX}_{BASEcase}$ |
|------|-----|--------|--------|---|--------|------|
| 81 | 82 | 0,0021 | 0,0005 | 0 | 156,25 | 0,26 |
| 47 | 83 | 0,0055 | 0,0040 | 0 | 156,25 | 0,13 |
| 49 | 84 | 0,0332 | 0,0289 | 0 | 156,25 | 0,39 |
| 50 | 85 | 0,0095 | 0,0023 | 0 | 156,25 | 0,51 |
| 85 | 86 | 0,0024 | 0,0010 | 0 | 156,25 | 0,51 |
| 86 | 87 | 0,0112 | 0,0149 | 0 | 156,25 | 0,57 |
| 7 | 88 | 0,0112 | 0,0149 | 0 | 156,25 | 2,91 |
| 88 | 89 | 0,0302 | 0,0402 | 0 | 156,25 | 2,82 |
| 89 | 90 | 0,0192 | 0,0256 | 0 | 156,25 | 1,93 |
| 90 | 91 | 0,0136 | 0,0182 | 0 | 156,25 | 1,93 |
| 91 | 92 | 0,0203 | 0,0270 | 0 | 156,25 | 1,22 |
| 92 | 93 | 0,0180 | 0,0240 | 0 | 156,25 | 0,88 |
| 93 | 94 | 0,0132 | 0,0176 | 0 | 156,25 | 0,88 |
| 94 | 95 | 0,0132 | 0,0176 | 0 | 156,25 | 0,01 |
| 89 | 96 | 0,0442 | 0,0313 | 0 | 156,25 | 0,94 |
| 96 | 97 | 0,0624 | 0,0441 | 0 | 156,25 | 0,71 |
| 97 | 98 | 0,0580 | 0,0126 | 0 | 156,25 | 0,43 |
| 97 | 99 | 0,0021 | 0,0005 | 0 | 156,25 | 0,34 |
| 99 | 100 | 0,0021 | 0,0005 | 0 | 156,25 | 0,34 |
| 91 | 101 | 0,0149 | 0,0105 | 0 | 156,25 | 0,88 |
| 101 | 102 | 0,0372 | 0,0263 | 0 | 156,25 | 0,87 |
| 102 | 103 | 0,0572 | 0,0140 | 0 | 156,25 | 0,87 |
| 103 | 104 | 0,0404 | 0,0098 | 0 | 156,25 | 0,72 |
| 104 | 105 | 0,0752 | 0,0183 | 0 | 156,25 | 0,50 |
| 104 | 106 | 0,0073 | 0,0017 | 0 | 156,25 | 0,26 |
| 92 | 107 | 0,0546 | 0,0133 | 0 | 156,25 | 0,56 |
| 94 | 108 | 0,0394 | 0,0167 | 0 | 156,25 | 0,67 |
| 108 | 109 | 0,0291 | 0,0123 | 0 | 156,25 | 0,67 |

| From | To | R (%) | X (%) | B (%) | $Z_{BASE}$ ($\Omega$) | $I_{BASEcase}^{MAX}$ |
|------|------|--------|--------|-------|-----------------------|----------------------|
| 94 | 110 | 0,0021 | 0,0005 | 0 | ,25 | 0,44 |
| 7 | 111 | 0,0462 | 0,0327 | 0 | 156,25 | 0,09 |
| 10 | 112 | 0,0688 | 0,0168 | 0 | 156,25 | 0,62 |
| 11 | 113 | 0,0223 | 0,0158 | 0 | 156,25 | 0,00 |
| 13 | 114 | 0,0401 | 0,0284 | 0 | 156,25 | 0,26 |
| 114 | 115 | 0,0430 | 0,0304 | 0 | 156,25 | 0,26 |
| 115 | 116 | 0,0026 | 0,0006 | 0 | 156,25 | 0,26 |
| 14 | 117 | 0,0325 | 0,0235 | 0 | 156,25 | 0,09 |
| 15 | 118 | 0,0104 | 0,0073 | 0 | 156,25 | 0,95 |
| 118 | 119 | 0,0297 | 0,0210 | 0 | 156,25 | 0,95 |
| 119 | 120 | 0,0273 | 0,0193 | 0 | 156,25 | 0,62 |
| 120 | 121 | 0,0326 | 0,0231 | 0 | 156,25 | 0,62 |
| 121 | 122 | 0,0471 | 0,0333 | 0 | 156,25 | 0,57 |
| 122 | 123 | 0,0376 | 0,0266 | 0 | 156,25 | 0,57 |
| 123 | 124 | 0,0392 | 0,0278 | 0 | 156,25 | 0,57 |
| 124 | 125 | 0,0504 | 0,0356 | 0 | 156,25 | 0,49 |
| 125 | 126 | 0,0536 | 0,0390 | 0 | 156,25 | 0,49 |
| 126 | 127 | 0,0223 | 0,0158 | 0 | 156,25 | 0,49 |
| 127 | 128 | 0,0367 | 0,0270 | 0 | 156,25 | 0,39 |
| 128 | 129 | 0,0376 | 0,0273 | 0 | 156,25 | 0,30 |
| 129 | 130 | 0,0066 | 0,0047 | 0 | 156,25 | 0,14 |
| 119 | 131 | 0,0228 | 0,0163 | 0 | 156,25 | 0,17 |
| 131 | 132 | 0,0223 | 0,0158 | 0 | 156,25 | 0,00 |
| 131 | 133 | 0,0592 | 0,0430 | 0 | 156,25 | 0,17 |
| 121 | 134 | 0,0541 | 0,0394 | 0 | 156,25 | 0,06 |
| 16 | 135 | 0,0339 | 0,0240 | 0 | 156,25 | 0,04 |
| 16 | 136 | 0,0194 | 0,0138 | 0 | 156,25 | 0,10 |
| 18 | 137 | 0,0376 | 0,0266 | 0 | 156,25 | 0,11 |
| 23 | 138 | 0,0495 | 0,0359 | 0 | 156,25 | 0,10 |
| 25 | 139 | 0,0611 | 0,0433 | 0 | 156,25 | 0,11 |
| 30 | 140 | 0,0334 | 0,0242 | 0 | 156,25 | 0,30 |
| 31 | 141 | 0,0376 | 0,0266 | 0 | 156,25 | 0,12 |

**Table 41.** Modified parameters of 141-bus IEEE scenario imported from MATPOWER library. Line data.

| Bus Nr. | Node type | $G_S$ | $B_S$ | $V_N$ (kV) | $V_{max}$ (p.u.) | $V_{min}$ (p.u.) |
|---|---|---|---|---|---|---|
| 1 | Slack | 0 | 0 | 12,5 | 1,1 | 0,9 |
| 2 | PQ | 0 | 0 | 12,5 | 1,1 | 0,9 |
| 3 | PQ | 0 | 0 | 12,5 | 1,1 | 0,9 |
| 4 | PQ | 0 | 0 | 12,5 | 1,1 | 0,9 |
| 5 | PQ | 0 | 0 | 12,5 | 1,1 | 0,9 |
| 6 | PQ | 0 | 0 | 12,5 | 1,1 | 0,9 |
| 7 | PQ | 0 | 0 | 12,5 | 1,1 | 0,9 |
| 8 | PQ | 0 | 0 | 12,5 | 1,1 | 0,9 |
| 9 | PQ | 0 | 0 | 12,5 | 1,1 | 0,9 |
| 10 | PQ | 0 | 0 | 12,5 | 1,1 | 0,9 |
| 11 | PQ | 0 | 0 | 12,5 | 1,1 | 0,9 |
| 12 | PQ | 0 | 0 | 12,5 | 1,1 | 0,9 |
| 13 | PQ | 0 | 0 | 12,5 | 1,1 | 0,9 |
| 14 | PQ | 0 | 0 | 12,5 | 1,1 | 0,9 |
| 15 | PQ | 0 | 0 | 12,5 | 1,1 | 0,9 |
| 16 | PQ | 0 | 0 | 12,5 | 1,1 | 0,9 |
| 17 | PQ | 0 | 0 | 12,5 | 1,1 | 0,9 |
| 18 | PQ | 0 | 0 | 12,5 | 1,1 | 0,9 |
| 19 | PQ | 0 | 0 | 12,5 | 1,1 | 0,9 |
| 20 | PQ | 0 | 0 | 12,5 | 1,1 | 0,9 |
| 21 | PQ | 0 | 0 | 12,5 | 1,1 | 0,9 |
| 22 | PQ | 0 | 0 | 12,5 | 1,1 | 0,9 |
| 23 | PQ | 0 | 0 | 12,5 | 1,1 | 0,9 |
| 24 | PQ | 0 | 0 | 12,5 | 1,1 | 0,9 |
| 25 | PQ | 0 | 0 | 12,5 | 1,1 | 0,9 |
| 26 | PQ | 0 | 0 | 12,5 | 1,1 | 0,9 |
| 27 | PQ | 0 | 0 | 12,5 | 1,1 | 0,9 |
| 28 | PQ | 0 | 0 | 12,5 | 1,1 | 0,9 |
| 29 | PQ | 0 | 0 | 12,5 | 1,1 | 0,9 |
| 30 | PQ | 0 | 0 | 12,5 | 1,1 | 0,9 |
| 31 | PQ | 0 | 0 | 12,5 | 1,1 | 0,9 |
| 32 | PQ | 0 | 0 | 12,5 | 1,1 | 0,9 |
| 33 | PQ | 0 | 0 | 12,5 | 1,1 | 0,9 |
| 34 | PQ | 0 | 0 | 12,5 | 1,1 | 0,9 |
| 35 | PQ | 0 | 0 | 12,5 | 1,1 | 0,9 |
| 36 | PQ | 0 | 0 | 12,5 | 1,1 | 0,9 |
| 37 | PQ | 0 | 0 | 12,5 | 1,1 | 0,9 |
| 38 | PQ | 0 | 0 | 12,5 | 1,1 | 0,9 |
| 39 | PQ | 0 | 0 | 12,5 | 1,1 | 0,9 |

| Bus Nr. | Node type | $G_S$ | $B_S$ | $V_N$ (kV) | $V_{max}$ (p.u.) | $V_{min}$ (p.u.) |
|---------|-----------|-------|-------|------------|------------------|------------------|
| 40 | PQ | 0 | 0 | 12,5 | 1,1 | 0,9 |
| 41 | PQ | 0 | 0 | 12,5 | 1,1 | 0,9 |
| 42 | PQ | 0 | 0 | 12,5 | 1,1 | 0,9 |
| 43 | PQ | 0 | 0 | 12,5 | 1,1 | 0,9 |
| 44 | PQ | 0 | 0 | 12,5 | 1,1 | 0,9 |
| 45 | PQ | 0 | 0 | 12,5 | 1,1 | 0,9 |
| 46 | PQ | 0 | 0 | 12,5 | 1,1 | 0,9 |
| 47 | PQ | 0 | 0 | 12,5 | 1,1 | 0,9 |
| 48 | PQ | 0 | 0 | 12,5 | 1,1 | 0,9 |
| 49 | PQ | 0 | 0 | 12,5 | 1,1 | 0,9 |
| 50 | PQ | 0 | 0 | 12,5 | 1,1 | 0,9 |
| 51 | PQ | 0 | 0 | 12,5 | 1,1 | 0,9 |
| 52 | PQ | 0 | 0 | 12,5 | 1,1 | 0,9 |
| 53 | PQ | 0 | 0 | 12,5 | 1,1 | 0,9 |
| 54 | PQ | 0 | 0 | 12,5 | 1,1 | 0,9 |
| 55 | PQ | 0 | 0 | 12,5 | 1,1 | 0,9 |
| 56 | PQ | 0 | 0 | 12,5 | 1,1 | 0,9 |
| 57 | PQ | 0 | 0 | 12,5 | 1,1 | 0,9 |
| 58 | PQ | 0 | 0 | 12,5 | 1,1 | 0,9 |
| 59 | PQ | 0 | 0 | 12,5 | 1,1 | 0,9 |
| 60 | PQ | 0 | 0 | 12,5 | 1,1 | 0,9 |
| 61 | PQ | 0 | 0 | 12,5 | 1,1 | 0,9 |
| 62 | PQ | 0 | 0 | 12,5 | 1,1 | 0,9 |
| 63 | PQ | 0 | 0 | 12,5 | 1,1 | 0,9 |
| 64 | PQ | 0 | 0 | 12,5 | 1,1 | 0,9 |
| 65 | PQ | 0 | 0 | 12,5 | 1,1 | 0,9 |
| 66 | PQ | 0 | 0 | 12,5 | 1,1 | 0,9 |
| 67 | PQ | 0 | 0 | 12,5 | 1,1 | 0,9 |
| 68 | PQ | 0 | 0 | 12,5 | 1,1 | 0,9 |
| 69 | PQ | 0 | 0 | 12,5 | 1,1 | 0,9 |
| 70 | PQ | 0 | 0 | 12,5 | 1,1 | 0,9 |
| 71 | PQ | 0 | 0 | 12,5 | 1,1 | 0,9 |
| 72 | PQ | 0 | 0 | 12,5 | 1,1 | 0,9 |
| 73 | PQ | 0 | 0 | 12,5 | 1,1 | 0,9 |
| 74 | PQ | 0 | 0 | 12,5 | 1,1 | 0,9 |
| 75 | PQ | 0 | 0 | 12,5 | 1,1 | 0,9 |
| 76 | PQ | 0 | 0 | 12,5 | 1,1 | 0,9 |
| 77 | PQ | 0 | 0 | 12,5 | 1,1 | 0,9 |
| 78 | PQ | 0 | 0 | 12,5 | 1,1 | 0,9 |
| 79 | PQ | 0 | 0 | 12,5 | 1,1 | 0,9 |

| Bus Nr. | Node type | $G_S$ | $B_S$ | $V_N$ (kV) | $V_{max}$ (p.u.) | $V_{min}$ (p.u.) |
|---|---|---|---|---|---|---|
| 80 | PQ | 0 | 0 | 12,5 | 1,1 | 0,9 |
| 81 | PQ | 0 | 0 | 12,5 | 1,1 | 0,9 |
| 82 | PQ | 0 | 0 | 12,5 | 1,1 | 0,9 |
| 83 | PQ | 0 | 0 | 12,5 | 1,1 | 0,9 |
| 84 | PQ | 0 | 0 | 12,5 | 1,1 | 0,9 |
| 85 | PQ | 0 | 0 | 12,5 | 1,1 | 0,9 |
| 86 | PQ | 0 | 0 | 12,5 | 1,1 | 0,9 |
| 87 | PQ | 0 | 0 | 12,5 | 1,1 | 0,9 |
| 88 | PQ | 0 | 0 | 12,5 | 1,1 | 0,9 |
| 89 | PQ | 0 | 0 | 12,5 | 1,1 | 0,9 |
| 90 | PQ | 0 | 0 | 12,5 | 1,1 | 0,9 |
| 91 | PQ | 0 | 0 | 12,5 | 1,1 | 0,9 |
| 92 | PQ | 0 | 0 | 12,5 | 1,1 | 0,9 |
| 93 | PQ | 0 | 0 | 12,5 | 1,1 | 0,9 |
| 94 | PQ | 0 | 0 | 12,5 | 1,1 | 0,9 |
| 95 | PQ | 0 | 0 | 12,5 | 1,1 | 0,9 |
| 96 | PQ | 0 | 0 | 12,5 | 1,1 | 0,9 |
| 97 | PQ | 0 | 0 | 12,5 | 1,1 | 0,9 |
| 98 | PQ | 0 | 0 | 12,5 | 1,1 | 0,9 |
| 99 | PQ | 0 | 0 | 12,5 | 1,1 | 0,9 |
| 100 | PQ | 0 | 0 | 12,5 | 1,1 | 0,9 |
| 101 | PQ | 0 | 0 | 12,5 | 1,1 | 0,9 |
| 102 | PQ | 0 | 0 | 12,5 | 1,1 | 0,9 |
| 103 | PQ | 0 | 0 | 12,5 | 1,1 | 0,9 |
| 104 | PQ | 0 | 0 | 12,5 | 1,1 | 0,9 |
| 105 | PQ | 0 | 0 | 12,5 | 1,1 | 0,9 |
| 106 | PQ | 0 | 0 | 12,5 | 1,1 | 0,9 |
| 107 | PQ | 0 | 0 | 12,5 | 1,1 | 0,9 |
| 108 | PQ | 0 | 0 | 12,5 | 1,1 | 0,9 |
| 109 | PQ | 0 | 0 | 12,5 | 1,1 | 0,9 |

| Bus Nr. | Node type | $G_S$ | $B_S$ | $V_N\ (kV)$ | $V_{max}\ (p.u.)$ | $V_{min}\ (p.u.)$ |
|---|---|---|---|---|---|---|
| 110 | PQ | 0 | 0 | 12,5 | 1,1 | 0,9 |
| 111 | PQ | 0 | 0 | 12,5 | 1,1 | 0,9 |
| 112 | PQ | 0 | 0 | 12,5 | 1,1 | 0,9 |
| 113 | PQ | 0 | 0 | 12,5 | 1,1 | 0,9 |
| 114 | PQ | 0 | 0 | 12,5 | 1,1 | 0,9 |
| 115 | PQ | 0 | 0 | 12,5 | 1,1 | 0,9 |
| 116 | PQ | 0 | 0 | 12,5 | 1,1 | 0,9 |
| 117 | PQ | 0 | 0 | 12,5 | 1,1 | 0,9 |
| 118 | PQ | 0 | 0 | 12,5 | 1,1 | 0,9 |
| 119 | PQ | 0 | 0 | 12,5 | 1,1 | 0,9 |
| 120 | PQ | 0 | 0 | 12,5 | 1,1 | 0,9 |
| 121 | PQ | 0 | 0 | 12,5 | 1,1 | 0,9 |
| 122 | PQ | 0 | 0 | 12,5 | 1,1 | 0,9 |
| 123 | PQ | 0 | 0 | 12,5 | 1,1 | 0,9 |
| 124 | PQ | 0 | 0 | 12,5 | 1,1 | 0,9 |
| 125 | PQ | 0 | 0 | 12,5 | 1,1 | 0,9 |
| 126 | PQ | 0 | 0 | 12,5 | 1,1 | 0,9 |
| 127 | PQ | 0 | 0 | 12,5 | 1,1 | 0,9 |
| 128 | PQ | 0 | 0 | 12,5 | 1,1 | 0,9 |
| 129 | PQ | 0 | 0 | 12,5 | 1,1 | 0,9 |
| 130 | PQ | 0 | 0 | 12,5 | 1,1 | 0,9 |
| 131 | PQ | 0 | 0 | 12,5 | 1,1 | 0,9 |
| 132 | PQ | 0 | 0 | 12,5 | 1,1 | 0,9 |
| 133 | PQ | 0 | 0 | 12,5 | 1,1 | 0,9 |
| 134 | PQ | 0 | 0 | 12,5 | 1,1 | 0,9 |
| 135 | PQ | 0 | 0 | 12,5 | 1,1 | 0,9 |
| 136 | PQ | 0 | 0 | 12,5 | 1,1 | 0,9 |
| 137 | PQ | 0 | 0 | 12,5 | 1,1 | 0,9 |
| 138 | PQ | 0 | 0 | 12,5 | 1,1 | 0,9 |
| 139 | PQ | 0 | 0 | 12,5 | 1,1 | 0,9 |
| 140 | PQ | 0 | 0 | 12,5 | 1,1 | 0,9 |
| 141 | PQ | 0 | 0 | 12,5 | 1,1 | 0,9 |

**Table 42.** Modified parameters of 141-bus IEEE scenario imported from MATPOWER library. Bus data.

# ANNEX B: EV Demand Distribution

This chapter presents the number of EVs that charge at each bus of the system and its charging behaviour. Note that the value reflects the number of EVs which charge at each node during the whole simulation, but the arrival times must not be necessarily the same. Tables 43 and 44 include the information regarding the 18-bus IEEE scenario for Low and High EV demand respectively. Likewise, Tables 45 and 46 show the information regarding the 141-bus IEEE scenario for Low and High EV demand respectively.

| Node | Node Type | Nr Houses | N | D |
|------|-----------|-----------|-----|-----|
| 1 | - | - | - | - |
| 2 | - | - | - | - |
| 3 | - | - | - | - |
| 4 | H | 200 | - | - |
| 5 | H | 400 | - | - |
| 6 | H,C2 | 200 | - | - |
| 7 | C1 | - | - | - |
| 8 | H, I1,I2 | 600 | 200 | 300 |
| 9 | H | 200 | - | - |
| 10 | O1 | - | - | - |
| 11 | H | 500 | 250 | 50 |
| 12 | H,C2 | 100 | - | - |
| 13 | H | 300 | 150 | 50 |
| 14 | H | 200 | - | - |
| 15 | H,O2 | 250 | 125 | 150 |
| 16 | H | 450 | 225 | 50 |
| 17 | I3,I4,I5 | - | 50 | 400 |
| 18 | H,Sc | 150 | - | - |

**Table 43.** 18-bus IEEE Low EV demand case - Number of EV per charging station. N denotes night charging behaviour, whereas D denotes day charging behaviour.

| Node | Node Type | Nr. Houses | N | D |
|------|-----------|------------|-----|-----|
| 1 | - | - | - | - |
| 2 | - | - | - | - |
| 3 | - | - | - | - |
| 4 | H | 200 | 200 | 50 |
| 5 | H | 400 | 400 | 100 |
| 6 | H,C2 | 200 | 200 | 300 |
| 7 | C1 | - | - | 500 |
| 8 | H, I1,I2 | 600 | 600 | 400 |
| 9 | H | 200 | 200 | - |
| 10 | O1 | - | - | 500 |
| 11 | H | 500 | 500 | 50 |
| 12 | H,C2 | 100 | 100 | 250 |
| 13 | H | 300 | 300 | 50 |
| 14 | H | 200 | 200 | 50 |
| 15 | H,O2 | 250 | 250 | 500 |
| 16 | H | 450 | 450 | 50 |
| 17 | I3,I4,I5 | - | - | 700 |
| 18 | H,Sc | 150 | 150 | 50 |

**Table 44.** 18-bus IEEE High EV demand case - Number of EV per charging station. N denotes night charging behaviour, whereas D denotes day charging behaviour.

| Node | Node Type | Nr. Houses | N | D |
|------|-----------|-----------|-----|-----|
| 1 | - | - | - | - |
| 2 | - | - | - | - |
| 3 | - | - | - | - |
| 4 | - | - | - | - |
| 5 | - | - | - | - |
| 6 | - | - | - | - |
| 7 | - | - | - | - |
| 8 | H | 60 | 20 | 0 |
| 9 | H | 20 | - | - |
| 10 | - | - | - | - |
| 11 | - | - | - | - |
| 12 | H | 30 | - | - |
| 13 | H | 60 | - | - |
| 14 | - | - | - | - |
| 15 | - | - | - | - |
| 16 | - | - | - | - |
| 17 | C2,H | 50 | 30 | 100 |
| 18 | - | - | - | - |
| 19 | - | - | - | - |
| 20 | H | 60 | 30 | - |
| 21 | H | 60 | - | - |
| 22 | - | - | - | - |
| 23 | H | 60 | 30 | - |
| 24 | - | - | - | - |
| 25 | - | - | - | - |
| 26 | H,I1 | 50 | 30 | 150 |
| 27 | H | 60 | - | - |
| 28 | - | - | - | - |
| 29 | H | 60 | - | - |
| 30 | - | - | - | - |
| 31 | - | - | - | - |
| 32 | H,I3 | 50 | 25 | - |
| 33 | - | - | - | - |
| 34 | I4 | - | - | - |
| 35 | H,I5 | 200 | 150 | 250 |
| 36 | H,Sc | 50 | - | - |
| 37 | H | 50 | - | - |
| 38 | - | - | - | - |
| 39 | H | 40 | - | - |

| Node | Node Type | Nr. Houses | N | D |
|------|-----------|------------|-----|-----|
| 40 | - | - | - | - |
| 41 | H | 60 | 40 | 0 |
| 42 | - | - | - | - |
| 43 | - | - | - | - |
| 44 | H | 50 | 25 | - |
| 45 | - | - | - | - |
| 46 | - | - | - | - |
| 47 | - | - | - | - |
| 48 | O2,H | 50 | 25 | 50 |
| 49 | H,C1 | 50 | 10 | 70 |
| 50 | - | - | - | - |
| 51 | H,I5 | 40 | - | - |
| 52 | H | 60 | - | - |
| 53 | H | 50 | - | - |
| 54 | - | - | - | - |
| 55 | - | - | - | - |
| 56 | H | 50 | - | - |
| 57 | - | - | - | - |
| 58 | I1,I3 | - | 0 | 190 |
| 59 | C2 | - | - | - |
| 60 | - | - | - | - |
| 61 | O1,H | 50 | - | - |
| 62 | H,O2 | 100 | 75 | 150 |
| 63 | - | - | - | - |
| 64 | H,C2 | 20 | - | - |
| 65 | H | 150 | 120 | 0 |
| 66 | H,O1 | 200 | 150 | 110 |
| 67 | H | 50 | - | - |
| 68 | H | 80 | - | - |
| 69 | I1,I5,C2 | - | 0 | 100 |
| 70 | - | - | - | - |
| 71 | I4 | - | 0 | 75 |
| 72 | H,I5 | 200 | 100 | 50 |
| 73 | O2,O1 | - | - | - |
| 74 | H,C2 | 150 | 80 | 50 |
| 75 | H | 40 | - | - |
| 76 | H | 70 | - | - |
| 77 | O1 | - | - | - |
| 78 | - | - | - | - |
| 79 | I4 | - | - | - |

| Node | Node Type | Nr. Houses | N | D |
|------|-----------|------------|-----|-----|
| 80 | O1,O2 | - | - | - |
| 81 | - | - | - | - |
| 82 | H | 150 | 75 | - |
| 83 | H | 60 | - | - |
| 84 | H,I1 | 150 | 75 | 50 |
| 85 | - | - | - | - |
| 86 | O1,I1,Sc | - | - | 100 |
| 87 | I5,I1,H | 50 | - | 25 |
| 88 | H | 60 | - | - |
| 89 | H | 50 | - | - |
| 90 | - | - | - | - |
| 91 | - | - | - | - |
| 92 | - | - | - | - |
| 93 | - | - | - | - |
| 94 | GEN | - | - | 50 |
| 95 | - | - | - | - |
| 96 | H | 150 | 80 | - |
| 97 | - | - | - | - |
| 98 | O1,H | 150 | 70 | 30 |
| 99 | - | - | - | - |
| 100 | O2,H | 150 | 80 | - |
| 101 | H | 10 | - | - |
| 102 | - | - | - | - |
| 103 | H | 100 | 75 | - |
| 104 | - | - | - | - |
| 105 | I3 | - | - | - |
| 106 | Sc,H | 70 | - | - |
| 107 | C1 | - | - | 60 |
| 108 | - | - | - | - |
| 109 | C2 | - | - | 80 |
| 110 | O2 | - | - | - |
| 111 | H | 50 | - | - |
| 112 | O1 | - | - | - |
| 113 | GEN | - | - | - |
| 114 | - | - | - | - |
| 115 | - | - | - | - |
| 116 | I1,I5,C2 | - | - | - |
| 117 | H | 50 | - | - |
| 118 | - | - | - | - |
| 119 | H | 90 | 60 | - |

| Node | Node Type | Nr. Houses | N | D |
|------|-----------|------------|-----|-----|
| 120 | - | - | - | - |
| 121 | - | - | - | - |
| 122 | - | - | - | - |
| 123 | GEN | - | - | - |
| 124 | Sc | - | - | - |
| 125 | - | - | - | - |
| 126 | - | - | - | - |
| 127 | H | 60 | 40 | - |
| 128 | H | 60 | - | - |
| 129 | H | 90 | 60 | - |
| 130 | H | 90 | - | - |
| 131 | - | - | - | - |
| 132 | GEN | - | - | - |
| 133 | H,I5 | 100 | 40 | 50 |
| 134 | O1,H | 30 | - | - |
| 135 | H | 20 | - | - |
| 136 | H | 60 | 45 | - |
| 137 | H | 50 | - | - |
| 138 | H | 50 | - | - |
| 139 | H | 50 | - | - |
| 140 | H | 150 | 100 | 0 |
| 141 | H | 70 | 50 | - |

**Table 45.** 141-bus IEEE Low EV demand case - Number of EV per charging station. N denotes night charging behaviour, whereas D denotes day charging behaviour.

| Node | Node Type | Nr. Houses | N | D |
|:----:|:---------:|:----------:|:---:|:---:|
| 1 | - | - | - | - |
| 2 | - | - | - | - |
| 3 | - | - | - | - |
| 4 | - | - | - | - |
| 5 | - | - | - | - |
| 6 | - | - | - | - |
| 7 | - | - | - | - |
| 8 | H | 60 | 60 | - |
| 9 | H | 20 | 20 | - |
| 10 | - | - | - | - |
| 11 | - | - | - | - |
| 12 | H | 30 | 30 | - |
| 13 | H | 60 | 60 | - |
| 14 | - | - | - | - |
| 15 | - | - | - | - |
| 16 | - | - | - | - |
| 17 | C2,H | 50 | 50 | 150 |
| 18 | - | - | - | - |
| 19 | - | - | - | - |
| 20 | H | 60 | 60 | - |
| 21 | H | 60 | 60 | - |
| 22 | - | - | - | - |
| 23 | H | 60 | 60 | - |
| 24 | - | - | - | - |
| 25 | - | - | - | - |
| 26 | H,I1 | 50 | 50 | 150 |
| 27 | H | 60 | 60 | - |
| 28 | - | - | - | - |
| 29 | H | 60 | 60 | - |
| 30 | - | - | - | - |
| 31 | - | - | - | - |
| 32 | H,I3 | 50 | 50 | 150 |
| 33 | - | - | - | - |
| 34 | I4 | - | - | - |
| 35 | H,I5 | 200 | 200 | 250 |
| 36 | H,Sc | 50 | 50 | 200 |
| 37 | H | 50 | 50 | 100 |
| 38 | - | - | - | - |
| 39 | H | 40 | 40 | - |

| Node | Node Type | Nr. Houses | N | D |
|------|-----------|-----------|-----|-----|
| 40 | - | - | - | - |
| 41 | H | 60 | 60 | - |
| 42 | - | - | - | - |
| 43 | - | - | - | - |
| 44 | H | 50 | 50 | - |
| 45 | - | - | - | - |
| 46 | - | - | - | - |
| 47 | - | - | - | - |
| 48 | O2,H | 50 | 50 | 300 |
| 49 | H,C1 | 50 | 50 | 70 |
| 50 | - | - | - | - |
| 51 | H,I5 | 40 | 40 | 100 |
| 52 | H | 60 | 60 | - |
| 53 | H | 50 | 50 | - |
| 54 | - | - | - | - |
| 55 | - | - | - | - |
| 56 | H | 50 | 50 | - |
| 57 | - | - | - | - |
| 58 | I1,I3 | - | - | 300 |
| 59 | C2 | - | - | 100 |
| 60 | - | - | - | - |
| 61 | O1,H | 50 | 50 | 100 |
| 62 | H,O2 | 100 | 100 | 150 |
| 63 | - | - | - | - |
| 64 | H,C2 | 20 | 20 | 200 |
| 65 | H | 150 | 150 | - |
| 66 | H,O1 | 200 | 200 | 70 |
| 67 | H | 50 | 50 | - |
| 68 | H | 80 | 80 | - |
| 69 | I1,I5,C2 | - | - | 100 |
| 70 | - | - | - | - |
| 71 | I4 | - | - | 75 |
| 72 | H,I5 | 200 | 200 | 50 |
| 73 | O2,O1 | - | - | 70 |
| 74 | H,C2 | 150 | 150 | 50 |
| 75 | H | 40 | 40 | - |
| 76 | H | 70 | 70 | - |
| 77 | O1 | - | - | 150 |
| 78 | - | - | - | - |
| 79 | I4 | - | - | 100 |

| Node | Node Type | Nr. Houses | N | D |
|------|-----------|------------|-----|-----|
| 80 | O1,O2 | - | - | 80 |
| 81 | - | - | - | - |
| 82 | H | 150 | 150 | - |
| 83 | H | 60 | 60 | - |
| 84 | H,I1 | 150 | 150 | 50 |
| 85 | - | - | - | - |
| 86 | O1,I1,Sc | - | - | 100 |
| 87 | I5,I1,H | 50 | 50 | 100 |
| 88 | H | 60 | 60 | - |
| 89 | H | 50 | 50 | - |
| 90 | - | - | - | - |
| 91 | - | - | - | - |
| 92 | - | - | - | - |
| 93 | - | - | - | - |
| 94 | GEN | - | - | 100 |
| 95 | - | - | - | - |
| 96 | H | 150 | 150 | - |
| 97 | - | - | - | - |
| 98 | O1,H | 150 | 150 | 100 |
| 99 | - | - | - | - |
| 100 | O2,H | 150 | 150 | 100 |
| 101 | H | 10 | 10 | - |
| 102 | - | - | - | - |
| 103 | H | 100 | 100 | - |
| 104 | - | - | - | - |
| 105 | I3 | - | - | 150 |
| 106 | Sc,H | 70 | 70 | 50 |
| 107 | C1 | - | - | 70 |
| 108 | - | - | - | - |
| 109 | C2 | - | - | 100 |
| 110 | O2 | - | - | 150 |
| 111 | H | 50 | 50 | - |
| 112 | O1 | - | - | 100 |
| 113 | GEN | - | - | - |
| 114 | - | - | - | - |
| 115 | - | - | - | - |
| 116 | I1,I5,C2 | - | - | 200 |
| 117 | H | 50 | 50 | - |
| 118 | - | - | - | - |
| 119 | H | 90 | 90 | - |

| Node | Node Type | Nr. Houses | N | D |
|------|-----------|------------|-----|-----|
| 120 | - | - | - | - |
| 121 | - | - | - | - |
| 122 | - | - | - | - |
| 123 | GEN | - | - | - |
| 124 | Sc | - | - | 50 |
| 125 | - | - | - | - |
| 126 | - | - | - | - |
| 127 | H | 60 | 60 | - |
| 128 | H | 60 | 60 | - |
| 129 | H | 90 | 90 | - |
| 130 | H | 90 | 90 | - |
| 131 | - | - | - | - |
| 132 | GEN | - | - | - |
| 133 | H,I5 | 100 | 100 | 100 |
| 134 | O1,H | 30 | 30 | 115 |
| 135 | H | 20 | 20 | - |
| 136 | H | 60 | 60 | - |
| 137 | H | 50 | 50 | - |
| 138 | H | 50 | 50 | - |
| 139 | H | 50 | 50 | - |
| 140 | H | 150 | 150 | - |
| 141 | H | 70 | 70 | - |

**Table 46.** 141-bus IEEE High EV demand case - Number of EV per charging station. N denotes night charging behaviour, whereas D denotes day charging behaviour.